Abstract

Traditionally, finite element methods generate progressively higher order accurate solutions by use of higher degree trial space bases for the weak statement construction. This invariably yields matrix equations of greater bandwidth thus increasing implementational and computational costs.

A new approach to designing high order - defined here to exceed third - accurate methods has been developed and tested. The systematic construction of progressively higher order spatial approximations is achieved via a modified equation analysis, which allows one to clearly identify correction terms appropriate for a desired accuracy order. The resulting perturbed PDE is shown to be consistent with the Taylor Weak Statement formulation. It confirms the expected high order of spatial accuracy in TWS constructions and provides a highly efficient dispersion error control mechanism whose application is based on the specifics of the solution domain discretization and physics of the problem. A distinguishing desirable property of the developed method is solution matrix bandwidth containment, i.e. bandwidth always remains equal to that of the linear basis (second order) discretization. This permits combining the computational efficiency of the lower order methods with superior accuracy inherent in higher order approximations.

Numerical simulations compare performance of the developed method to that of the GWS and TWS formulations. Uniform mesh refinement convergence results con-

firm the order of truncation error for each method. High order formulation is shown to require significantly fewer nodes to accurately resolve solution gradients for convection dominated problems. Benchmark problem applications for the compressible Euler and incompressible Navier-Stokes equations complete the manuscript. In both cases the developed high order formulation is shown to result in more accurate solutions on coarser discretizations, thus preserving the design trends illustrated for the model advection-diffusion equation.

Contents.

Chapter **Page**

1. Introduction **1**

1.1 Finite differences approach 1

1.2 Finite element approach 4

1.3 This dissertation 6

2. Weak statement formulation **8**

2.1 Error minimization via a weak statement 8

2.2 Solution domain discretization 9

2.3 Element assembly procedure 10

2.4 Accuracy and asymptotic convergence 13

3. Undetermined coefficients approach **16**

3.1 High order formulation. Theoretical approach 16

3.2 One-dimensional unsteady case 24

3.3 Two-dimensional steady-state case 28

4. Perturbed PDE approach **40**

4.1 One-dimensional steady-state formulation 40

4.2 Non-uniform mesh implementation 48

4.3 Two-dimensional steady-state case 53

4.4 2D steady-state verification problems 58

4.5 Unsteady two-dimensional formulation 62

4.6 High order formulation for hyperbolic problems 69

5. Lax-Wendroff, upwind formulations.

Monotonicity vs. accuracy 73

5.1 Perturbed PDE analysis error correction 73

5.2 Lax-Wendroff formulation for the linear unsteady case 74

5.3 Generalized Taylor Weak Statement approach 77

5.4 Upwind formulation 79

5.5 Upwind vs. High order = monotonicity vs. accuracy 80

5.6 Uniformly high order time-space corrections 82

Chapter **Page**

6. High order formulation for non-linear equation systems 89

6.1 Flows in a converging-diverging nozzle. Euler equations 89

6.1.1 Problem statement 89

6.1.2 High order formulation 91

6.1.3 Diffusion term introduction 95

6.1.4 High order formulation for Euler equations 96

6.1.5 Spatial filtering 101

6.1.6 Time dependent formulation 103

6.2 Incompressible Navier-Stokes equations 108

6.2.1 $\Omega - \Psi$ algorithm 108

6.2.2 High order formulation 110

6.2.3 High order formulation for general Navier-Stokes equation forms 113

6.2.4 FE-like matrix formulation. Assembly procedure 115

7. Results and discussion 118

7.1 Undetermined coefficients approach 118

7.1.1 Convergence study results 118

7.1.2 One-dimensional steady-state problems 119

7.1.3 One-dimensional unsteady problems 120

7.1.4 Two-dimensional steady-state problems 122

7.2 Perturbed equation approach 124

7.2.1 One-dimensional problems on uniform mesh 124

7.2.2 One-dimensional problems on non-uniform mesh 125

7.2.3 Two-dimensional steady-state problems 126

7.2.4 Two-dimensional unsteady problems 128

7.2.5 Two-dimensional hyperbolic problems 130

7.3 Non-linear equation systems 130

7.3.1 Flows in a converging-diverging nozzle 130

7.3.2 Driven cavity benchmark solutions 135

Chapter **Page**

8. Summary and conclusions **140**

Bibliography **142**

Appendices **149**

Appendix I Figures 150

Appendix II Tables 180

Appendix III Template file for the high order formulation implementation. Driven cavity benchmark 190

Appendix IV Model file for the high order formulation implementation. Driven cavity benchmark 198

Appendix V Driven cavity benchmark. Integer print-field after 40 time steps. High order formulation, Re=3000, 31×31 locally uniform mesh 203

Vita **223**

List of figures

Figure **Page**

5.1 Steady-state advection-diffusion. Uniform 21-node mesh.

Performance comparison for $\varepsilon = 0.001$ 151

5.2 Steady-state advection diffusion. Uniform mesh.

Performance comparison 152

7.1 1D Steady-state problem, solution dependence on *Nnode*, $\varepsilon = 0.001$.

High order and GWS performance comparison. 153

7.2 1D Stationary wave problem, solution dependence on *Nnode*, $\varepsilon = 0.001$.

High order and GWS performance comparison. 154

7.3 1D Unsteady problem, solution dependence on C and ε.

High order and GWS performance comparison. 155

7.4 1D Unsteady problem, solution behavior at small ε, C=1.

High order and GWS performance comparison. 156

7.5 2D Steady-state problem, solution dependence on ε, 11×11 square

mesh. High order and GWS performance comparison. 157

7.6 2D Steady-state problem, solution dependence on *Nnode*, $\varepsilon = 0.005$

High order and GWS performance comparison. 158

7.7 Linear advection-diffusion, solution dependence on *Nnode*, $\varepsilon = 0.001$.
High order and GWS performance comparison. 159
7.8 Burgers equation. Fourth order method solutions on uniform mesh,
$\varepsilon = 0.001$. 160
7.9 Linear advection-diffusion. Non-uniform mesh comparison, p=0.8. ... 161
7.10 Linear advection-diffusion. Locally uniform mesh comparison. 162
7.11 Burgers equation. Locally uniform mesh comparison. 163
7.12 Linear advection-diffusion, uniform mesh, solution dependence on
Nnode, $\varepsilon = 0.005$. 164
7.13 Non-linear problem, uniform mesh, solution dependence on
ε, *Nnode*=31×31. 165
7.14 Unsteady advection-diffusion. Analytical distributions. 166
7.15 Unsteady advection-diffusion. Uniform 26×26-node mesh, $\varepsilon = 0.005$.
Solution dependence on Courant number. 167
7.16 Unsteady convection. 31×31-node uniform mesh.
High order solution. 168

Figure **Page**

7.17 Converging-diverging nozzle flow. Steady-state.

Solution comparison, 101-node uniform mesh. 169

7.18 Converging-diverging nozzle flow. Steady-state.

Fourth/Second order comparison, 101-node uniform mesh, $\varepsilon = 0.1$. . 170

7.19 Converging-diverging nozzle flow. Steady-state.

Fourth/Second order comparison, 101-node uniform mesh,

$\varepsilon = 0.0004$. 171

7.20 Converging-diverging nozzle flow. Steady-state.

Fourth order method with spatial filtering,

101-node uniform mesh, $\varepsilon = 0.0004$, $\alpha = -0.49$. 172

7.21 Converging-diverging nozzle flow. Transient problem.

Fourth/Second order comparison,

$\varepsilon = 0.0008$, $\alpha = 0.4$. 173

7.22 Converging-diverging nozzle flow. Transient problem.

Accelerated second order method,

$\varepsilon = 0.000001$, $\alpha = -0.05$. 174

7.23 Driven cavity benchmark solutions. Re=1000,

33×33-node uniform mesh. 175

7.24 Driven cavity benchmark solutions. Re=3000, 33×33-node
locally-uniform mesh. X1: [33(0. 8R1.0 .02 16R1.0 .98 8R1.0 1)],
X2: [-33(0. 20R1.0 .98 12R1.0 1)]. 176

7.25 Driven cavity benchmark solutions.
Vorticity high order formulation. 33×33-node uniform mesh. 177

7.26 Driven cavity benchmark solutions.
Vorticity high order formulation. 33×33-node
locally-uniform mesh. X1: [33(0. 8R1.0 .02 16R1.0 .98 8R1.0 1)],
X2: [-33(0. 20R1.0 .98 12R1.0 1)]. 178

7.27 Driven cavity benchmark solutions.
Stream-function high order formulation. 33×33-node
locally-uniform mesh. X1: [33(0. 8R1.0 .02 16R1.0 .98 8R1.0 1)],
X2: [-33(0. 20R1.0 .98 12R1.0 1)]. 179

List of tables

Table **Page**

1. Undetermined coefficients method.

1D linear advection-diffusion, $\varepsilon = 0.1$ 181

2. Undetermined coefficients method.

2D linear advection-diffusion, $\varepsilon = 1$ 182

3. Perturbed PDE method.

1D linear advection-diffusion, $\varepsilon = 0.1$ 183

4. Perturbed PDE method.

1D Burgers equation, $\varepsilon = 0.1$ 184

5. Perturbed PDE method.

2D linear advection-diffusion. Fourth order convergence data. 185

6. Perturbed PDE method. 1D converging-diverging

nozzle flow. Velocity convergence data. 186

7. Perturbed PDE method. 1D converging-diverging

nozzle flow modified for the diffusion term introduction, $\varepsilon = 0.1$. 187

8. Driven cavity benchmark convergence study.

Stream-function in energy norm. 188

9. Driven cavity benchmark accuracy comparison. 189

Chapter 1
Introduction.

1.1. Finite differences approach.

High order methods can generate highly accurate results for problems with smooth data, hence solutions for which the physical domain is smoothly mapped onto the computational space. Invariably, this is accomplished by increasing the width of the computational stencil, which yields matrix equations of greater bandwidth. This increases the implementational cost, but by lowering the truncation error can reduce the number of nodes needed to obtain a given accuracy numerical solution.

Finite difference methods treat partial derivative entries of a given PDE separately. The value of each derivative at a generic computational node is approximated by a linear combination of function values at the adjacent nodes. Consequently, coefficients of this combination are derived by matching Taylor series coefficients. For example, in one dimension

$$\begin{aligned} \frac{\partial q(x)}{\partial x} &= a_1 Q_{j-1} + a_2 Q_j + a_3 Q_{j+1} \\ \frac{\partial^2 q(x)}{\partial x^2} &= a_4 Q_{j-1} + a_5 Q_j + a_6 Q_{j+1} \end{aligned} \tag{1.1}$$

and coefficients a_i can be shown to be

$$a_1 = -\frac{1}{2h}, \qquad a_2 = 0, \qquad a_3 = \frac{1}{2h},$$
$$a_4 = \frac{1}{h^2}, \qquad a_5 = -\frac{2}{h^2}, \qquad a_6 = \frac{1}{h^2} \tag{1.2}$$

Wider computational stencil therefore permits higher order accuracy by introducing more unknowns into the approximation expression, as in Thomas (1995)

$$a_1 Q_{j-2} + a_2 Q_{j-1} + a_3 Q_j + a_4 Q_{j+1} + a_5 Q_{j+2} = 0 \tag{1.3}$$

Generalization of this approach is provided by Pade or compact finite difference schemes (Kopal, 1961, Lomax, 1976)

Alternatively, a higher order approximation for select elliptic problem statements can be achieved using Hermitian type discretization methods (Collatz, 1960) without adding additional pivotal points. In this case, nodal values of high order derivatives are used to introduce more coefficients in the stencil expressions as

$$a_1 Q_{j-1} + a_2 Q_j + a_3 Q_{j+1} + a_4 Q''_{j-1} + a_5 Q''_j + a_6 Q''_{j+1} = 0 \tag{1.4}$$

Once stencil coefficients are determined by Taylor series analysis, solution matrix bandwidth expansion is contained by expressing high order derivatives via nodal function values. Unless this transition can be provided by the partial differential equation itself, solution matrix bandwidth must be expanded to accommodate the extra unknowns resulting from introducing nodal values of high order derivatives into

the stencil expression. Here, high order approximation again comes at a computational price of solving matrix equation of greater bandwidth. In particular, this is clearly the case when considering the advection-diffusion equation. It does not provide a required dependence between derivatives and corresponding function values, rendering Hermitian methods ineffective in reducing computational costs.

Approximation can be further optimized by introducing additional theoretical considerations, suitable for a particular physical problem. Optimized compact finite difference schemes (Tam and Webb, 1993, Kim and Lee, 1996, Visbal and Gaitonde, 1998) utilize Fourier analysis to achieve maximum resolution by minimizing dispersive (phase) errors in the differencing approximation. Resolution of abrupt boundary layers in convection dominated problems and shock-like discontinuities caused by local non-linearities can be enhanced by promoting the scheme's "monotonicity".

Thus the analysis of a normalized-variable diagram leads to the restrictions being placed on time-averaged normalized face values of the solution resulting in the ULTIMATE strategy (Leonard, 1991) for correcting the numerical solution, which can be applied for arbitrary high order schemes. Similarly, comparison of relevant divided differences to select the locally smoothest stencil, used on the reconstruction stage of the interpolation procedure described by Shu (1997) for ENO and WENO type schemes, yields highly accurate solutions.

1.2. Finite element approach.

Finite element methods proceed in a somewhat different manner. The cornerstone of the theoretical development is the "weak form" formulation (Baker, 1983) requiring the measure of the error in the approximate solution to vanish in an integrated sense. Introduction of the solution domain discretization further replaces the continuous solution approximation with its appropriate piecewise-continuous form, resulting in generation of the "weak statement" extremum, leading to a precise derivation of the computational stencil expression upon specification of suitable test and trial basis function sets. Higher order of approximation is achieved by general or local embedding of higher degree interpolants (p-refinement) (Baker, 1983, Oden, 1994). Method performance can be enhanced by optimizing test and trial basis function sets leading to various Petrov-Galerkin approximations (Brooks and Hughes, 1980, Chaffin and Baker, 1995).

Optimal $h-p$ finite element methods (Oden, 1994) use bilinear form symmetrization to derive problem specific test and trial functions. The existence of an accurate fine mesh solution to a given problem is assumed, and the corresponding optimal test and trial functions are designed to match this solution at the nodes of a significantly coarser grid. This leads to the "extrasuperconvergence" result which allows for an *a posteriori* error estimate on each of the finite elements of the solution domain discretization yielding an adaptive mesh refinement strategy.

Early Petrov-Galerkin methods (Heinrich et.al., 1977, Christie and Mitchell, 1978) introduced excessive amounts of diffusion into the numerical solution and SUPG methods (Brooks and Highes, 1980) were designed to counter this problem. Extension of the Lax-Wendroff method (Lax and Wendroff, 1960), which uses the governing equation to cancel error terms in time and space to a finite element formulation, lead to development of the Taylor-Galerkin method of Donea (1984), which was generalized as the Taylor weak statement (TWS) by Baker and Kim (1987). Detailed investigation of the TWS method performance for various multi-dimensional problems can be found in Chaffin and Baker (1995) and Chaffin (1997).

Matrix/static condensation techniques, unique for finite element formulations, provide another powerful tool for method optimization. The SGM method of Roy and Baker (1997, 1998), and Galerkin methods with bubble functions (Baiocchi and Brezzi, 1993), successfully use this approach to promote solution stability and monotonicity. Finite element methods specificly designed for shock-capturing were shown to significantly improve the method ability to resolve sharp solution discontinuities. Examples include discontinuous Galerkin methods (Hu and Shu, 1998) and a non-linear element-upstream weak statement (NEWS) algorithm (Iannelli, 1996, 1999), that achieve accurate monotone solutions for various conservation law system forms.

1.3. This dissertation.

Overall, upon discretization of the solution domain, virtually all high order methods result in matrix equations with larger bandwidth thus increasing the computational cost. Such wider stencils cannot be implemented at the boundaries, leading to a local loss of accuracy, especially in multi-dimensional cases, hence requiring additional theoretical consideration. Grid generation around complex geometries also becomes extremely complicated, since a smooth grid is dictated by the design of high order methods.

In this dissertation a method resolving this dilemma is developed and tested. The theory provides high order accurate solutions at no added computational cost, by retaining the solution matrix bandwidth of the second order methods. This is potentially of significance, in simplifying multi-dimensional grid generation procedures necessary for the implementation of high order methods. This development utilizes the ideas of "modified" partial differential equation analysis of Warming and Hyett (1974) (see also Shokin (1983)) to derive the problem-specific computational stencil coefficients appropriate for the desired order of accuracy. This allows for avoiding implementational difficulties encountered by Hermitian type methods.

The systematic construction of progressively higher order spatial approximations is achieved via a modified equation analysis, which allows one to clearly identify correction terms appropriate for a desired accuracy order. The resulting perturbed PDE

is shown to be consistent with the Taylor Weak Statement formulation. It confirms the expected high order of spatial accuracy in TWS constructions and provides a highly efficient dispersion error control mechanism whose application is based on the specifics of the solution domain discretization and physics of the problem.

Benchmark problem applications for non-linear Euler and Navier-Stokes equations document the performance of the disturbed equation methods developed in this research.

Chapter 2

Weak statement formulation.

2.1. Error minimization via a weak statment.

Consider the linear scalar multi-dimensional advection-diffusion equation with the corresponding Dirichlet and Neumann boundary conditions

$$L(q(\mathbf{x},t)) = \frac{\partial q(\mathbf{x},t)}{\partial t} + \mathbf{u}(\mathbf{x}) \cdot \nabla q(\mathbf{x},t)$$
$$- \varepsilon \nabla \cdot \nabla q(\mathbf{x},t) = 0 \qquad in \quad \Omega \in \mathbf{R}^n \times R^1 \tag{2.1}$$

$$q = q_b \qquad on \quad \partial\Omega_1 \tag{2.2}$$

$$\frac{\partial q}{\partial \mathbf{n}} = g(\mathbf{x}) \qquad \text{on} \quad \partial\Omega_2; \qquad \partial\Omega_1 \cup \partial\Omega_2 = \partial\Omega \tag{2.3}$$

where viscosity ε, velocity $\mathbf{u}(\mathbf{x})$, and boundary data $g(\mathbf{x})$, q_b are given.

Since in general the approximate solution $q^N(\mathbf{x},t)$ will not coincide with the exact solution $q(\mathbf{x},t)$, one can express the associated error in the numerical solution as

$$e^N(\mathbf{x},t) = q(\mathbf{x},t) - q^N(\mathbf{x},t) \tag{2.4}$$

One possible measure of the size of $e^N(\mathbf{x},t)$ can be obtained by substituting (2.4) into (2.1), which yields the following differential equation for the error

$$L(e^N(\mathbf{x},t)) = L(q(\mathbf{x},t)) - L(q^N(\mathbf{x},t)) = -L(q^N(\mathbf{x},t)) \tag{2.5}$$

The weak form construction requires the measure of the approximation error, which from the above equation is $L(q^N(\mathbf{x},t))$, to vanish in an overall integrated sense, resulting in

$$WF(L(q^N(\mathbf{x},t))) = \int_\Omega \omega(\mathbf{x}) L(q^N(\mathbf{x},t)) d\Omega = 0 \tag{2.6}$$

Here $\omega(\mathbf{x}) \in H^1(\Omega)$ is an arbitrary non-zero test function. Substituting (2.1) into (2.6) and applying the Green-Gauss theorem yields

$$WF(L(q^N(\mathbf{x},t))) =$$

$$\int_\Omega \left[\omega(\mathbf{x}) \left(\frac{\partial q^N(\mathbf{x},t)}{\partial t} + \mathbf{u}(\mathbf{x}) \cdot \nabla q^N(\mathbf{x},t) \right) + \varepsilon \nabla \omega(\mathbf{x}) \cdot \nabla q^N(\mathbf{x},t) \right] d\Omega \tag{2.7}$$

$$- \int_{\partial\Omega_2} \varepsilon \omega(\mathbf{x}) \frac{\partial q^N(\mathbf{x},t)}{\partial \mathbf{n}} d\partial\Omega_2 = 0 \qquad \forall \omega(\mathbf{x}) \in H^1(\Omega), \qquad \omega(\mathbf{x}) = 0 \in \partial\Omega_1$$

2.2. Solution domain discretization

The introduction of the solution domain discretization Ω^h replaces the continuous solution approximation $q^N(\mathbf{x},t)$ and test function $\omega(\mathbf{x})$ with their appropriate piecewise-continuous forms

$$q(\mathbf{x},t) \approx q^N(\mathbf{x},t) = \sum_{m=1}^{N} \psi_m(\mathbf{x})\, Q_m(t) = \{\Psi(\mathbf{x})\}\{Q(t)\} \tag{2.8}$$

$$\omega(\mathbf{x}) \approx \omega^I(\mathbf{x},t) = \sum_{p=1}^{I} \chi_p(\mathbf{x})\, W(t)_p = \{\chi(\mathbf{x})\}\{W(t)\} \tag{2.9}$$

Here $\chi(\mathbf{x}), \psi(\mathbf{x}) \in V_h \subset H^1(\Omega)$ are the test and trial functions with compact support; $\{Q(t)\}$ are the unknown nodal values of the approximate solution, and coefficients

$\{W(t)\}$ are still absolutely arbitrary. Since (2.7) holds for any interpolation $\omega^I(\mathbf{x})$, the extremum of (2.7) with respect to the arbitrariness, now only the coefficients $\{W(t)\}$, must vanish producing the weak statement (WS). Substituting (2.8) and (2.9) into (2.7) yields

$$WS^h(L(q^N(\mathbf{x},t))) =$$

$$\int_{\Omega^h} \{\chi(\mathbf{x})\} \left(\{\Psi(\mathbf{x})\}^T \frac{d\{Q(t)\}}{dt} + \mathbf{u}(\mathbf{x}) \cdot \nabla \{\Psi(\mathbf{x})\}^T \{Q(t)\} \right) d\Omega \tag{2.10}$$

$$+ \int_{\Omega^h} \varepsilon \nabla \{\chi(\mathbf{x})\} \cdot \nabla \{\Psi(\mathbf{x})\}^T \{Q(t)\} d\Omega - \int_{\partial\Omega_2} \varepsilon \{\chi(\mathbf{x})\} \{\Psi(\mathbf{x})\}^T \{G\} d\partial\Omega_2 = 0$$

where $\{G\}$ are the nodal values of the bounday data.

2.3. Element assembly procedure.

The form of (2.10) as a matrix sum of integrals, allows for subdivision of the domain Ω^h of the integrals in (2.10) into N finite elements Ω_e. The integral entries in (2.10) may then be computed individually on each element and summed or "assembled" over the domain. Because the compact interpolation (2.8) and (2.9) are at least piecewise-continuous, only elements adjacent to a node are assembled into the equation for that node, thus leading to the concept of the finite element stencil, finite element counterpart of the finite difference scheme.

The end point of the formulation involves evaluation of the integrals in (2.10),

which in turn requires specification of test and trial function sets. Denoting

$$[K]_e = \int_{\Omega_e} \varepsilon \nabla\{\chi(\mathbf{x})\} \cdot \nabla\{\Psi(\mathbf{x})\}^T d\Omega_{\mathrm{e}} \tag{2.11}$$

$$[M]_e = \int_{\Omega_e} \{\chi(\mathbf{x})\} \cdot \{\Psi(\mathbf{x})\}^T d\Omega_{\mathrm{e}} \tag{2.12}$$

$$[U]_e = \int_{\Omega_e} \{\chi(\mathbf{x})\} \cdot \mathbf{u}(\mathbf{x}) \nabla\{\Psi(\mathbf{x})\}^T d\Omega_{\mathrm{e}} \tag{2.13}$$

one obtains (10) in the matrix form

$$WS^h(L(q^N(\mathbf{x},t) = S_e \left([M]_e \frac{d\{Q(t)\}_e}{dt} + [U+K]_e \{Q(t)\}_e - \{b\}_e \right) = \{0\} \tag{2.14}$$

where S_e denotes the assembly operator and $\{b\}_e$ is the known boundary data. Performing the assembly results in an ordinary differential equation system

$$[M]\frac{d\{Q\}}{dt} + \{RQ\} = 0 \tag{2.15}$$

where $[M]$ is the assembly of the element matrices $[M]_e$ evaluated on each element Ω_e and $\{RQ\}$ is finite element evaluation of all other terms including all boundary conditions.

In advancing the solution over the time interval $\triangle t = t^{n+1} - t^n$, one can enjoy the theoretical advancements made by the theory of ordinary differential equations, while accounting for the additional details brought upon by a particular spatial discretization. For example, defining the variable-implicit family of single-step (Euler)

ODE algorithms via the introduction of the Taylor series expansion

$$\{Q(t_{n+1})\} = \{Q\}_{n+1} = \{Q_n\} + \triangle t \frac{d\{Q\}}{dt}|_{n+\theta} + \frac{\triangle t^2}{2}\frac{d^2\{Q\}}{dt^2}|_{n+\theta} + O(\triangle t^3) \tag{2.16}$$

For $\theta = 0$, (2.16) is explicit and first order accurate; for $\theta = 1$, (2.16) is backwards implicit and of the first order, while if $\theta = 0.5$, (2.16) produces the second order accurate trapezoidal rule. For arbitrary θ substituting (2.15) into (2.16) yields

$$\begin{aligned} \{Q\}_{n+1} = \{Q\}_n - \triangle t[M]^{-1}\{RQ\}_{n+\theta} \\ - \frac{\triangle t^2}{2}[M]^{-1}[M]^{-1}\frac{d\{RQ\}}{dt}|_{n+\theta} + O(\triangle t^{f(\theta)}) \end{aligned} \tag{2.17}$$

Neglecting $d\{RQ\}/dt$ at this point, multiplying through by $[M]$ and collecting the terms produces a potentially non-linear algebraic equation system

$$\{FQ\} = [M]\{Q_{n+1} - Q_n\} + \triangle t\{RQ\}_{n+\theta} = \{0\} \tag{2.18}$$

Equation (2.18) is the computable GWS^h finite element form, which in the linear case can be solved directly to provide a numerical "nodal" solution to the original equation. In the non-linear case one can proceed by employing a Newton iteration algorithm as

$$[JAC]^p\{\delta Q\}^{p+1} = -\{FQ\}^p \tag{2.19}$$

$$\{FQ\}^p = [M]\{Q^p_{n+1} - Q_n\} + \triangle t\{RQ\}^p_{n+\theta} \tag{2.20}$$

$$[JAC]^p = \frac{\partial\{FQ\}^p}{\partial\{Q\}^p} = [M] + \theta\triangle t\frac{\partial\{RQ\}^p}{\partial\{Q\}^p} \tag{2.21}$$

$$\{Q\}_{n+1}^{p+1} = \{Q\}_{n+1}^{p} + \{\delta Q\}^{p+1} = \{Q\}_n + \sum_{i=0}^{p} \{\delta Q\}^{i+1} \tag{2.22}$$

where $p = 0, 1, 2, ...$ is the integer index for iteration and $n + 1$ is the time station where the nodal solution is sought. The iteration converges when $max|\{\delta Q\}^{p+1}| < \varepsilon_0$ (Baker, 1997), where ε_0 is the convergence requirement. Since the Newton Jacobian $[JAC]$ is non-singular, this occurs when $max|\{FQ\}^{p}| < \delta$, where δ is an acceptable approximation to zero.

2.4. Accuracy and asymptotic convergence.

For any finite element approximate solution q^h, the semi-discrete approximation error is

$$e^h(x,t) = q(x,t) - q^h(x,t) \tag{2.23}$$

and since both q and q^h are continuous, the error e^h is also continuous. The error estimate employs resolution of $e^h(x,t)$ into spatial and temporal semi-discrete components. Using functional notation for clarity (Baker, 1997)

$$\sigma(j\triangle x, n\triangle t) = e^h(j\triangle x, t) + \tau(j\triangle x, n\triangle t) \tag{2.24}$$

where spatial semi-discretization error is

$$e^h(j\triangle x, t) = q(x,t) - q^h(j\triangle x, t) \tag{2.25}$$

while the temporal truncation error is

$$\tau(j\triangle x, n\triangle t) = q^h(j\triangle x, t) - Q_j(n\triangle t) \tag{2.26}$$

and the fully discrete error is given by

$$\sigma(j\triangle x, n\triangle t) = q(x,t) - Q_j(n\triangle t) \tag{2.27}$$

For any choice of norm the triangle identity results in

$$\|\sigma\| = \|e^h + \tau\| \leq \|e^h\| + \|\tau\| \tag{2.28}$$

It can be shown (Oden and Reddy, 1976) that for $u = 0$ in (2.1) and for the Euler explicit time integration $\theta = 0$ the finite element semi-discrete approximation error measured in H^1 Sobolev norm satisfies

$$\|e^h(t)\|_{H^1(\Omega)} \leq C_1 h^k \|q(t)\|_{H^{k+1}(\Omega)} + C_2 \triangle t \|q(t_0)\|_{H^1(\Omega)} \tag{2.29}$$

Here, h is the measure of the mesh size, $\triangle t$ is the time step, C_1 and C_2 are constants independent of h and k is the polynomial degree of the selected finite element basis.

In the case where $u > 0$ and $\varepsilon = 0$ this estimate is recast as

$$\begin{aligned} \|e^h(t)\|_{H^1(\Omega)} \leq C_1 h^{k+1} \|q(t)\|_{H^{k+1}(\Omega)} + C_2 \triangle t \|q(t_0)\|_{H^1(\Omega)} \\ + C_3 h \int_{t_0}^{t} \|q(\tau)\|_{H^{k+1}(\Omega)} d\tau \end{aligned} \tag{2.30}$$

This estimate states that the finite element semi-discrete error will proceed to zero in H^1 as the measure of the mesh independent of the polynomial degree k of the selected basis.

This theoretical prediction can be compared with an finite difference order of accuracy estimate by expressing it in the energy semi-norm as

$$\|e^h(t)\|_{E(\Omega)} \leq C_1^2 h^{2k}(\|s\|^2_{H^{k-1}(\Omega)} + \|p\|^2_{H^{k-1}(\partial\Omega)}) + C_2^2 \triangle t^{f(\theta)} \|q(t_0)\|^2_{H^1(\Omega)} \qquad (2.31)$$

stating that an $\{N_k\}$ finite element basis algorithm is $2k$ order accurate in space and first- or second-order accurate in time dependent on θ.

Chapter 3
Undetermined coefficients approach.

3.1 High order formulation. Theoretical approach

We first consider a one-dimensional steady-state case, for a constant velocity $\mathbf{u}(\mathbf{x})=u$ and Dirichlet boundary conditions. Equations (2.1),(2.2),(2.3) are rewritten as

$$L(q(x)) = \varepsilon \frac{d^2q(x)}{dx^2} - u\frac{dq(x)}{dx} = 0 \qquad in \quad x \in (0,1) \tag{3.1}$$

$$q(0) = 0 \qquad q(1) = 1 \quad on \quad \partial\Omega \tag{3.2}$$

Note, the original PDE (2.1) reduces to an ordinary differential equation in this case.

The exact solution in the case $u = 1$ is given by

$$q(x) = \frac{1 - e^{\frac{x}{\varepsilon}}}{1 - e^{\frac{1}{\varepsilon}}} \tag{3.3}$$

and its behavior for various values of ε is well known (see for example Fletcher, 1991, Roy and Baker, 1997). For sufficiently small values of ε, the solution remains constant over nearly all of the solution domain, while forming a "boundary" layer in a thin region of the domain, whose thickness is dictated by the boundary conditions and the value of viscosity parameter ε. In general, a very fine mesh is required to adequately resolve the "boundary" layer on a uniform mesh, while coarse (uniform) mesh solutions produce spurious $2\triangle x$ oscillations signaling the discretization's inability to

resolve this layer. Alternatively, a non-uniform mesh can be used for obtaining an acceptable solution. Unfortunately, the layer location must be known in this case.

For a given one-dimensional problem (3.1),(3.2), the discrete weak statement formulation becomes

$$WS^h = S_e([U + K]_e\{Q\}_e) = S_e([A(h, \varepsilon)]_e\{Q\}_e) = \{0\} \tag{3.4}$$

For an arbitrary two-node finite element trial and test function sets $\{\chi(x)\}, \{\Psi(x)\}$ one can evaluate the element matrix $[A]_e$ as a function of the element length h and given data. A fully discrete equivalent of (3.4), obtained by assembling the element matrix $[A]_e$ on two adjacent elements and presented in a finite element stencil form becomes

$$a_1 Q_{j-1} + a_2 Q_j + a_3 Q_{j+1} = 0 \tag{3.5}$$

Here $a_i, i = 1, 2, 3$ are the coefficients dependent on a specific choice of finite element trial and test functions, and Q_{j-1}, Q_j, Q_{j+1} are the unknown nodal values of the approximate solution.

Assuming a uniform mesh with $\triangle x = h$, which is sufficiently small, and writing a Taylor series expansion at node j yields

$$\begin{aligned}(a_1 + a_2 + a_3)Q_j + h(a_3 - a_1)Q_j^{'} + \frac{h^2}{2}(a_3 + a_1)Q_j^{''} + \sum_{n=3,2}^{\infty}(a_3 - a_1)\frac{h^n}{n!}Q_j^{(n)} \\ + \sum_{n=4,2}^{\infty}(a_3 + a_1)\frac{h^n}{n!}Q_j^{(n)} = 0\end{aligned} \tag{3.6}$$

Since in the end one desires to approximate equation (3.1), the general idea behind all types of consistency, convergence, order of the method and accuracy estimates is for a_i in (3.6) to satisfy the following equations

$$a_1 + a_2 + a_3 = 0$$

$$a_3 - a_1 = \frac{u}{h} \tag{3.7}$$

$$a_3 + a_1 = -\frac{2\varepsilon}{h^2}$$

As an example, solution of system (3.7) for the coefficients a_i gives Galerkin linear basis coefficients that are consistent with a centered three-node finite difference approximation, and clearly yields a second order method. If a higher order approximation is desired, finite difference method proceeds by increasing the width of the stencil to the form

$$a_1 Q_{j-2} + a_2 Q_{j-1} + a_3 Q_j + a_4 Q_{j+1} + a_5 Q_{j+2} = 0 \tag{3.8}$$

This introduces more coefficients and allows for solving more equations in (3.6), thus increasing the order of the method.

Alternatively, higher order approximation can be obtained by considering the following stencil (Collatz, 1960):

$$a_1 Q_{j-1} + a_2 Q_j + a_3 Q_{j+1} + a_4 Q''_{j-1} + a_5 Q''_j + a_6 Q''_{j+1} = 0 \tag{3.9}$$

Here, more coefficients are introduced not by expanding the stencil, but by utilizing nodal values of high order derivatives themselves. In order to reduce (3.9) to a computable form, partial differential equation itself must be used to express high order derivatives through nodal values of the numerical solution. Clearly, this is impossible in a case of advection-diffusion equation, since it does not provide a relationship between Q_i'' and nodal values of solution vector $\{Q\}$.

Finite element methods proceed by embedding higher degree basis functions, thus also introducing more coefficients, and allowing for solving more equations in (3.6). Thus, most approaches produce higher order methods at the price of solving a matrix statement with larger bandwidth. At the same time, FD wider stencils cannot be implemented at the boundaries, leading to a local loss of accuracy, especially in multi-dimensional cases, and requiring additional theoretical consideration as well as programming effort.

While Hermitian type methods provide a theoretical alternative to computational stencil expansion, their implementation for different equation types is problematic. We use the idea of "modified" partial differential equation analysis of Warming and Hyett (1974) to develop a method which resolves this dilemma, and provides high order accurate solutions at no added computational cost, by retaining the solution matrix bandwidth of the second order methods. Towards this end, equation (3.7) is

replaced with

$$a_1 + a_2 + a_3 = 0$$

$$a_3 - a_1 = \frac{u}{h} \tag{3.10}$$

$$a_3 + a_1 = -\frac{2\varepsilon}{h^2} + 2B$$

where B is a free parameter to be determined. Equation (3.6) therefore becomes

$$\begin{aligned} & uQ_j^{'} - \varepsilon Q_j^{''} + Bh^2 Q_j^{''} + \sum_{n=3,2}^{\infty} \frac{uh^{n-1}}{n!} Q_j^{(n)} \\ & - \sum_{n=4,2}^{\infty} \frac{2\varepsilon h^{n-2}}{n!} Q_j^{(n)} + \sum_{n=4,2}^{\infty} \frac{2Bh^n}{n!} Q_j^{(n)} = 0 \end{aligned} \tag{3.11}$$

Retaining only the terms of the order *1* and h^2 one obtains

$$uQ_j^{'} - \varepsilon Q_j^{''} + h^2 \left[BQ_j^{''} + \frac{u}{6} Q_j^{'''} - \frac{\varepsilon}{12} Q_j^{''''} \right] + H.O.T. = 0 \tag{3.12}$$

Equation (3.12) represents an "infinite" order partial differential equation satisfied by the nodal numerical solution $\{Q\}$ (Warming and Hyett, 1960, Thomas, 1995). We therefore can differentiate it repeatedly with respect to x , thus expressing higher order derivatives present in (3.12), and then attempt to select parameter B which would "zero out" the term at h^2 in the "modified" equation (3.12) leading to a higher order approximation of the equation to be solved.

Differentiating (3.12) with respect to x yields

$$Q_j^{''} = \frac{\varepsilon}{u} Q_j^{'''} - h^2 \left[\frac{B}{u} Q_j^{'''} + \frac{1}{6} Q_j^{''''} - \frac{\varepsilon}{12u} Q_j^{'''''} \right] + H.O.T. \tag{3.13}$$

and substituting back into (3.12) one obtains

$$uQ_j^{'} - \varepsilon Q_j^{''} + h^2 \left[\left(\frac{B\varepsilon}{u} + \frac{u}{6} \right) Q_j^{'''} - \frac{\varepsilon}{12} Q_j^{''''} \right] - h^4 \left[\frac{B^2}{u} Q_j^{'''} + \frac{B}{6} Q_j^{''''} - \frac{B\varepsilon}{12u} Q_j^{'''''} \right] + H.O.T. = 0 \tag{3.14}$$

Since the goal at this point is to eliminate the term at h^2 in (3.12), one can neglect the contribution produced by the h^4 term resulting from differentiating in (3.14) and further concentrate only on the h^2 term in (3.12). Again, differentiating (3.12) twice with respect to x, and remembering to neglect all terms of the order h^4 that result from differentiation, leads to

$$Q_j^{'''} = \frac{\varepsilon}{u} Q_j^{''''} + H.O.T. \tag{3.15}$$

and substituting into (3.14)

$$uQ_j^{'} - \varepsilon Q_j^{''} + h^2 \varepsilon Q_j^{''''} \left(\frac{B\varepsilon}{u^2} + \frac{1}{12} \right) + H.O.T. = 0 \tag{3.16}$$

It is interesting to note that neglecting higher order terms in (3.14) significantly simplifies the task at hand, since we need only be concerned with the form of the actual equation (3.1) itself in finding expressions for higher order derivatives, as illustrated in (3.15).

It is clear now that setting

$$B = -\frac{u^2}{12\varepsilon} \tag{3.17}$$

in (3.16) results in a fourth order accurate method. One can now solve (3.10) for the computational stencil coefficients

$$a_1 = -\frac{6h\varepsilon u + 12\varepsilon^2 + u^2h^2}{12h^2\varepsilon}, \qquad a_2 = \frac{12\varepsilon^2 + u^2h^2}{6h^2\varepsilon}$$
$$a_3 = \frac{6h\varepsilon u - 12\varepsilon^2 - u^2h^2}{12h^2\varepsilon} \tag{3.18}$$

Of course, unlike conventional high order methods of the form (3.8), the width of the computational stencil in this case remains unchanged inducing no additional computational cost.

To obtain a sixth order accurate method, consider the following system

$$a_1 + a_2 + a_3 = 0$$
$$a_3 - a_1 = \frac{u}{h} \tag{3.19}$$
$$a_3 + a_1 = -\frac{2\varepsilon}{h^2} + 2B + 2Ah^2$$

where A and B are free coefficients to be determined. (3.6) now becomes

$$uQ_j^{'} - \varepsilon Q_j^{''} + Bh^2Q_j^{''} + Ah^4Q_j^{''} + \sum_{n=3,2}^{\infty} \frac{uh^{n-1}}{n!}Q_j^{(n)} - \sum_{n=4,2}^{\infty} \frac{2\varepsilon h^{n-2}}{n!}Q_j^{(n)}$$
$$+ \sum_{n=4,2}^{\infty} \frac{2Bh^n}{n!}Q_j^{(n)} + + \sum_{n=4,2}^{\infty} \frac{2Ah^{n+2}}{n!}Q_j^{(n)} = 0 \tag{3.20}$$

and retaining only the terms of the order 1, h^2, h^4

$$uQ_j^{'} - \varepsilon Q_j^{''} + h^2\left[BQ_j^{''} + \frac{u}{6}Q_j^{'''} - \frac{\varepsilon}{12}Q_j^{''''}\right]$$
$$+ h^4\left[AQ_j^{''} + \frac{u}{120}Q_j^{(v)} - \frac{\varepsilon}{360}Q_j^{(vi)} + \frac{B}{12}Q_j^{(iv)}\right] + H.O.T. = 0 \tag{3.21}$$

Even though this expression appears to require greater effort when determining free parameters, it can be greatly simplified by the fact that the terms of the order h^2 in both (3.12) and (3.21) are exactly the same, as dictated by the selection of the order of the new free parameter A in (3.19). Therefore setting B as in (3.17) yields

$$uQ_j^{'} - \varepsilon Q_j^{''} + h^4 \left[AQ_j^{''} - \frac{u^2}{144\varepsilon} Q_j^{(iv)} + \frac{u}{120} Q_j^{(v)} - \frac{\varepsilon}{360} Q_j^{(vi)} \right] + H.O.T. = 0 \qquad (3.22)$$

Differentiating (3.21) repeatedly with respect to x and substituting into (3.22) yields

$$uQ_j^{'} - \varepsilon Q_j^{''} + h^4 \varepsilon Q_j^{(vi)} \left(\frac{A\varepsilon^3}{u^4} - \frac{1}{720} \right) + H.O.T. = 0 \qquad (3.23)$$

Setting

$$A = \frac{u^4}{720\varepsilon^3} \qquad (3.24)$$

results in a sixth order method. Solving (3.19) for the computational stencil coefficients one obtains

$$\begin{aligned} a_1 &= \frac{-360hu\varepsilon^3 - 720\varepsilon^4 - 60u^2h^2\varepsilon^2u^4h^4}{720h^2\varepsilon^3} \\ a_2 &= \frac{720\varepsilon^4 + 60u^2h^2\varepsilon^2 - u^4h^4}{360h^2\varepsilon^3} \\ a_3 &= \frac{360hu\varepsilon^3 - 720\varepsilon^4 - 60u^2h^2\varepsilon^2 + u^4h^4}{720h^2\varepsilon^3} \end{aligned} \qquad (3.25)$$

Again, bandwidth of the solution matrix remains unchanged as compared to that of any two-node finite element basis, while the order of the method increases. This procedure can be repeated as many times as desired.

3.2 One-dimensional unsteady case

The unsteady advection-diffusion equation (2.1) written for constant velocity $\mathbf{u}(\mathbf{x}) = u$ becomes:

$$\frac{\partial q(x,t)}{\partial t} + u\frac{\partial q(x,t)}{\partial x} - \varepsilon\frac{\partial^2 q(x,t)}{\partial x^2} = 0 \tag{3.26}$$

One known analytical solution to (3.26) is

$$q(x,t) = \frac{e^{\frac{x}{\varepsilon}}}{2}\left[1 - erf\left(\sqrt{\frac{1}{\varepsilon t}}\left(\frac{x+t}{2}\right)\right)\right] + \left[1 - erf\left(\sqrt{\frac{1}{\varepsilon t}}\left(\frac{x-t}{2}\right)\right)\right] \tag{3.27}$$

The discrete weak statement formulation written in matrix notation remains (2.14). For an arbitrary two-node finite element trial and test function set, evaluating the matrix entries in (2.14) and assembling on two adjacent elements leads to the following semi-discrete equivalent

$$a_1 Q_{t,j-1} + a_2 Q_{t,j} + a_3 Q_{t,j+1} + a_4 Q_{j-1} + a_5 Q_j + a_6 Q_{j+1} = 0 \tag{3.28}$$

Here again, the a_i are stencil coefficients dependent on a specific choice of finite element trial and test basis functions in (2.14), Q_t denotes the time derivative, and Q_{j-1}, Q_j, Q_{j+1} are the unknown nodal values of the numerical solution. The time integration algorithm remains completely arbitrary at this point, to be specified later.

Assuming the spatial discretization to be sufficient, and performing Taylor series

expansion of (3.28) at node Q_j yields

$$\begin{aligned}
&(a_1+a_2+a_3)Q_t + h(a_3-a_1)Q_{tx} + \frac{h^2}{2}(a_3+a_1)Q_{txx} \\
&+(a_3-a_1)\sum_{n=3,2}^{\infty}\frac{h^n}{n!}Q_t^{(n)} + +(a_3+a_1)\sum_{n=4,2}^{\infty}\frac{h^n}{n!}Q_t^{(n)} + (a_4+a_5+a_6)Q \\
&+h(a_6-a_4)Q_x + \frac{h^2}{2}(a_6+a_4)Q_{xx} + (a_6-a_4)\sum_{n=3,2}^{\infty}\frac{h^n}{n!}Q^{(n)} \\
&+(a_6+a_4)\sum_{n=4,2}^{\infty}\frac{h^n}{n!}Q^{(n)}
\end{aligned} \tag{3.29}$$

where Q replaces Q_j for clarity.

In order for (3.29) to approximate the original equation (3.26), the computational coefficients a_4, a_5, a_6 must satisfy

$$a_4 + a_5 + a_6 = 0$$

$$a_6 - a_4 = \frac{u}{h} \tag{3.30}$$

$$a_6 + a_4 = -\frac{2\varepsilon}{h^2}$$

The requirement on coefficients a_1, a_2, a_3 is less restrictive, since the only condition from (3.29) is

$$a_1 + a_2 + a_3 = 1 \tag{3.31}$$

The particular choice of the other two parameter combinations, generally results from the specific finite element trial and test basis functions, leading to a first or second order of spatial approximation.

In concert with the ideas developed for the steady-state case, we propose placing the following restrictions on the stencil coefficients

$$a_1 + a_2 + a_3 = 1$$

$$a_3 - a_1 = Ch$$

$$a_3 + a_1 = 2B \tag{3.32}$$

$$a_4 + a_5 + a_6 = 0$$

$$a_6 - a_4 = \frac{u}{h}$$

$$a_6 + a_4 = -\frac{2\varepsilon}{h^2} + 2A$$

Substituting into (3.29) and retaining the terms of the order 1 and h^2 results in

$$\begin{aligned} Q_t + uQ_x - \varepsilon Q_{xx} + h^2(CQ_{tx} + BQ_{txx} + AQ_{xx} \\ + \frac{u}{6}Q_{xxx} - \frac{\varepsilon}{12}Q_{xxxx}) + H.O.T. = 0 \end{aligned} \tag{3.33}$$

Following developments of the previous sections, differentiate modified equation (3.33) with respect to x, and neglecting terms of the order h^4 resulting from this differentiation, one obtains

$$Q_{xx} = \frac{\varepsilon}{u} Q_{xxx} - \frac{1}{u} Q_{xt} + H.O.T. \tag{3.34}$$

which upon substitution reduces (3.33) to

$$\begin{aligned} Q_t + uQ_x - \varepsilon Q_{xx} + h^2 (Q_{tx}(C - \frac{A}{u}) + BQ_{txx} \\ + Q_{xxx}(\frac{u}{6} + \frac{A\varepsilon}{u}) - \frac{\varepsilon}{12} Q_{xxxx}) + H.O.T. = 0 \end{aligned} \tag{3.35}$$

Differentiating (3.33) twice with respect to x yields

$$Q_{xxx} = \frac{\varepsilon}{u} Q_{xxxx} - \frac{1}{u} Q_{txx} + H.O.T. \tag{3.36}$$

and thus (3.33) is reduced to

$$\begin{aligned} Q_t + uQ_x - \varepsilon Q_{xx} + h^2 (Q_{tx}(C - \frac{A}{u}) + Q_{txx}(B - \frac{1}{6} - \frac{A\varepsilon}{u^2}) \\ + Q_{xxxx}(\frac{\varepsilon}{6} + \frac{A\varepsilon^2}{u^2} - \frac{\varepsilon}{12})) + H.O.T. = 0 \end{aligned} \tag{3.37}$$

and selecting

$$A = -\frac{u^2}{12\varepsilon}, \qquad B = \frac{1}{12}, \qquad C = -\frac{u}{12\varepsilon} \tag{3.38}$$

leads to a fourth order spatial discretization.

With the weight parameters at hand, one can substitute them back into (3.32) to

derive expressions for coefficients a_i in (3.28) as

$$a_1 = \frac{2\varepsilon + hu}{24\varepsilon}, \qquad a_2 = \frac{5}{6}, \qquad a_3 = \frac{2\varepsilon - hu}{24\varepsilon}$$

$$a_4 = -\frac{6hu\varepsilon + 12\varepsilon^2 + h^2u^2}{12h^2\varepsilon}, \qquad a_5 = \frac{12\varepsilon^2 + h^2u^2}{6h^2\varepsilon}, \tag{3.39}$$

$$a_6 = \frac{6hu\varepsilon - 12\varepsilon^2 - h^2u^2}{12h^2\varepsilon}$$

Comparing (3.38) to the condition (3.17), developed for the steady-state one-dimensional case, note that the weight coefficient for the spatial derivative group remains identical, with two additional parameters introduced in the unsteady case to handle extra terms resulting from the presence of the time derivative in the semi-discrete finite element computational stencil (3.28). In fact, the approximation of the spatial derivatives group is absolutely unchanged for the high order formulation extended to unsteady problems, since the coefficients responsible for spatial discretization are identical (compare (3.39) to (3.18)).

3.3 Two-dimensional steady-state case.

In two dimensions, the advection-diffusion equation (1) written for constant velocity $\mathbf{u}(\mathbf{x}) = u\mathbf{i} + v\mathbf{j}$ becomes

$$L(q(x,y)) = \varepsilon\frac{\partial^2 q(x,y)}{\partial x^2} + \varepsilon\frac{\partial^2 q(x,y)}{\partial y^2} - u\frac{\partial q(x,y)}{\partial x} - v\frac{\partial q(x,y)}{\partial y} = 0 \tag{3.40}$$

$$in \quad x, y \in (0,1) \times (0,1)$$

The exact solution of (3.40) on a unit square, comparable to the 1-D problem is

$$q(x,y) = \left(\frac{e^{\frac{ux}{\varepsilon}} - 1}{e^{\frac{1}{\varepsilon}} - 1}\right)\left(\frac{e^{\frac{vy}{\varepsilon}} - 1}{e^{\frac{1}{\varepsilon}} - 1}\right) \tag{3.41}$$

To simplify theoretical assessments for establishing methods convergence rate, consider the boundary conditions

$$q(1,1) = 1 \qquad q(0,y) = q(x,0) = 0 \tag{3.42}$$

$$q(x,1) = \frac{e^{\frac{ux}{\varepsilon}} - 1}{e^{\frac{1}{\varepsilon}} - 1} \qquad q(1,y) = \frac{e^{\frac{vy}{\varepsilon}} - 1}{e^{\frac{1}{\varepsilon}} - 1} \tag{3.43}$$

that correspond with the exact solution (3.41).

The discrete weak statement formulation remains (3.4), where the element matrix $[A]_e$ is now a function of the element dimensions $\triangle x, \triangle y$, and given data. In accordance with the Galerkin bilinear basis two-dimensional weak statement formulation written on rectangular four-node element, a fully discrete equivalent of (3.4), obtained by assembling the element matrix on four adjacent elements sharing a common corner node, leads to the general nine-node computational stencil

$$\begin{aligned} &c_1 Q_{i-1,j-1} + c_2 Q_{i,j-1} + c_3 Q_{i+1,j-1} + c_4 Q_{i-1,j} + c_5 Q_{i,j} \\ &+ c_6 Q_{i+1,j} + c_7 Q_{i-1,j+1} + c_8 Q_{i,j+1} + c_9 Q_{i+1,j+1} = 0 \end{aligned} \tag{3.44}$$

Assuming a uniform square mesh with $\triangle x = \triangle y = h$, which is sufficiently small, and writing a Taylor series expansion at node *i,j* yields

$$Q \sum_{n=1}^{9} c_n + hQ_x(-c_1 + c_3 - c_4 + c_6 - c_7 + c_9)$$

$$+hQ_y(-c_1 - c_2 - c_3 + c_7 + c_8 + c_9)$$

$$+\frac{h^2}{2}Q_{xx}(c_1 + c_3 + c_4 + c_6 + c_7 + c_9)$$

$$+\frac{h^2}{2}Q_{yy}(c_1 + c_2 + c_3 + c_7 + c_8 + c_9)$$

$$+h^2Q_{xy}(c_1 - c_3 - c_7 + c_9) + (c_9 - c_1)\sum_{n=3,2}^{\infty}\frac{h^n}{n!}\left(\frac{\partial}{\partial x} + \frac{\partial}{\partial y}\right)^{(n)}Q$$

$$+(c_9 + c_1)\sum_{n=4,2}^{\infty}\frac{h^n}{n!}\left(\frac{\partial}{\partial x} + \frac{\partial}{\partial y}\right)^{(n)}Q \tag{3.45}$$

$$+(c_3 - c_7)\sum_{n=3,2}^{\infty}\frac{h^n}{n!}\left(\frac{\partial}{\partial x} - \frac{\partial}{\partial y}\right)^{(n)}Q$$

$$+(c_3 + c_7)\sum_{n=4,2}^{\infty}\frac{h^n}{n!}\left(\frac{\partial}{\partial x} - \frac{\partial}{\partial y}\right)^{(n)}Q + (c_8 - c_2)\sum_{n=3,2}^{\infty}\frac{h^n}{n!}\left(\frac{\partial}{\partial y}\right)^{(n)}Q$$

$$+(c_8 + c_2)\sum_{n=4,2}^{\infty}\frac{h^n}{n!}\left(\frac{\partial}{\partial y}\right)^{(n)}Q + (c_6 - c_4)\sum_{n=3,2}^{\infty}\frac{h^n}{n!}\left(\frac{\partial}{\partial x}\right)^{(n)}Q$$

$$+(c_6 + c_4)\sum_{n=4,2}^{\infty}\frac{h^n}{n!}\left(\frac{\partial}{\partial x}\right)^{(n)}Q = 0$$

where Q replaces $Q_{i,j}$ for clarity. As with (3.6), (3.45) represents an infinite order partial differential equation satisfied by the numerical solution.

In order for (3.45) to approximate the original equation (3.40), the minimum requirement on the coefficient set c_i is

$$\sum_{n=1}^{9} c_n = 0$$

$$-c_1 + c_3 - c_4 + c_6 - c_7 + c_9 = \frac{u}{h}$$

$$-c_1 - c_2 - c_3 + c_7 + c_8 + c_9 = \frac{v}{h}$$

$$c_1 + c_3 + c_4 + c_6 + c_7 + c_9 = -\frac{2\varepsilon}{h^2} \tag{3.46}$$

$$c_1 + c_2 + c_3 + c_7 + c_8 + c_9 = -\frac{2\varepsilon}{h^2}$$

$$c_1 - c_3 - c_7 + c_9 = 0$$

Indeed, the Galerkin bilinear basis discretization satisfies the required conditions (3.46), which allows for uniquely defining six of the nine coefficients, while the rest is determined by the particulars of a given discretization approach. To develop a higher order approximation, one proceeds in the manner of the one-dimensional case and replaces (3.46) with

$$\sum_{n=1}^{9} c_n = 0$$

$$-c_1 + c_3 - c_4 + c_6 - c_7 + c_9 = \frac{u}{h}$$

$$-c_1 - c_2 - c_3 + c_7 + c_8 + c_9 = \frac{v}{h}$$

$$c_1 + c_3 + c_4 + c_6 + c_7 + c_9 = -\frac{2\varepsilon}{h^2} + 2G$$

$$c_1 + c_2 + c_3 + c_7 + c_8 + c_9 = -\frac{2\varepsilon}{h^2} + 2A \tag{3.47}$$

$$c_1 - c_3 - c_7 + c_9 = B$$

$$c_9 - c_1 = \frac{D}{h}$$

$$c_9 + c_1 = \frac{H}{h^2}$$

$$c_3 - c_7 = \frac{F}{h}$$

This results in nine equations for nine unknown coefficients c_i and A, B, D, F, G, H are free parameters to be determined. The procedure is thus identical to the one-dimensional case. Namely, one includes several free parameters into the stencil coefficient expressions, by conveniently loading them into the h^2 order term of the truncation error expansion (3.45), while retaining the symmetric structure of the modified partial differential equation.

Substituting (3.47) into (3.45) and keeping the terms of the order 1 and h^2 yields

the following expression

$$uQ_x + vQ_y - \varepsilon Q_{xx} - \varepsilon Q_{yy} + h^2(BQ_{xy} + GQ_{xx} + AQ_{yy}$$

$$+\frac{vQ_{yyy}}{6} - \frac{\varepsilon Q_{yyyy}}{12} + \frac{uQ_{xxx}}{6} - \frac{\varepsilon Q_{xxxx}}{12} + \frac{DQ_{xxy}}{2} + \frac{DQ_{xyy}}{2} \tag{3.48}$$

$$+\frac{HQ_{xxyy}}{2} - \frac{FQ_{xxy}}{2} + \frac{FQ_{xyy}}{2}) + H.O.T. = 0$$

Differentiating (3.48) twice with respect to x, y and neglecting the terms of the order h^4 resulting from differentiating and subsequent substitution into (3.48) yields

$$uQ_{xxx} + vQ_{xxy} = \varepsilon Q_{xxxx} + \varepsilon Q_{xxyy} + H.O.T. \tag{3.49}$$

$$uQ_{xyy} + vQ_{yyy} = \varepsilon Q_{xxyy} + \varepsilon Q_{yyyy} + H.O.T. \tag{3.50}$$

or

$$\varepsilon(Q_{xxxx} + 2Q_{xxyy} + Q_{yyyy}) = uQ_{xxx} + uQ_{xyy} + vQ_{xxy} + vQ_{yyy} + H.O.T. \tag{3.51}$$

Setting

$$H = -\frac{\varepsilon}{3} \tag{3.52}$$

and substituting back into (3.48) yields

$$uQ_x + vQ_y - \varepsilon Q_{xx} - \varepsilon Q_{yy} + h^2(BQ_{xy} + GQ_{xx} + AQ_{yy}$$

$$+\frac{vQ_{yyy}}{12} + \frac{uQ_{xxx}}{12} + Q_{xxy}(\frac{D}{2} - \frac{F}{2} - \frac{v}{12}) \tag{3.53}$$

$$+Q_{xxy}(\frac{D}{2} + \frac{F}{2} - \frac{u}{12})) + H.O.T. = 0$$

Differentiating (3.48) by x, y and neglecting the terms of the order h^4 leads to

$$Q_{xxx} + Q_{xyy} = \frac{u}{\varepsilon} Q_{xx} + \frac{v}{\varepsilon} Q_{xy} + H.O.T. \tag{3.54}$$

$$Q_{xxy} + Q_{yyy} = \frac{u}{\varepsilon} Q_{xy} + \frac{v}{\varepsilon} Q_{yy} + H.O.T. \tag{3.55}$$

Therefore, setting

$$F = \frac{u - v}{6} \qquad D = \frac{u + v}{6} \tag{3.56}$$

reduces (3.48) to

$$\begin{gathered} uQ_x + vQ_y - \varepsilon Q_{xx} - \varepsilon Q_{yy} \\ +h^2(Q_{xy}(B + \frac{uv}{6\varepsilon}) + Q_{xx}(G + \frac{u^2}{12\varepsilon}) + Q_{yy}(A + \frac{v^2}{12\varepsilon})) + H.O.T. = 0 \end{gathered} \tag{3.57}$$

Setting

$$B = -\frac{uv}{6\varepsilon} \qquad G = -\frac{u^2}{12\varepsilon} \qquad A = -\frac{v^2}{12\varepsilon} \tag{3.58}$$

thus completes development of the fourth order method, with the computational stencil coefficients determined by substituting (3.52,3.56,3.58) into (3.47) and solving for c_i. For u =1 this leads to:

$$c_1 = -\frac{h + \varepsilon}{6h^2}, \qquad c_2 = -\frac{2h\varepsilon + 4\varepsilon^2 + h^2}{6h^2\varepsilon}, \qquad c_3 = \frac{-2\varepsilon^2 + h^2}{12h^2\varepsilon}$$

$$c_4 = -\frac{2h\varepsilon + 4\varepsilon^2 + h^2}{6h^2\varepsilon}, \qquad c_5 = \frac{20\varepsilon^2 + 3h^2}{6h^2\varepsilon}, \qquad c_6 = \frac{-4\varepsilon^2 + 2h\varepsilon - h^2}{6h^2\varepsilon} \tag{3.59}$$

$$c_7 = \frac{-2\varepsilon^2 + h^2}{12h^2\varepsilon}, \qquad c_8 = \frac{-4\varepsilon^2 + 2h\varepsilon - h^2}{6h^2\varepsilon}, \qquad c_9 = \frac{h - \varepsilon}{6h^2}$$

It is important to note that the coefficients of the first and second derivatives in (3.58) (compare to (3.17)) are exactly the same as in one-dimensional case. Extension of the method to two-dimensional problems thus requires addition of the weight parameters on the cross-derivatives, which are of course absent in one-dimensional considerations. This approach therefore provides desirable consistency and continuity when applied to multi-dimensional problems. And indeed, the size of the computational stencil remains equal to that of the second order Galerkin bilinear basis approximation, hence requiring no additional effort as normally associated with numerical implementation of higher order methods.

Extension to a sixth order accurate method is straightforward and follows the procedure as outlined. (3.47) is replaced by

$$\sum_{n=1}^{9} c_n = 0$$

$$-c_1 + c_3 - c_4 + c_6 - c_7 + c_9 = \frac{u}{h}$$

$$-c_1 - c_2 - c_3 + c_7 + c_8 + c_9 = \frac{v}{h}$$

$$c_1 + c_3 + c_4 + c_6 + c_7 + c_9 = -\frac{2\varepsilon}{h^2} + 2G + 2G_1 h^2$$

$$c_1 + c_2 + c_3 + c_7 + c_8 + c_9 = -\frac{2\varepsilon}{h^2} + 2A + 2A_1 h^2 \tag{3.60}$$

$$c_1 - c_3 - c_7 + c_9 = B + B_1 h^2$$

$$c_9 - c_1 = \frac{D}{h} + D_1 h$$

$$c_9 + c_1 = \frac{H}{h^2} + H_1$$

$$c_3 - c_7 = \frac{F}{h} + F_1 h$$

where $A, A_1, B, B_1, D, D_1, F, F_1, G, G_1, H, H_1$ are now free coefficients to be determined. Substituting (3.60) into (3.45) and retaining the terms of the order $1, h^2, h^4$ leads to

$$uQ_x + vQ_y - \varepsilon Q_{xx} - \varepsilon Q_{yy} + h^2(BQ_{xy} + GQ_{xx} + AQ_{yy}$$

$$+\frac{vQ_{yyy}}{6} - \frac{\varepsilon Q_{yyyy}}{12} + \frac{uQ_{xxx}}{6} - \frac{\varepsilon Q_{xxxx}}{12} + \frac{DQ_{xxy}}{2} + \frac{DQ_{xyy}}{2}$$

$$+\frac{HQ_{xxyy}}{2} - \frac{FQ_{xxy}}{2} + \frac{FQ_{xyy}}{2}) + h^4(G_1 Q_{xx} + A_1 Q_{yy} + B_1 Q_{xy}$$

$$+\frac{D}{120}\left(\frac{\partial}{\partial x} + \frac{\partial}{\partial y}\right)^5 Q + \frac{D_1}{6}\left(\frac{\partial}{\partial x} + \frac{\partial}{\partial y}\right)^3 Q$$

$$+\frac{H}{720}\left(\frac{\partial}{\partial x} + \frac{\partial}{\partial y}\right)^6 Q + \frac{H_1}{24}\left(\frac{\partial}{\partial x} + \frac{\partial}{\partial y}\right)^4 Q + \frac{F}{120}\left(\frac{\partial}{\partial x} - \frac{\partial}{\partial y}\right)^5 Q \qquad (3.61)$$

$$+\frac{F_1}{6}\left(\frac{\partial}{\partial x} - \frac{\partial}{\partial y}\right)^3 Q + \frac{H}{720}\left(\frac{\partial}{\partial x} - \frac{\partial}{\partial y}\right)^6 Q + \frac{H_1 - B}{24}\left(\frac{\partial}{\partial x} - \frac{\partial}{\partial y}\right)^4 Q$$

$$+\frac{F-D+v}{120}\left(\frac{\partial}{\partial y}\right)^5 Q+\frac{F_1-D_1}{6}\left(\frac{\partial}{\partial y}\right)^3 Q-\frac{H+\varepsilon}{360}\left(\frac{\partial}{\partial y}\right)^6 Q$$

$$+\frac{B-2H_1+2A}{24}\left(\frac{\partial}{\partial y}\right)^4 Q+\frac{u-F-D}{120}\left(\frac{\partial}{\partial x}\right)^5 Q-\frac{F_1+D_1}{6}\left(\frac{\partial}{\partial x}\right)^3 Q$$

$$-\frac{H+\varepsilon}{360}\left(\frac{\partial}{\partial x}\right)^6 Q++\frac{B-2H_1+2C}{24}\left(\frac{\partial}{\partial x}\right)^4 Q)+H.O.T.=0$$

Comparing (3.61) to (3.48) and noticing that h^2 order term is zero for parameters A, B, D, G and H satisfying (3.52,3.56,3.58), yields (3.61) in the form

$$uQ_x+vQ_y-\varepsilon Q_{xx}-\varepsilon Q_{yy}-\frac{h^4}{720\varepsilon}(-720B_1\varepsilon Q_{xy}-20\varepsilon uQ_{xxxyy}$$

$$-10\varepsilon uQ_{xyyyy}-10\varepsilon vQ_{xxxxy}-20\varepsilon vQ_{xxyyy}-360D_1\varepsilon Q_{xxy}-360D_1\varepsilon Q_{xyy}$$

$$-360H_1\varepsilon Q_{xxyy}+360F_1\varepsilon Q_{xxy}-360F_1\varepsilon Q_{xyy}+20uvQ_{xxxy} \tag{3.62}$$

$$-30uvQ_{xxyy}+20uvQ_{xyyy}-720G_1\varepsilon Q_{xx}-720A_1\varepsilon Q_{yy}-6v\varepsilon Q_{yyyyy}$$

$$+2\varepsilon^2 Q_{yyyyyy}+2\varepsilon^2 Q_{xxxxxx}+10\varepsilon^2 Q_{xxxxyy}+10\varepsilon^2 Q_{xxyyyy}$$

$$-6u\varepsilon Q_{xxxxx}+5v^2 Q_{yyyy}+5u^2 Q_{xxxx})+H.O.T.=0$$

Performing differentiation in a manner similar to (3.48-3.58) leads to the following restrictions on the introduced coefficients

$$A_1=\frac{v^4}{720\varepsilon^3},\qquad B_1=\frac{v^3u+u^3v}{720\varepsilon^3}=\frac{uv\parallel\mathbf{u}\parallel}{720\varepsilon^3},\qquad G_1=\frac{u^4}{720\varepsilon^3}$$

$$D_1 = -\frac{1}{720\varepsilon^2}(-9u^2v + v^3 - 9uv^2 + u^3) \tag{3.63}$$

$$F_1 = -\frac{1}{720\varepsilon^2}(-9uv^2 + u^3 + 9u^2v - v^3)$$

$$H_1 = -\frac{uv}{12} - \frac{v^2}{40} - \frac{u^2}{40}$$

Again, similarity between one and two-dimensional coefficients is evident, compare (3.63) to (3.24).

The computational stencil coefficient set c_i is evaluated by substituting (3.63) into (3.60) and solving the resulting algebraic system to obtain, for u =1

$$c_1 = -\frac{h^3 + 15\varepsilon^4 + 6h^2\varepsilon^3 + 15h\varepsilon^3}{90h^2\varepsilon^3}$$

$$c_2 = \frac{4h^3 - 120h\varepsilon^3 - 240\varepsilon^4 + 48h^2\varepsilon^3 - 60h^2\varepsilon^2 + h^4}{360h^2\varepsilon^3}$$

$$c_3 = -\frac{120\varepsilon^4 + 48h^2\varepsilon^3 - 60h^2\varepsilon^2 + h^4}{720h^2\varepsilon^3}$$

$$c_4 = \frac{4h^3 - 120h\varepsilon^3 - 240\varepsilon^4 + 48h^2\varepsilon^3 - 60h^2\varepsilon^2 + h^4}{360h^2\varepsilon^3}$$

$$c_5 = \frac{400\varepsilon^4 - 32h^2\varepsilon^3 + 60h^2\varepsilon^2 - h^4}{120h^2\varepsilon^3} \tag{3.64}$$

$$c_6 = \frac{-240\varepsilon^4 + 48h^2\varepsilon^3 - 4h^3 + 120h\varepsilon^3 - 60h^2\varepsilon^2 + h^4}{360h^2\varepsilon^3}$$

$$c_7 = -\frac{120\varepsilon^4 + 48h^2\varepsilon^3 - 60h^2\varepsilon^2 + h^4}{720h^2\varepsilon^3}$$

$$c_8 = \frac{-240\varepsilon^4 + 48h^2\varepsilon^3 - 4h^3 + 120h\varepsilon^3 - 60h^2\varepsilon^2 + h^4}{360h^2\varepsilon^3}$$

$$c_9 = \frac{h^3 - 15\varepsilon^4 - 6h^2\varepsilon^3 + 15h\varepsilon^3}{90h^2\varepsilon 3}$$

Chapter 4
Perturbed PDE approach.

4.1 One-dimensional steady-state formulation.

Model equation (2.1) rewritten for the non-linear one-dimensional steady-state case becomes

$$f(q,x)\frac{dq(x)}{dx} - \varepsilon(x)\frac{d^2q}{dx^2} = 0 \tag{4.1}$$

Assuming the existence of appropriate boundary conditions, the discrete weak statement formulation remains

$$WS^h = S_e([U+D]_e\{Q\}_e) = S_e([A(h,\varepsilon)]_e\{Q\}_e) = \{0\} \tag{4.2}$$

A fully discrete equivalent of (4.2), obtained by assembling the element matrix $[A]_e$ on two adjacent elements and presented in a pseudo-finite element stencil form now is

$$f_j\left(a_1Q_{j-1} + a_2Q_j + a_3Q_{j+1}\right) - \varepsilon_j\left(a_4Q_{j-1} + a_5Q_j + a_6Q_{j+1}\right) = 0 \tag{4.3}$$

or

$$(f_ja_1 - \varepsilon_ja_4)Q_{j-1} + (f_ja_2 - \varepsilon_ja_5)Q_j + (f_ja_3 - \varepsilon_ja_6)Q_{j+1} = 0 \tag{4.4}$$

Here a_i are the coefficients dependent on a specific choice of finite element trial and test functions, and Q_{j-1}, Q_j, Q_{j+1} are the unknown nodal values of the approximate

solution. A genuine finite element formulation would require interpolation of functions $f(q,x)$ and $\varepsilon(x)$, thus adding complexity to the stencil expression in (4.4). Without the loss in generality, in the present analysis interpolated functional expressions are replaced with their respective nodal values f_j and ε_j.

Assuming a locally uniform mesh with $\triangle x = h$, which is sufficiently small, and writing a Taylor series expansion at node j yields

$$f_j[(a_1+a_2+a_3)Q + (a_3-a_1)hQ_x + (a_3+a_1)\frac{h^2}{2}Q_{xx}$$

$$+(a_3-a_1)\sum_{n=3,2}^{\infty}\frac{h^n}{n!}Q^{(n)} + (a_3+a_1)\sum_{n=4,2}^{\infty}\frac{h^n}{n!}Q^{(n)}] - \varepsilon_j[(a_4+a_5+a_6)Q \qquad (4.5)$$

$$+(a_6-a_4)hQ_x + (a_6+a_4)\frac{h^2}{2}Q_{xx} + (a_6-a_4)\sum_{n=3,2}^{\infty}\frac{h^n}{n!}Q^{(n)}$$

$$+(a_6+a_4)\sum_{n=4,2}^{\infty}\frac{h^n}{n!}Q^{(n)}] = 0$$

where Q replaces Q_j for clarity.

Naturally, for (4.5) to approximate equation (4.1), a_i in (4.5) must satisfy the following conditions.

$$a_1 + a_2 + a_3 = 0$$

$$a_3 - a_1 = \frac{1}{h} \qquad (4.6)$$

$$a_3 + a_1 = 0$$

and

$$a_4 + a_5 + a_6 = 0$$

$$a_6 - a_4 = 0 \tag{4.7}$$

$$a_3 + a_1 = \frac{2}{h^2}$$

Coefficient groups $[a_1, a_2, a_3]$ and $[a_4, a_5, a_6]$ are responsible for the second order discretization of the first and second order derivatives respectively and conditions (4.6-4.7) must be satisfied independently of a particular approximation technique selected to arrive at (4.2). Therefore,

$$\begin{aligned} \frac{\partial q(x)}{\partial x} &= a_1 Q_{j-1} + a_2 Q_j + a_3 Q_{j+1} \\ \frac{\partial^2 q(x)}{\partial x^2} &= a_4 Q_{j-1} + a_5 Q_j + a_6 Q_{j+1} \end{aligned} \tag{4.8}$$

and coefficients a_i are uniquely determined by solving (4.6) and (4.7)

$$\begin{aligned} a_1 &= -\frac{1}{2h}, \qquad a_2 = 0, \qquad a_3 = \frac{1}{2h} \\ a_4 &= \frac{1}{h^2}, \qquad a_5 = -\frac{2}{h^2}, \qquad a_6 = \frac{1}{h^2} \end{aligned} \tag{4.9}$$

Another approach providing higher order accurate solutions at no added computational cost by retaining the solution matrix bandwidth of the second order methods is developed below.

For the computational stencil coefficients a_i satisfying (4.9), (4.5) becomes

$$f_j Q_x - \varepsilon_j Q_{xx} + h^2 \left(\frac{f_j Q_{xxx}}{6} - \frac{\varepsilon_j Q_{xxxx}}{12} \right) + H.O.T. = 0 \tag{4.10}$$

Rewriting (4.10) yields the convenient form

$$\varepsilon Q_{xx} = f Q_x - h^2 \left(\frac{f Q_{xxx}}{6} - \frac{\varepsilon Q_{xxxx}}{12} \right) + H.O.T. \tag{4.11}$$

where f and ε replace f_j and ε_j respectively.

Equation (4.11) represents an "infinite" order partial differential equation satisfied by the nodal numerical solution $\{Q\}$ (Warming and Hyett, 1974, Thomas, 1995). We therefore can differentiate it repeatedly with respect to x , thus expressing higher order derivatives present in (4.11), and then attempt to derive a second order PDE (ODE in the one-dimensional steady-state case), whose second order approximation would result in a higher order approximation of the equation to be solved. Obtaining this "perturbed" second order ODE is a key to this theoretical development, since any second order ODE can be discretized on three nodes in the one-dimensional case.

Assuming for simplicity the viscosity parameter ε is constant, differentiating (4.11) repeatedly with respect to x and neglecting high order terms leads to

$$\varepsilon Q_{xxx} = f_x Q_x + f Q_{xx} - H.O.T. \tag{4.12}$$

$$\varepsilon Q_{xxxx} = f_{xx} Q_x + f_x Q_{xx} + f_x Q_{xx} + f Q_{xxx} - H.O.T. \tag{4.13}$$

Substituting (4.12) and (4.13) into (4.10) and neglecting the terms of the order greater than 4, one obtains

$$fQ_x - \varepsilon Q_{xx} + h^2 Q_x \left(\frac{f f_x}{12\varepsilon} - \frac{f_{xx}}{12} \right) + h^2 Q_{xx} \left(\frac{f^2}{12\varepsilon} - \frac{f_x}{6} \right) = 0 \tag{4.14}$$

which represents the equation satisfied by the nodal approximate solution Q including the second order error terms resulting from the selected second order approximation. Clearly, reversing the sign of the error terms in (4.14) yields the sought "perturbed" PDE as

$$fq_x - \varepsilon q_{xx} - h^2 q_x \left(\frac{f f_x}{12\varepsilon} - \frac{f_{xx}}{12} \right) - h^2 q_{xx} \left(\frac{f^2}{12\varepsilon} - \frac{f_x}{6} \right) = 0 \tag{4.15}$$

In applications, viscosity parameter ε is usually small, making it possible to neglect the terms of the order unity as compared to those of the order $1/\varepsilon$, thus reducing (4.15) to

$$fq_x - \varepsilon q_{xx} - h^2 q_x \frac{f f_x}{12\varepsilon} - h^2 q_{xx} \frac{f^2}{12\varepsilon} = 0 \tag{4.16}$$

and combining the terms, the perturbed ODE becomes

$$f \frac{\partial q}{\partial x} - \varepsilon \frac{\partial^2 q}{\partial x^2} - \frac{h^2}{12\varepsilon} f \frac{\partial}{\partial x} \left(f \frac{\partial q}{\partial x} \right) = 0 \tag{4.17}$$

Numerical solution of (4.17) obtained using the approximation consistent with (4.8-4.9) will provide the fourth order accurate solution to the original equation (4.1) by eliminating the second order error terms in (4.5).

Similar arguments yield the following sixth order perturbed ODE, illustrated for the linear $f(q,x) = u(x)$ case as

$$uq_x - \varepsilon q_{xx} - h^2 q_x \left(\frac{uu_x}{12\varepsilon} - \frac{u_{xx}}{12}\right) - h^2 q_{xx}\left(\frac{u^2}{12\varepsilon} - \frac{u_x}{6}\right)$$

$$- h^4 q_x \left(\frac{uu_x^2}{180\varepsilon^2} - \frac{u^3 u_x}{720\varepsilon^3} - \frac{u_{xxxx}}{360} - \frac{u^2 u_{xx}}{720\varepsilon^2} + \frac{uu_{xxx}}{180\varepsilon}\right) \tag{4.18}$$

$$- h^4 q_{xx}\left(\frac{u_{xx}^2}{180\varepsilon} - \frac{u_{xxx}}{90} + \frac{uu_{xx}}{72\varepsilon} + \frac{u^2 u_x}{360\varepsilon^2} - \frac{u^4}{720\varepsilon^3}\right) = 0$$

It is important to note that the terms of the order h^2 remain unchanged from the fourth order ODE, thus allowing for recursive development of higher order approximations.

First consider a one-dimensional steady-state case for a constant velocity $\mathbf{u}(\mathbf{x})=u\mathbf{i}$ and Dirichlet boundary conditions. Equation (4.1) is

$$L(q(x)) = \varepsilon \frac{d^2 q(x)}{dx^2} - u\frac{dq(x)}{dx} = 0 \qquad in \quad x \in (0,1) \tag{4.19}$$

$$q(0) = 0 \qquad q(1) = 1 \quad on \quad \partial\Omega \tag{4.20}$$

The exact solution in the case $u = 1$ is given by (3.3)

Via the developed methodology, perturbed ODE (4.17) becomes

$$uQ_x - \varepsilon Q_{xx} - Q_{xx}\frac{h^2 u^2}{12\varepsilon} = 0 \tag{4.21}$$

indicating that only the second order derivative perturbation term is required to achieve a higher order numerical solution in this case.

The computational stencil expression (4.4) reduces to

$$\begin{aligned} u(a_1Q_{j-1} + a_2Q_j + a_3Q_{j+1}) - \varepsilon(a_4Q_{j-1} + a_5Q_j + a_6Q_{j+1}) \\ - \frac{h^2u^2}{12\varepsilon}(a_4Q_{j-1} + a_5Q_j + a_6Q_{j+1}) = 0 \end{aligned} \tag{4.22}$$

where coefficients a_i are given in (4.9). Collecting the terms, the three node stencil is

$$\begin{aligned} \left[-\frac{6h\varepsilon u + 12\varepsilon^2 + h^2u^2}{12\varepsilon h^2}\right] Q_{j-1} + \left[\frac{12\varepsilon^2 + h^2u^2}{6\varepsilon h^2}\right] Q_j \\ + \left[\frac{6h\varepsilon u - 12\varepsilon^2 - h^2u^2}{12\varepsilon h^2}\right] Q_{j+1} = 0 \end{aligned} \tag{4.23}$$

With this linear case development now complete one can proceed to the non-linear Burger's equation case, $f(x,q) = q(x)$. The one-dimensional steady-state equation is now of the form

$$L(q(x)) = \varepsilon\frac{d^2q(x)}{dx^2} - q\frac{dq(x)}{dx} = 0 \qquad in \quad x \in (0,1) \tag{4.24}$$

with boundary conditions

$$q(0) = 1 \qquad q(1) = -1 \tag{4.25}$$

The perturbed ODE form remains (4.17), with $f(x,q)$ replaced by $q(x)$. Replacing continuous derivative expressions with their discrete counterparts via (4.8), the

computational stencil (4.4) takes the homogeneous form

$$F_j = Q_j\left(-\frac{Q_{j-1}}{2h}+\frac{Q_{j+1}}{2h}\right)-\varepsilon\left(\frac{Q_{j-1}}{h^2}-\frac{2Q_j}{h^2}+\frac{Q_{j+1}}{h^2}\right)$$

$$-\frac{h^2Q_j}{12\varepsilon}\left(-\frac{Q_{j-1}}{2h}+\frac{Q_{j+1}}{2h}\right)^2-\frac{h^2Q_j^2}{12\varepsilon}\left(\frac{Q_{j-1}}{h^2}-\frac{2Q_j}{h^2}+\frac{Q_{j+1}}{h^2}\right) \tag{4.26}$$

$$+\frac{h^2}{4}\left(-\frac{Q_{j-1}}{2h}+\frac{Q_{j+1}}{2h}\right)\left(\frac{Q_{j-1}}{h^2}-\frac{2Q_j}{h^2}+\frac{Q_{j+1}}{h^2}\right)=0$$

The non-linear system of equations (4.26) is solved using Newton's iterative procedure, with tridiagonal Jacobian matrix $\{JAC_{j-1}, JAC_j, JAC_{j+1}\}$ evaluated from (4.26) as

$$JAC_{j-1}=\frac{\partial F_j}{\partial Q_{j-1}}= \tag{4.27}$$

$$-\frac{1}{24\varepsilon h^2}(6Q_j\varepsilon h+24\varepsilon^2+h^2Q_jQ_{j-1}-h^2Q_jQ_{j+1}+2Q_j^2h^2+6Q_{j-1}\varepsilon h)$$

$$JAC_j=\frac{\partial F_j}{\partial Q_j}=$$

$$-\frac{1}{48\varepsilon h^2}(12Q_{j-1}\varepsilon h-12Q_{j+1}\varepsilon h-96\varepsilon^2+h^2Q_{j-1}^2-2h^2Q_{j-1}Q_{j+1} \tag{4.28}$$

$$+h^2Q_{j+1}^2+8h^2Q_jQ_{j-1}-24Q_j^2h^2+8h^2Q_jQ_{j+1})$$

$$JAC_{j+1}=\frac{\partial F_j}{\partial Q_{j+1}}= \tag{4.29}$$

$$\frac{1}{24\varepsilon h^2}(6Q_j\varepsilon h-24\varepsilon^2+h^2Q_jQ_{j-1}-h^2Q_jQ_{j+1}-2Q_j^2h^2+6Q_{j+1}\varepsilon h)$$

For comparison, presented below are Jacobian matrix elements corresponding to the second order approximation.

$$JAC_{j-1} = -\frac{Q_j}{2h} - \frac{\varepsilon}{h^2}, \quad JAC_j = -\frac{Q_{j-1}}{2h} + \frac{2\varepsilon}{h^2} + \frac{Q_j}{2h}, \quad JAC_{j+1} = \frac{Q_j}{2h} - \frac{\varepsilon}{h^2} \quad (4.30)$$

4.2 Non-uniform mesh implementation.

Theoretical analysis of the above sections assumes a uniform discretization of the solution domain, thus imposing a rather serious restriction on the method's practical applicability. Herein, the theory is naturally extended to incorporate a non-uniform mesh implementation. This development is shown to be greatly simplified by the method's design goal of solution matrix bandwidth containment. Combination of a uniform and non-uniform discretizations leads to the idea of a *locally* uniform mesh which is more suited for "real life" problems.

One-dimensional model equation remains (4.1). Non-uniform discretization of the solution domain is introduced via geometric progression expression of the form (Baker, 1991)

$$h_{i+1} = ph_i \quad (4.31)$$

where h_i is the discretization size, and p is geometric progression ratio. Discretization nodal coordinates are determined via (Baker, 1991)

$$XR_{i+1} = XR_i + \frac{Lp^{i-1}}{\sum_{j=1}^{M} p^{j-1}} \quad (4.32)$$

Here XR is the nodal coordinate, L is one-dimensional length measure of the solution domain, and $M+1$ is the total number of discretization nodes.

Taylor series expansion at node j yields

$$f_j[(a_1+a_2+a_3)Q+(a_3p-a_1)hQ_x+(a_3p^2+a_1)\frac{h^2}{2}Q_{xx}$$

$$+\sum_{n=3,2}^{\infty}\frac{h^n}{n!}Q^{(n)}(a_3p^n-a_1)+\sum_{n=4,2}^{\infty}\frac{h^n}{n!}Q^{(n)}(a_3p^n+a_1)] \tag{4.33}$$

$$-\varepsilon_j[(a_4+a_5+a_6)Q+(a_6p-a_4)hQ_x+(a_6p^2+a_4)\frac{h^2}{2}Q_{xx}+$$

$$\sum_{n=3,2}^{\infty}\frac{h^n}{n!}Q^{(n)}(a_6p^n-a_4)+\sum_{n=4,2}^{\infty}\frac{h^n}{n!}Q^{(n)}(a_6p^n+a_4)]=0$$

The approximation requirement (4.6-4.7) is modified to

$$a_1+a_2+a_3=0$$

$$a_3p-a_1=\frac{1}{h} \tag{4.34}$$

$$a_3p^2+a_1=0$$

and

$$a_4+a_5+a_6=0$$

$$a_6p-a_4=0 \tag{4.35}$$

$$a_3 p^2 + a_1 = \frac{2}{h^2}$$

uniquely providing coefficients a_i as

$$\begin{aligned} a_1 &= -\frac{p}{h(1+p)}, \quad a_2 = \frac{p-1}{ph}, \quad a_3 = \frac{1}{ph(1+p)}, \\ a_4 &= \frac{2}{h^2(1+p)}, \quad a_5 = -\frac{2}{ph^2}, \quad a_6 = \frac{2}{ph^2(1+p)} \end{aligned} \tag{4.36}$$

Substituting into (4.33) and neglecting terms of the order greater than h^2 yields Taylor series expansion in the form

$$fQ_x - \varepsilon Q_{xx} - \frac{\varepsilon(p-1)h}{3} Q_{xxx} + \frac{fph^2}{6} Q_{xxx} + H.O.T. = 0 \tag{4.37}$$

The lowest order truncation error term appearance indicates that any three-node discretization on a non-uniform mesh can at best achieve a first order approximation of the original equation. In fact, unlike the uniform mesh case, where discretization symmetry allows for elimination of the odd order error terms (4.5), here one must deal with both odd and even order error terms in order to design higher order approximations. The only potential drawback resulting from switching to more realistic non-uniform approximations is therefore the increased amount of algebraic calculation required in evaluating correction terms providing higher order approximation. This is a minor inconvenience, easily offset by taking advantage of any symbolic manipulation language (e.g. MAPLE or MATLAB). Otherwise, all theoretical developments of the previous sections remain valid on a non-uniform discretization.

Hence, proceeding along the basic steps outlined before one rewrites (4.37) in the form

$$Q_{xx} = \frac{1}{\varepsilon} f Q_x + H.O.T. \tag{4.38}$$

and differentiating (4.38) by x obtains the following expression

$$Q_{xxx} = \frac{1}{\varepsilon}(f_x Q_x + f Q_{xx}) \tag{4.39}$$

Substituting (4.39) into (4.37) yields the second order perturbed ODE in the form

$$f q_x - \varepsilon q_{xx} + \frac{(p-1)h}{3}(f_x q_x + f q_{xx}) = 0 \tag{4.40}$$

which nicely reduces to the original ODE (4.1) on a uniform mesh ($p = 1$).

The design of the third order method follows the well known route. Rewriting (4.40) as

$$\left(f + \frac{(p-1)h}{3} f_x\right) q_x + \left(\frac{(p-1)h}{3} f - \varepsilon\right) q_{xx} = 0 \tag{4.41}$$

one can now substitute partial derivative expressions from (4.8) and writing Taylor series at node j obtain

$$\begin{aligned} &\left(f + \frac{(p-1)h}{3} f_x\right) \left[Q_x + \sum_{n=3,2}^{\infty} \frac{h^n}{n!}(a_3 p^n - a_1) + \sum_{n=4,2}^{\infty} \frac{h^n}{n!}(a_3 p^n + a_1)\right] \\ &- \left(\frac{(p-1)h}{3} f - \varepsilon\right) \left[Q_{xx} + \sum_{n=3,2}^{\infty} \frac{h^n}{n!}(a_6 p^n - a_4) + \sum_{n=4,2}^{\infty} \frac{h^n}{n!}(a_6 p^n + a_4)\right] = 0 \end{aligned} \tag{4.42}$$

Remembering (4.36) and retaining the terms of the order h^2 results in

$$\left(f + \frac{(p-1)h}{3} f_x\right) \left[Q_x + \frac{ph^2}{6}\right]$$

$$- \left(\frac{(p-1)h}{3} f - \varepsilon\right) [Q_{xx} + \frac{(p-1)h}{3} Q_{xxx} \tag{4.43}$$

$$+ \frac{(p^2-p+1)h^2}{12} Q_{xxxx}] + H.O.T. = 0$$

Provided one began this process with the second order perturbed ODE (4.40) as the starting point, one can immediately simplify the task at hand by noting that first order terms in (4.43) must cancel out reducing it to

$$\begin{aligned} fQ_x - \varepsilon Q_{xx} + \frac{p^2h^2}{6} Q_{xxx} - \frac{\varepsilon(p^2-p+1)h^2}{12} Q_{xxxx} \\ + \frac{(p-1)^2h^2 f}{9} Q_{xxx} + H.O.T. = 0 \end{aligned} \tag{4.44}$$

Lowering the order of this equation from fourth to second, which is a focal point in developing third order approximation, now requires evaluating fourth and third order derivatives via their lower order counterparts. Differentiating (4.38) twice with respect to x

$$Q_{xxxx} = \frac{1}{\varepsilon}(f_{xx}Q_x + 2f_xQ_{xx} + fQ_{xxx}) \tag{4.45}$$

and recalling (4.39) one obtains (4.44) in the form

$$\begin{aligned} fQ_x - \varepsilon Q_{xx} - \frac{(p^2-p+1)h^2}{12} f_{xx}Q_x - \frac{(p^2-p+1)h^2}{6} f_xQ_{xx} \\ + \frac{(p^2+p+1)h^2 f}{36\varepsilon}(f_xQ_x + fQ_{xx}) + H.O.T. = 0 \end{aligned} \tag{4.46}$$

Collecting the terms and reversing signs on the correction error entries yields the third order perturbed PDE as

$$\begin{aligned} fq_x - \varepsilon q_{xx} + q_x \left[\frac{(p^2-p+1)h^2 f_{xx}}{12} - \frac{(p^2+p+1)h^2 f f_x}{36\varepsilon} \right] \\ + q_{xx} \left[\frac{(p^2-p+1)h^2 f_x}{6} - \frac{(p^2+p+1)h^2 f^2}{36\varepsilon} \right] = 0 \end{aligned} \tag{4.47}$$

Similarly to the uniform mesh development, order of magnitude and vector analyses reduce (4.47) to

$$f\frac{\partial q}{\partial x} - \varepsilon \frac{\partial^2 q}{\partial x^2} - \frac{h^2(p^2+p+1)}{36\varepsilon} f \frac{\partial}{\partial x}\left(f \frac{\partial q}{\partial x} \right) = 0 \tag{4.48}$$

Again for $p = 1$ this equation reduces to the fourth order approximation (4.17), ensuring compatibility of the approach developed herein.

4.3 Two-dimensional steady-state case.

Model equation (1) rewritten for the two-dimensional steady-state case, written for velocity $\mathbf{u}(\mathbf{x},\mathbf{y}) = u(x,y)\mathbf{i} + v(x,y)\mathbf{j}$ becomes

$$\begin{aligned} L(q(x,y)) = \varepsilon \frac{\partial^2 q(x,y)}{\partial x^2} + \varepsilon \frac{\partial^2 q(x,y)}{\partial y^2} - u(x,y)\frac{\partial q(x,y)}{\partial x} - v(x,y)\frac{\partial q(x,y)}{\partial y} = 0 \\ in \quad x, y \in (0,1) \times (0,1) \end{aligned} \tag{4.49}$$

In accordance with the Galerkin bilinear basis two-dimensional weak statement formulation written on rectangular four-node element, a fully discrete equivalent of (4.49), obtained by assembling the element matrix on four adjacent elements sharing

a common corner node, leads to the general nine-node computational stencil

$$c_1Q_{i-1,j-1} + c_2Q_{i,j-1} + c_3Q_{i+1,j-1} + c_4Q_{i-1,j} + c_5Q_{i,j} \\ + c_6Q_{i+1,j} + c_7Q_{i-1,j+1} + c_8Q_{i,j+1} + c_9Q_{i+1,j+1} = 0 \tag{4.50}$$

As shown in the previous chapter, assuming a uniform square mesh with $\triangle x = \triangle y = h$, which is sufficiently small, and writing a Taylor series expansion at node *i,j* yields (3.45) with Q replacing $Q_{i,j}$ for clarity. Equation (3.45) represents an infinite order partial differential equation satisfied by the numerical solution. Retaining only the terms of the order lower or equal than four yields

$$(c_1 + c_2 + c_3 + c_4 + c_5 + c_6 + c_7 + c_8 + c_9)Q$$

$$+hQ_x(-c_1 + c_3 - c_4 + c_6 - c_7 + c_9)$$

$$+hQ_y(-c1 - c_2 - c_3 + c_7 + c_8 + c_9)$$

$$+\frac{h^2}{2}Q_{xx}(c_1 + c_3 + c_4 + c_6 + c_7 + c_9)$$

$$+\frac{h^2}{2}Q_{yy}(c_1 + c_2 + c_3 + c_7 + c_8 + c_9)$$

$$+h^2Q_{xy}(c_1 - c_3 - c_7 + c_9) + +\frac{h^3}{6}Q_{xxx}(c_9 - c_1 + c_3 - c_7 + c_6 - c_4) \tag{4.51}$$

$$+\frac{h^3}{6}Q_{yyy}(c_9 - c_1 - c_3 + c_7 + c_8 - c_2) + \frac{h^3}{2}Q_{xxy}(c_9 - c_1 - c_3 + c_7)$$

$$+\frac{h^3}{2}Q_{xyy}(c_9 - c_1 + c_3 - c_7) + \frac{h^4}{24}Q_{xxxx}(c_9 + c_1 + c_3 + c_7 + c_6 + c_4)$$

$$+\frac{h^4}{24}Q_{yyyy}(c_9 + c_1 + c_3 + c_7 + c_8 + c_2) + \frac{h^4}{6}Q_{xxxy}(c_9 + c_1 - c_3 - c_7)$$

$$+\frac{h^4}{6}Q_{xyyy}(c_9 + c_1 - c_3 - c_7) + \frac{h^4}{4}Q_{xxyy}(c_9 + c_1 + c_3 + c_7) + H.O.T. = 0$$

As shown in Chapter 3, the necessary symmetrization of the selected discretization is achieved via

$$\sum_{n=1}^{9} c_n = 0$$

$$-c_1 + c_3 - c_4 + c_6 - c_7 + c_9 = \frac{u}{h}$$

$$-c_1 - c_2 - c_3 + c_7 + c_8 + c_9 = \frac{v}{h}$$

$$c_1 + c_3 + c_4 + c_6 + c_7 + c_9 = -\frac{2\varepsilon}{h^2}$$

$$c_1 + c_2 + c_3 + c_7 + c_8 + c_9 = -\frac{2\varepsilon}{h^2} \tag{4.52}$$

$$c_1 - c_3 - c_7 + c_9 = 0$$

$$c_9 - c_1 = \frac{u + v}{6h}$$

$$c_9 + c_1 = \frac{-\varepsilon}{3h^2}$$

$$c_3 - c_7 = \frac{u - v}{6h}$$

which reduces (4.51) to

$$\begin{aligned} uQ_x + vQ_y - \varepsilon Q_{xx} - \varepsilon Q_{yy} + h^2(\frac{vQ_{yyy}}{6} + \frac{uQ_{xxx}}{6} + \frac{vQ_{xxy}}{6} + \frac{uQ_{xyy}}{6}) \\ - h^2\varepsilon(\frac{Q_{xxxx}}{12} + \frac{Q_{yyyy}}{12} + \frac{Q_{xxyy}}{6}) + H.O.T. = 0 \end{aligned} \tag{4.53}$$

In concert with the theoretical developments of the previous chapters one can now differentiate (4.53) twice with respect to x and y and neglecting higher order terms obtain

$$u_{xx}Q_x + 2u_xQ_{xx} + uQ_{xxx} + v_{xx}Q_y + 2v_xQ_{xy} + vQ_{xxy} = \varepsilon Q_{xxxx} + \varepsilon Q_{xxyy} \tag{4.54}$$

$$u_{yy}Q_x + 2u_yQ_{xy} + uQ_{xyy} + v_{yy}Q_y + 2v_yQ_{yy} + vQ_{yyy} = \varepsilon Q_{xxyy} + \varepsilon Q_{yyyy} \tag{4.55}$$

Similarly, differentiating (4.53) with respect to x and y produces

$$u_xQ_x + uQ_{xx} + v_xQ_y + vQ_{xy} = \varepsilon Q_{xxx} + \varepsilon Q_{xyy} \tag{4.56}$$

$$u_yQ_x + uQ_{xy} + v_yQ_y + vQ_{yy} = \varepsilon Q_{xxy} + \varepsilon Q_{yyy} \tag{4.57}$$

Substituting expressions (4.54-4.57) into (4.53) leads to

$$\begin{aligned} uQ_x + vQ_y - \varepsilon Q_{xx} - \varepsilon Q_{yy} + h^2\left(\frac{vu_yQ_x}{12\varepsilon} + \frac{vuQ_{xy}}{6\varepsilon} + \frac{vv_yQ_y}{12\varepsilon} + \frac{v^2Q_{yy}}{12\varepsilon}\right) \\ + h^2\left(\frac{uu_xQ_x}{12\varepsilon} + \frac{u^2Q_{xx}}{12\varepsilon} + \frac{uv_xQ_y}{12\varepsilon} - \frac{u_{xx}Q_x}{12} - \frac{u_xQ_{xx}}{6}\right) \\ + h^2\left(-\frac{v_{xx}Q_y}{12} - \frac{v_xQ_{xy}}{6} - \frac{u_{yy}Q_x}{12} - \frac{u_yQ_{xy}}{6} - \frac{v_{yy}Q_y}{12} - \frac{v_yQ_{yy}}{6}\right) = 0 \end{aligned} \tag{4.58}$$

which after reversing the sign on the correction error terms yields the modified fourth order perturbed PDE in the form

$$uQ_x + vQ_y - \varepsilon Q_{xx} - \varepsilon Q_{yy} - h^2 \left(\frac{vu_y Q_x}{12\varepsilon} + \frac{vuQ_{xy}}{6\varepsilon} + \frac{vv_y Q_y}{12\varepsilon} + \frac{v^2 Q_{yy}}{12\varepsilon} \right)$$

$$- h^2 \left(\frac{uu_x Q_x}{12\varepsilon} + \frac{u^2 Q_{xx}}{12\varepsilon} + \frac{uv_x Q_y}{12\varepsilon} - \frac{u_{xx} Q_x}{12} - \frac{u_x Q_{xx}}{6} \right) \tag{4.59}$$

$$- h^2 \left(-\frac{v_{xx} Q_y}{12} - \frac{v_x Q_{xy}}{6} - \frac{u_{yy} Q_x}{12} - \frac{u_y Q_{xy}}{6} - \frac{v_{yy} Q_y}{12} - \frac{v_y Q_{yy}}{6} \right) = 0$$

Again, note that for most applications the $1/\varepsilon$ terms dominate the solution behavior. Hence, neglecting high order correction terms of the order of 1, the remaining terms can be combined for perturbed PDE (4.59) to be conveniently recast in continuum vector-form

$$\mathbf{u} \cdot \nabla q - \varepsilon \nabla \cdot \nabla q - \frac{h^2}{12\varepsilon} \mathbf{u} \cdot \nabla (\mathbf{u} \cdot \nabla q) = 0 \tag{4.60}$$

As before, its discretization (consistent with (4.52)) will yield a fourth order method due to the developed cancellation of the correction error terms. The partial derivatives of the order h^2 present in (4.59) can be discretized via any conventional FD/FV/FE method, since the error terms in their respective approximate expressions on a uniform mesh will be of the order h^4. The following are used in this development

$$Q_x = -\frac{1}{2h} Q_{i-1,j} + \frac{1}{2h} Q_{i+1,j} \tag{4.61}$$

$$Q_y = -\frac{1}{2h} Q_{i,j-1} + \frac{1}{2h} Q_{i,j+1} \tag{4.62}$$

$$Q_{xy} = \frac{1}{4h^2}Q_{i-1,j-1} - \frac{1}{4h^2}Q_{i+1,j-1} - \frac{1}{4h^2}Q_{i-1,j+1} + \frac{1}{4h^2}Q_{i+1,j+1} \tag{4.63}$$

$$Q_{xx} = \frac{1}{h^2}Q_{i-1,j} - \frac{2}{h^2}Q_{i,j} + \frac{1}{h^2}Q_{i+1,j} \tag{4.64}$$

$$Q_{yy} = \frac{1}{h^2}Q_{i,j-1} - \frac{2}{h^2}Q_{i,j} + \frac{1}{h^2}Q_{i,j+1} \tag{4.65}$$

Indeed, all approximations satisfy the matrix bandwidth restriction requirement and some maybe easily recognized as their one-dimensional counterparts. While the approximation selection in (4.61-4.65) does not compromise the fourth order accuracy of the method, the algorithm performance can be further optimized by customizing these discrete expressions.

4.4 2D steady-state verification problems

The first problem under consideration is a linear advection-diffusion equation with constant coefficients $u = v = const$. The modified PDE (4.60) reduces to

$$uQ_x + vQ_y - \varepsilon Q_{xx} - \varepsilon Q_{yy} - h^2\left(\frac{vuQ_{xy}}{6\varepsilon} + \frac{v^2Q_{yy}}{12\varepsilon} + \frac{u^2Q_{xx}}{12\varepsilon}\right) = 0 \tag{4.66}$$

and using discrete approximations in (4.52), (4.61-4.65) one obtains the coefficients in the nine-node stencil in the form

$$c_1 = -\frac{2\varepsilon hu + 2\varepsilon hv + 4\varepsilon^2 + uvh^2}{24h^2\varepsilon}, \qquad c_2 = -\frac{8\varepsilon^2 + 4\varepsilon hv + v^2h^2}{12h^2\varepsilon}$$

$$c_3 = \frac{2\varepsilon hu - 2\varepsilon hv - 4\varepsilon^2 + uvh^2}{24h^2\varepsilon}, \qquad c_4 = -\frac{8\varepsilon^2 + 4\varepsilon hu + u^2h^2}{12h^2\varepsilon}$$

$$c_5 = \frac{20\varepsilon^2 + v^2h^2 + u^2h^2}{6h^2\varepsilon}, \qquad c_6 = -\frac{8\varepsilon^2 - 4\varepsilon hu + u^2h^2}{12h^2\varepsilon} \tag{4.67}$$

$$c_7 = -\frac{2\varepsilon hu - 2\varepsilon hv + 4\varepsilon^2 - uvh^2}{24h^2\varepsilon}, \qquad c_8 = -\frac{8\varepsilon^2 - 4\varepsilon hv + v^2h^2}{12h^2\varepsilon}$$

$$c_9 = \frac{2\varepsilon hu + 2\varepsilon hv - 4\varepsilon^2 - uvh^2}{24h^2\varepsilon}$$

It is important to note that the stencil coefficients in (4.67) are not the same as those obtained for the same equation using the undetermined coefficients method of the previous section. This proves that these two theoretical approaches for implementing high order methods are indeed different and their respective future development can proceed in distinct directions.

Selecting $u(x,y) = v(x,y) = \frac{1}{\sqrt{2}}q(x,y)$ in (4.49) provides the non-linear verification case in the form

$$\frac{1}{\sqrt{2}}q\frac{\partial q}{\partial x} + \frac{1}{\sqrt{2}}q\frac{\partial q}{\partial y} - \varepsilon\frac{\partial^2 q}{\partial x^2} - \varepsilon\frac{\partial^2 q}{\partial y^2} = 0 \tag{4.68}$$

The modified PDE (4.60) in this case becomes

$$\frac{1}{\sqrt{2}}q\frac{\partial q}{\partial x} + \frac{1}{\sqrt{2}}q\frac{\partial q}{\partial y} - \varepsilon\frac{\partial^2 q}{\partial x^2} - \varepsilon\frac{\partial^2 q}{\partial y^2} - h^2\left(\frac{1}{12\varepsilon}q\frac{\partial q}{\partial x}\frac{\partial q}{\partial y} + \frac{1}{12\varepsilon}q^2\frac{\partial^2 q}{\partial x\partial y}\right)$$

$$-h^2\frac{1}{24\varepsilon}q\left(\frac{\partial q}{\partial y}\right)^2 + \frac{1}{24\varepsilon}q\left(\frac{\partial q}{\partial x}\right)^2 + \frac{1}{24\varepsilon}q^2\frac{\partial^2 q}{\partial y^2} \tag{4.69}$$

$$+\frac{1}{24\varepsilon}q^2\frac{\partial^2 q}{\partial x^2} - \frac{1}{4\sqrt{2}}\frac{\partial q}{\partial x}\frac{\partial^2 q}{\partial x^2} - \frac{1}{4\sqrt{2}}\frac{\partial q}{\partial y}\frac{\partial^2 q}{\partial y^2})$$

$$-h^2\left(-\frac{1}{12\sqrt{2}}\frac{\partial^2 q}{\partial x^2}\frac{\partial q}{\partial y}-\frac{1}{12\sqrt{2}}\frac{\partial^2 q}{\partial y^2}\frac{\partial q}{\partial x}-\frac{1}{6\sqrt{2}}\frac{\partial q}{\partial x}\frac{\partial^2 q}{\partial x\partial y}-\frac{1}{6\sqrt{2}}\frac{\partial q}{\partial y}\frac{\partial^2 q}{\partial x\partial y}\right)=0$$

Discretizing (4.69) via (4.52), (4.61-4.65) one can calculate the Newton algorithm jacobian expressions for the fourth order method as

$$\begin{aligned}\frac{\partial F}{\partial Q_{i-1,j-1}} =& -(8\varepsilon ahQ_{i,j}+8\varepsilon^2+Q_{i,j}^2h^2+ah\varepsilon Q_{i-1,j}\\ &-ah\varepsilon Q_{i+1,j}+ah\varepsilon Q_{i,j-1}-ah\varepsilon Q_{i,j+1})/48h^2\varepsilon\end{aligned} \tag{4.70}$$

$$\begin{aligned}\frac{\partial F}{\partial Q_{i,j-1}} =& -(32\varepsilon^2+h^2Q_{i,j}Q_{i-1,j}-h^2Q_{i,j}Q_{i+1,j}+h^2Q_{i,j}Q_{i,j-1}\\ &-h^2Q_{i,j}Q_{i,j+1}+2Q_{i,j}^2h^2+12ah\varepsilon Q_{i,j-1}+4ah\varepsilon Q_{i-1,j}\\ &+ah\varepsilon Q_{i-1,j-1}-ah\varepsilon Q_{i+1,j-1}-ah\varepsilon Q_{i-1,j+1}+ah\varepsilon Q_{i+1,j+1})/48h^2\varepsilon\end{aligned} \tag{4.71}$$

$$\begin{aligned}\frac{\partial F}{\partial Q_{i+1,j-1}} =&(8\varepsilon^2+Q_{i,j}^2h^2+ah\varepsilon Q_{i-1,j}-ah\varepsilon Q_{i+1,j}\\ &+ah\varepsilon Q_{i,j-1}-ah\varepsilon Q_{i,j+1})/48h^2\varepsilon\end{aligned} \tag{4.72}$$

$$\begin{aligned}\frac{\partial F}{\partial Q_{i-1,j}} =& -(32\varepsilon^2+h^2Q_{i,j}Q_{i,j-1}-h^2Q_{i,j}Q_{i,j+1}+h^2Q_{i,j}Q_{i-1,j}\\ &-h^2Q_{i,j}Q_{i+1,j}+2Q_{i,j}^2h^2+12ah\varepsilon Q_{i-1,j}+4ah\varepsilon Q_{i,j-1}\\ &+ah\varepsilon Q_{i-1,j-1}-ah\varepsilon Q_{i+1,j-1}-ah\varepsilon Q_{i-1,j+1}\\ &+ah\varepsilon Q_{i+1,j+1})/48h^2\varepsilon\end{aligned} \tag{4.73}$$

$$\frac{\partial F}{\partial Q_{i,j}} = (48Q_{i,j}^2h^2 - 16ah\varepsilon Q_{i-1,j-1} + 16ah\varepsilon Q_{i+1,j+1} + 320\varepsilon^2$$

$$-8h^2Q_{i,j}Q_{i-1,j} - 8h^2Q_{i,j}Q_{i+1,j} - 8h^2Q_{i,j}Q_{i,j-1} - 8h^2Q_{i,j}Q_{i,j+1}$$

$$-h^2Q_{i-1,j}^2 - h^2Q_{i+1,j}^2 + 2h^2Q_{i,j-1}Q_{i,j+1} - h^2Q_{i,j-1}^2 - h^2Q_{i,j+1}^2 \tag{4.74}$$

$$+4h^2Q_{i,j}Q_{i+1,j-1} + 4h^2Q_{i,j}Q_{i-1,j+1} - 4h^2Q_{i,j}Q_{i+1,j+1} - 2h^2Q_{i-1,j}Q_{i,j-1}$$

$$+2h^2Q_{i-1,j}Q_{i,j+1} + 2h^2Q_{i+1,j}Q_{i,j-1} - 2h^2Q_{i+1,j}Q_{i,j+1}$$

$$+2h^2Q_{i-1,j}Q_{i+1,j} - 4h^2Q_{i,j}Q_{i-1,j-1})/96h^2\varepsilon$$

$$\frac{\partial F}{\partial Q_{i+1,j}} = -(32\varepsilon^2 - h^2Q_{i,j}Q_{i,j-1} + h^2Q_{i,j}Q_{i,j+1} - h^2Q_{i,j}Q_{i-1,j}$$

$$+ h^2Q_{i,j}Q_{i+1,j} + 2Q_{i,j}^2h^2 - 12ah\varepsilon Q_{i+1,j} - 4ah\varepsilon Q_{i,j+1} \tag{4.75}$$

$$- ah\varepsilon Q_{i-1,j-1} + ah\varepsilon Q_{i+1,j-1} + ah\varepsilon Q_{i-1,j+1} - ah\varepsilon Q_{i+1,j+1})/48h^2\varepsilon$$

$$\frac{\partial F}{\partial Q_{i-1,j+1}} =(-8\varepsilon^2 + Q_{i,j}^2h^2 + ah\varepsilon Q_{i-1,j} - ah\varepsilon Q_{i+1,j}$$

$$+ ah\varepsilon Q_{i,j-1} - ah\varepsilon Q_{i,j+1})/48h^2\varepsilon \tag{4.76}$$

$$\frac{\partial F}{\partial Q_{i,j+1}} = -(32\varepsilon^2 - h^2Q_{i,j}Q_{i-1,j} + h^2Q_{i,j}Q_{i+1,j} - h^2Q_{i,j}Q_{i,j-1}$$

$$+ h^2Q_{i,j}Q_{i,j+1} + 2Q_{i,j}^2h^2 - 12ah\varepsilon Q_{i,j+1} - 4ah\varepsilon Q_{i+1,j} \tag{4.77}$$

$$- ah\varepsilon Q_{i-1,j-1} + ah\varepsilon Q_{i+1,j-1} + ah\varepsilon Q_{i-1,j+1} - ah\varepsilon Q_{i+1,j+1})/48h^2\varepsilon$$

$$\frac{\partial F}{\partial Q_{i+1,j+1}} =(8\varepsilon ahQ_{i,j} - 8\varepsilon^2 - Q_{i,j}^2 h^2 - ah\varepsilon Q_{i-1,j} + ah\varepsilon Q_{i+1,j} - ah\varepsilon Q_{i,j-1} + ah\varepsilon Q_{i,j+1})/48h^2\varepsilon \tag{4.78}$$

4.5 Unsteady two-dimensional formulation.

The unsteady advection-diffusion equation (1) in two dimensions is

$$\frac{\partial q(x,y,t)}{\partial t} - \varepsilon\frac{\partial^2 q(x,y,t)}{\partial x^2} - \varepsilon\frac{\partial^2 q(x,y,t)}{\partial y^2} + u(x,y,t)\frac{\partial q(x,y,t)}{\partial x} + v(x,y,t)\frac{\partial q(x,y,t)}{\partial y} = 0 \tag{4.79}$$

Following the theoretical development of Lax and Wendroff (1960) outlined in detail by Chaffin (1997), two forward Taylor series, for a full timestep $\triangle t$ and for a partial timestep $(1-\alpha)\triangle t$

$$q^{n+1} = q^n + \triangle t\frac{\partial q^n}{\partial t} + \frac{\triangle t^2}{2}\frac{\partial^2 q^n}{\partial t^2} + \frac{\triangle t^3}{6}\frac{\partial^3 q^n}{\partial t^3} + \frac{\triangle t^4}{24}\frac{\partial^4 q^n}{\partial t^4} + H.O.T. \tag{4.80}$$

$$q^{n+1-\alpha} = q^n + (1-\alpha)\triangle t\frac{\partial q^n}{\partial t} + \frac{(1-\alpha)^2\triangle t^2}{2}\frac{\partial^2 q^n}{\partial t^2} + \frac{(1-\alpha)^3\triangle t^3}{6}\frac{\partial^3 q^n}{\partial t^3} + \frac{(1-\alpha)^4\triangle t^4}{24}\frac{\partial^4 q^n}{\partial t^4} + H.O.T. \tag{4.81}$$

and two corresponding backward series

$$q^n = q^{n+1} - \triangle t\frac{\partial q^{n+1}}{\partial t} + \frac{\triangle t^2}{2}\frac{\partial^2 q^{n+1}}{\partial t^2} - \frac{\triangle t^3}{6}\frac{\partial^3 q^{n+1}}{\partial t^3} + \frac{\triangle t^4}{24}\frac{\partial^4 q^{n+1}}{\partial t^4} + H.O.T. \tag{4.82}$$

$$q^{n-\alpha} = q^{n+1} - \alpha\triangle t\frac{\partial q^n}{\partial t} + \frac{\alpha^2\triangle t^2}{2}\frac{\partial^2 q^{n+1}}{\partial t^2} - \frac{\alpha^3\triangle t^3}{6}\frac{\partial^3 q^{n+1}}{\partial t^3} + \frac{\alpha^4\triangle t^4}{24}\frac{\partial^4 q^{n+1}}{\partial t^4} + H.O.T. \tag{4.83}$$

are used in designing the temporal discretization.

A linear combination of the four series is then taken to eliminate third order terms as

$$\begin{aligned} q^{n+1} - q^n - \triangle t \left[\theta \frac{\partial q^{n+1}}{\partial t} + (1+\theta)\frac{\partial q^n}{\partial t}\right] = \\ - \frac{\triangle t^2}{6}\left[(3\theta - 1)\frac{\partial^2 q^{n+1}}{\partial t^2} + (3\theta - 2)\frac{\partial^2 q^n}{\partial t^2}\right] \\ - \frac{\triangle t^4}{72}\left[-(3\theta - 1)^2\frac{\partial^4 q^{n+1}}{\partial t^4} + (3\theta - 2)^2\frac{\partial^4 q^n}{\partial t^4}\right] + H.O.T. \end{aligned} \tag{4.84}$$

Here, the left had side is the θ-implicit approximation, and the right hand side consists of the correction error terms. Selecting the non-dissipative, second-order accurate trapesoidal rule $\theta = 1/2$ for time integration and replacing the corresponding time derivatives with their space counterparts via the Lax-Wendroff substitution utilizing the original equation (4.79) as

$$\frac{\partial q}{\partial t} = \left(-u\frac{\partial}{\partial x} - v\frac{\partial}{\partial y} + \varepsilon\frac{\partial^2}{\partial x^2} + \varepsilon\frac{\partial^2}{\partial y^2}\right) q \tag{4.85}$$

yields the following semi-discrete equation

$$\begin{aligned} Q^{n+1} + \frac{\triangle t}{2}\left(u\frac{\partial Q^{n+1}}{\partial x} + v\frac{\partial Q^{n+1}}{\partial y} - \varepsilon\frac{\partial^2 Q^{n+1}}{\partial x^2} - \varepsilon\frac{\partial^2 Q^{n+1}}{\partial x^2}\right) = \\ Q^n - \frac{\triangle t}{2}\left(u\frac{\partial Q^n}{\partial x} + v\frac{\partial Q^n}{\partial y} - \varepsilon\frac{\partial^2 Q^n}{\partial x^2} - \varepsilon\frac{\partial^2 Q^n}{\partial x^2}\right) \end{aligned} \tag{4.86}$$

Introduction of the nine-node spatial discretization (4.50) leads to

$$Q_j^{n+1} + \frac{\triangle t}{2}(c_1 Q_{i-1,j-1}^{n+1} + c_2 Q_{i,j-1}^{n+1} + c_3 Q_{i+1,j-1}^{n+1} + c_4 Q_{i-1,j}^{n+1} + c_5 Q_{i,j}^{n+1}$$

$$+c_6Q^{n+1}_{i+1,j} + c_7Q^{n+1}_{i-1,j+1} + c_8Q^{n+1}_{i,j+1} + c_9Q^{n+1}_{i+1,j+1}) = \tag{4.87}$$

$$Q^n_j - \frac{\triangle t}{2}(c_1Q^n_{i-1,j-1} + c_2Q^n_{i,j-1} + c_3Q^n_{i+1,j-1} + c_4Q^n_{i-1,j} + c_5Q^n_{i,j}$$

$$+c_6Q^n_{i+1,j} + c_7Q^n_{i-1,j+1} + c_8Q^n_{i,j+1} + c_9Q^n_{i+1,j+1})$$

with a subsequent Taylor series expansion, whose existence is postulated via the usual assumptions, producing

$$Q^{n+1} + \frac{\triangle t}{2}((c_1 + c_2 + c_3 + c_4 + c_5 + c_6 + c_7 + c_8 + c_9)Q^{n+1}$$

$$+hQ^{n+1}_x(-c_1 + c_3 - c_4 + c_6 - c_7 + c_9)$$

$$+hQ^{n+1}_y(-c1 - c_2 - c_3 + c_7 + c_8 + c_9)$$

$$+\frac{h^2}{2}Q^{n+1}_{xx}(c_1 + c_3 + c_4 + c_6 + c_7 + c_9)$$

$$+\frac{h^2}{2}Q^{n+1}_{yy}(c_1 + c_2 + c_3 + c_7 + c_8 + c_9) + h^2Q^{n+1}_{xy}(c_1 - c_3 - c_7 + c_9)$$

$$+\frac{h^3}{6}Q^{n+1}_{xxx}(c_9 - c_1 + c_3 - c_7 + c_6 - c_4)$$

$$+\frac{h^3}{6}Q^{n+1}_{yyy}(c_9 - c_1 - c_3 + c_7 + c_8 - c_2)$$

$$+\frac{h^3}{2}Q^{n+1}_{xxy}(c_9 - c_1 - c_3 + c_7) + \frac{h^3}{2}Q^{n+1}_{xyy}(c_9 - c_1 + c_3 - c_7)$$

$$+\frac{h^4}{24}Q^{n+1}_{xxxx}(c_9+c_1+c_3+c_7+c_6+c_4)$$

$$+\frac{h^4}{24}Q^{n+1}_{yyyy}(c_9+c_1+c_3+c_7+c_8+c_2)+\frac{h^4}{6}Q^{n+1}_{xxxy}(c_9+c_1-c_3-c_7)$$

$$+\frac{h^4}{6}Q^{n+1}_{xyyy}(c_9+c_1-c_3-c_7)+\frac{h^4}{4}Q^{n+1}_{xxyy}(c_9+c_1+c_3+c_7))= \tag{4.88}$$

$$Q^n-\frac{\triangle t}{2}((c_1+c_2+c_3+c_4+c_5+c_6+c_7+c_8+c_9)Q^n$$

$$+hQ^n_x(-c_1+c_3-c_4+c_6-c_7+c_9)$$

$$+hQ^n_y(-c1-c_2-c_3+c_7+c_8+c_9)$$

$$+\frac{h^2}{2}Q^n_{xx}(c_1+c_3+c_4+c_6+c_7+c_9)$$

$$+\frac{h^2}{2}Q^n_{yy}(c_1+c_2+c_3+c_7+c_8+c_9)+h^2Q^n_{xy}(c_1-c_3-c_7+c_9)$$

$$+\frac{h^3}{6}Q^n_{xxx}(c_9-c_1+c_3-c_7+c_6-c_4)$$

$$+\frac{h^3}{6}Q^n_{yyy}(c_9-c_1-c_3+c_7+c_8-c_2)$$

$$+\frac{h^3}{2}Q^n_{xxy}(c_9-c_1-c_3+c_7)+\frac{h^3}{2}Q^n_{xyy}(c_9-c_1+c_3-c_7)$$

$$+\frac{h^4}{24}Q^n_{xxxx}(c_9+c_1+c_3+c_7+c_6+c_4)$$

$$+\frac{h^4}{24}Q^n_{yyyy}(c_9+c_1+c_3+c_7+c_8+c_2)+\frac{h^4}{6}Q^n_{xxxy}(c_9+c_1-c_3-c_7)$$

$$+\frac{h^4}{6}Q^n_{xyyy}(c_9+c_1-c_3-c_7)+\frac{h^4}{4}Q^n_{xxyy}(c_9+c_1+c_3+c_7))$$

Introduction of symmetrized spatial approximation of the form (4.52) further yields

$$Q^{n+1}+\frac{\triangle tu}{2}Q^{n+1}_x+\frac{\triangle tv}{2}Q^{n+1}_y-\frac{\triangle t\varepsilon}{2}Q^{n+1}_{xx}-\frac{\triangle t\varepsilon}{2}Q^{n+1}_{yy}$$

$$-Q^n+\frac{\triangle tu}{2}Q^n_x+\frac{\triangle tv}{2}Q^n_y-\frac{\triangle t\varepsilon}{2}Q^n_{xx}-\frac{\triangle t\varepsilon}{2}Q^n_{yy}$$

$$+\frac{h^2\triangle t}{2}(\frac{vQ^{n+1}_{yyy}}{6}+\frac{uQ^{n+1}_{xxx}}{6}+\frac{vQ^{n+1}_{xxy}}{6}+\frac{uQ^{n+1}_{xyy}}{6} \tag{4.89}$$

$$+\frac{vQ^n_{yyy}}{6}+\frac{uQ^n_{xxx}}{6}+\frac{vQ^n_{xxy}}{6}+\frac{uQ^n_{xyy}}{6})$$

$$-\frac{h^2\triangle t\varepsilon}{2}(\frac{Q^{n+1}_{xxxx}}{12}+\frac{Q^{n+1}_{yyyy}}{12}+\frac{Q^{n+1}_{xxyy}}{6}+\frac{Q^n_{xxxx}}{12}+\frac{Q^n_{yyyy}}{12}+\frac{Q^n_{xxyy}}{6})$$

Differentiating (4.89) twice with respect to x and y and combining the terms produces

$$\triangle tu_yQ^{n+1}_{xy}+\frac{\triangle t}{2}uQ^n_{xxx}+Q^{n+1}_{xx}+Q^{n+1}_{yy}-Q^n_{xx}-Q^n_{yy}$$

$$+\frac{\triangle t}{2}vQ^n_{yyy}+\frac{\triangle t}{2}uQ^n_{xyy}+\frac{\triangle t}{2}u_{xx}Q^{n+1}_x+\triangle tu_xQ^{n+1}_{xx}+\frac{\triangle t}{2}uQ^{n+1}_{xxx}$$

$$+\frac{\triangle t}{2}v_{xx}Q^{n+1}_y+\triangle tv_xQ^{n+1}_{xy}+\frac{\triangle t}{2}vQ^{n+1}_{xxy}+\frac{\triangle t}{2}u_{xx}Q^n_x+\triangle tu_xQ^n_{xx}$$

$$+\frac{\triangle t}{2}v_{xx}Q_y^n + \triangle t v_x Q_{xy}^n + \frac{\triangle t}{2}vQ_{xxy}^n + \frac{\triangle t}{2}u_{yy}Q_x^{n+1} + \frac{\triangle t}{2}uQ_{xyy}^{n+1} \tag{4.90}$$

$$+\frac{\triangle t}{2}v_{yy}Q_y^{n+1} + \triangle t v_y Q_{yy}^{n+1} + \frac{\triangle t}{2}vQ_{yyy}^{n+1} + \frac{\triangle t}{2}u_{yy}Q_x^n + \triangle t u_y Q_{xy}^n$$

$$+\frac{\triangle t}{2}v_{yy}Q_y^n + \triangle t v_y Q_{yy}^n = \triangle t\varepsilon Q_{xxyy}^{n+1} + \frac{\triangle t\varepsilon}{2}Q_{xxxx}^{n+1} + \frac{\triangle t\varepsilon}{2}Q_{xxxx}^n$$

$$+\triangle t\varepsilon Q_{xxyy}^n + \frac{\triangle t\varepsilon}{2}Q_{yyyy}^n + \frac{\triangle t\varepsilon}{2}Q_{yyyy}^{n+1}$$

Similarly, differentiating with respect to x and y yields

$$Q_x^{n+1} + \frac{\triangle t}{2}u_x Q_x^{n+1} + \frac{\triangle t}{2}uQ_{xx}^{n+1} + \frac{\triangle t}{2}v_x Q_y^{n+1} + \frac{\triangle t}{2}vQ_{xy}^{n+1}$$

$$-Q_x^n + \frac{\triangle t}{2}u_x Q_x^n + \frac{\triangle t}{2}uQ_{xx}^n + \frac{\triangle t}{2}v_x Q_y^n + \frac{\triangle t}{2}vQ_{xy}^n = \tag{4.91}$$

$$\frac{\triangle t\varepsilon}{2}Q_{xxx}^{n+1} + \frac{\triangle t\varepsilon}{2}Q_{xyy}^{n+1} + \frac{\triangle t\varepsilon}{2}Q_{xxx}^n + \frac{\triangle t\varepsilon}{2}Q_{xyy}^n$$

and

$$Q_y^{n+1} + \frac{\triangle t}{2}u_y Q_x^{n+1} + \frac{\triangle t}{2}uQ_{xy}^{n+1} + \frac{\triangle t}{2}v_y Q_y^{n+1} + \frac{\triangle t}{2}vQ_{yy}^{n+1}$$

$$-Q_y^n + \frac{\triangle t}{2}u_y Q_x^n + \frac{\triangle t}{2}uQ_{xy}^n + \frac{\triangle t}{2}v_y Q_y^n + \frac{\triangle t}{2}vQ_{yy}^n = \tag{4.92}$$

$$\frac{\triangle t\varepsilon}{2}Q_{xxy}^{n+1} + \frac{\triangle t\varepsilon}{2}Q_{xxy}^n + \frac{\triangle t\varepsilon}{2}Q_{yyy}^{n+1} + \frac{\triangle t\varepsilon}{2}Q_{yyy}^n$$

respectively.

Substituting (4.90-4.92) into (4.89) to eliminate higher order derivatives from the fourth order error contribution, combining the terms and reversing the signs on the error entries of the modified PDE one obtains the fourth order space accurate perturbed

PDE in the form

$$Q^{n+1} + \frac{\triangle t u}{2} Q_x^{n+1} + \frac{\triangle t v}{2} Q_y^{n+1} - \frac{\triangle t \varepsilon}{2} Q_{xx}^{n+1} - \frac{\triangle t \varepsilon}{2} Q_{yy}^{n+1}$$

$$- \frac{h^2 \triangle t}{2} Q_x^{n+1} \left(\frac{u}{6 \triangle t \varepsilon} + \frac{u u_x}{12 \varepsilon} - \frac{u_{xx}}{12} - \frac{u_{yy}}{12} + \frac{v u_y}{12 \varepsilon} \right)$$

$$- \frac{h^2 \triangle t}{2} Q_y^{n+1} \left(\frac{u v_x}{12 \varepsilon} - \frac{v_{xx}}{12} - \frac{v_{yy}}{12} + \frac{v}{6 \triangle t \varepsilon} + \frac{v v_y}{12 \varepsilon} \right)$$

$$- \frac{h^2 \triangle t}{2} Q_{yy}^{n+1} \left(\frac{v^2}{12 \varepsilon} - \frac{1}{6 \triangle t} - \frac{v_y}{6} \right) - \frac{h^2 \triangle t}{2} Q_{xx}^{n+1} \left(\frac{u^2}{12 \varepsilon} - \frac{1}{6 \triangle t} - \frac{u_x}{6} \right)$$

$$- \frac{h^2 \triangle t}{2} Q_{xy}^{n+1} \left(\frac{u v}{6 \varepsilon} - \frac{u_y}{6} - \frac{v_x}{6} \right) = \tag{4.93}$$

$$Q^n - \frac{\triangle t u}{2} Q_x^n - \frac{\triangle t v}{2} Q_y^n + \frac{\triangle t \varepsilon}{2} Q_{xx}^n + \frac{\triangle t \varepsilon}{2} Q_{yy}^n$$

$$+ \frac{h^2 \triangle t}{2} Q_x^n \left(- \frac{u}{6 \triangle t \varepsilon} + \frac{u u_x}{12 \varepsilon} - \frac{u_{xx}}{12} - \frac{u_{yy}}{12} + \frac{v u_y}{12 \varepsilon} \right)$$

$$+ \frac{h^2 \triangle t}{2} Q_y^n \left(\frac{u v_x}{12 \varepsilon} - \frac{v_{xx}}{12} - \frac{v_{yy}}{12} - \frac{v}{6 \triangle t \varepsilon} + \frac{v v_y}{12 \varepsilon} \right)$$

$$+ \frac{h^2 \triangle t}{2} Q_{yy}^n \left(\frac{v^2}{12 \varepsilon} + \frac{1}{6 \triangle t} - \frac{v_y}{6} \right) + \frac{h^2 \triangle t}{2} Q_{xx}^n \left(\frac{u^2}{12 \varepsilon} + \frac{1}{6 \triangle t} - \frac{u_x}{6} \right)$$

$$+ \frac{h^2 \triangle t}{2} Q_{xy}^n \left(\frac{u v}{6 \varepsilon} - \frac{u_y}{6} - \frac{v_x}{6} \right)$$

Finally, performing order of magnitude analysis consistent with the steady-state case and proceeding to the limit as $\triangle t \to \gamma \geq 0$ yields the continuum form

$$\begin{aligned} &\frac{\partial q}{\partial t} + \mathbf{u} \cdot \nabla q - \varepsilon \nabla \cdot \nabla q - \frac{h^2}{12\varepsilon} \mathbf{u} \cdot \nabla (\mathbf{u} \cdot \nabla q) \\ &\quad + \frac{h^2}{6 \triangle t \varepsilon} \mathbf{u} \cdot \nabla q - \frac{h^2}{6 \triangle t} \nabla \cdot \nabla q = 0 \end{aligned} \tag{4.94}$$

Note that (4.94) recovers the steady-state modified PDE form (4.60), when temporal error terms are taken into account. The theory is therefore complete. The symmetry of the developed discretization in (4.52) would provide a natural extension to three-dimensional problems, with the continuum perturbed equation forms (4.60) and (4.94) remaining unchanged from the two-dimensional case, granted the mesh size measure h is evaluated as an appropriate combination of $\triangle x$, $\triangle y$ and $\triangle z$.

4.6. High order formulation for hyperbolic problems.

The advection-diffusion equation (1) written for zero physical diffusion is written as

$$\frac{\partial q(x,y,t)}{\partial t} + +u(x,y,t) \frac{\partial q(x,y,t)}{\partial x} + v(x,y,t) \frac{\partial q(x,y,t)}{\partial y} = 0 \tag{4.95}$$

Introducing the temporal discretization in the manner illustrated in (4.80-4.84), selecting trapesoidal integration rule and substituting the corresponding time error

terms via (4.95) yields

$$Q^{n+1} + \frac{\triangle t}{2}\left(u\frac{\partial Q^{n+1}}{\partial x} + v\frac{\partial Q^{n+1}}{\partial y}\right) =$$

$$Q^{n} - \frac{\triangle t}{2}\left(u\frac{\partial Q^{n}}{\partial x} + v\frac{\partial Q^{n}}{\partial y}\right) \tag{4.96}$$

The nine-node spatial discretization (4.50) is then introduced to produce (4.51), with the symmetrized spatial approximation requirement (4.52) now being replaced by

$$\sum_{n=1}^{9} c_n = 0$$

$$-c_1 + c_3 - c_4 + c_6 - c_7 + c_9 = \frac{u}{h}$$

$$-c_1 - c_2 - c_3 + c_7 + c_8 + c_9 = \frac{v}{h}$$

$$c_1 + c_3 + c_4 + c_6 + c_7 + c_9 = 0$$

$$c_1 + c_2 + c_3 + c_7 + c_8 + c_9 = 0 \tag{4.97}$$

$$c_1 - c_3 - c_7 + c_9 = 0$$

$$c_9 - c_1 = \frac{u+v}{6h}$$

$$c_9 + c_1 = 0$$

$$c_3 - c_7 = \frac{u - v}{6h}$$

Substituting (4.97) into (4.51) and neglecting error terms of the order greater than four yields

$$\begin{aligned} & Q^{n+1} + \frac{\triangle t u}{2} Q_x^{n+1} + \frac{\triangle t v}{2} Q_y^{n+1} - Q^n + \frac{\triangle t u}{2} Q_x^n + \frac{\triangle t v}{2} Q_y^n \\ & + \frac{h^2 \triangle t}{12} (v Q_{yyy}^{n+1} + u Q_{xxx}^{n+1} + v Q_{xxy}^{n+1} + u Q_{xyy}^{n+1} \\ & + v Q_{yyy}^n + u Q_{xxx}^n + v Q_{xxy}^n + u Q_{xyy}^n) = 0 \end{aligned} \tag{4.98}$$

Differentiating twice with respect to x and y one obtains

$$\begin{aligned} & Q_{xx}^{n+1} + \frac{\triangle t}{2} u_{xx} Q_x^{n+1} + \triangle t u_x Q_{xx}^{n+1} + \frac{\triangle t}{2} v_{xx} Q_y^{n+1} + \triangle t v_x Q_{xy}^{n+1} \\ & + \frac{\triangle t}{2} v Q_{xxy}^{n+1} + \frac{\triangle t}{2} u_{xx} Q_x^n + \triangle t u_x Q_{xx}^n + \frac{\triangle t}{2} v_{xx} Q_y^n + \triangle t v_x Q_{xy}^n \\ & + \frac{\triangle t}{2} v Q_{xxy}^n - Q_{xx}^n = -\frac{\triangle t}{2} u Q_{xxx}^n - \frac{\triangle t}{2} u Q_{xxx}^{n+1} \end{aligned} \tag{4.99}$$

and

$$\begin{aligned} & Q_{yy}^{n+1} + \frac{\triangle t}{2} u_{yy} Q_x^{n+1} + \triangle t u_y Q_{xy}^{n+1} + \frac{\triangle t}{2} u Q_{xyy}^{n+1} + \frac{\triangle t}{2} v_{yy} Q_y^{n+1} \\ & + \triangle t v_y Q_{yy}^{n+1} + \frac{\triangle t}{2} u_{yy} Q_x^n + \triangle t u_y Q_{xy}^n + \frac{\triangle t}{2} u Q_{xyy}^n \\ & + \frac{\triangle t}{2} v_{yy} Q_y^n + \triangle t v_y Q_{yy}^n - Q_{yy}^n = -\frac{\triangle t}{2} v Q_{yyy}^n - \frac{\triangle t}{2} v Q_{yyy}^{n+1} \end{aligned} \tag{4.100}$$

respectively.

Substituting (4.99,4.100) into (4.98), collecting the terms and reversing the signs on the error contributions results in the modified fourth order space accurate PDE in

the form

$$Q^{n+1} + \frac{\triangle tu}{2} Q_x^{n+1} + \frac{\triangle tv}{2} Q_y^{n+1} + \frac{h^2 \triangle t}{2} Q_{xx}^{n+1} \left(\frac{1}{3\triangle t} + \frac{u_x}{3} \right)$$

$$+ \frac{h^2 \triangle t}{2} Q_{yy}^{n+1} \left(\frac{1}{3\triangle t} + \frac{v_y}{3} \right) + \frac{h^2 \triangle t}{2} Q_x^{n+1} \left(\frac{u_{xx}}{6} + \frac{u_{yy}}{6} \right)$$

$$+ \frac{h^2 \triangle t}{2} Q_y^{n+1} \left(\frac{v_{xx}}{6} + \frac{v_{yy}}{6} \right) + \frac{h^2 \triangle t}{2} Q_{xy}^{n+1} \left(\frac{v_x}{3} + \frac{u_y}{3} \right) = \tag{4.101}$$

$$Q^n - \frac{\triangle tu}{2} Q_x^n - \frac{\triangle tv}{2} Q_y^n + \frac{h^2 \triangle t}{2} Q_{xx}^n \left(\frac{1}{3\triangle t} - \frac{u_x}{3} \right)$$

$$+ \frac{h^2 \triangle t}{2} Q_{yy}^n \left(\frac{1}{3\triangle t} - \frac{v_y}{3} \right) - \frac{h^2 \triangle t}{2} Q_x^n \left(\frac{u_{xx}}{6} + \frac{u_{yy}}{6} \right)$$

$$- \frac{h^2 \triangle t}{2} Q_y^n \left(\frac{v_{xx}}{6} + \frac{v_{yy}}{6} \right) + \frac{h^2 \triangle t}{2} Q_{xy}^n \left(\frac{v_x}{3} + \frac{u_y}{3} \right)$$

Order of magnitude ordering combined with taking $\triangle t \to \gamma \geq 0$ results in

$$\frac{\partial q}{\partial t} + \mathbf{u} \cdot \nabla q - \frac{h^2}{3\triangle t} \nabla \cdot \nabla q = 0 \tag{4.102}$$

which conveniently adds an artificial diffusion operator to the original equation, whose application is balanced by the respective measures of temporal and spatial discretizations.

Chapter 5

Lax-Wendroff, upwind formulations. Monotonicity vs. accuracy.

5.1 Perturbed PDE analysis error correction.

The high order spatial multidimensional formulation developed herein has been shown to eliminate oscillatory dispersive error modes thus promoting solution monotonicity and accuracy on a sufficiently refined computational grid. The developed perturbed PDE methodology also allows for qualitative analysis of the error control mechanism by clearly specifying the error terms corrected to the higher order of accuracy. In the one-dimensional steady-state case the perturbed PDE is shown to be

$$u\frac{\partial q}{\partial x} - \varepsilon\frac{\partial^2 q}{\partial x^2} - \frac{h^2}{12\varepsilon}u\frac{\partial}{\partial x}u\frac{\partial q}{\partial x} = 0 \tag{5.1}$$

on uniform, and

$$u\frac{\partial q}{\partial x} - \varepsilon\frac{\partial^2 q}{\partial x^2} - \frac{h^2(p^2+p+1)}{36\varepsilon}u\frac{\partial}{\partial x}u\frac{\partial q}{\partial x} = 0 \tag{5.2}$$

non-uniform discretizations.

The uniform-mesh perturbed PDE (5.1) reduces to

$$uq_x - \varepsilon q_{xx} - h^2 q_{xx}\frac{u^2}{12\varepsilon} = 0 \tag{5.3}$$

in the linear case.

Similarly, in two dimensions the perturbed PDE is

$$\mathbf{u} \cdot \nabla q - \varepsilon \nabla \cdot \nabla q - \frac{h^2}{12\varepsilon} \mathbf{u} \cdot \nabla (\mathbf{u} \cdot \nabla q) = 0 \tag{5.4}$$

with the linear case resulting in

$$uQ_x + vQ_y - \varepsilon Q_{xx} - \varepsilon Q_{yy} - h^2 \frac{vuQ_{xy}}{6\varepsilon} - h^2 \frac{v^2 Q_{yy}}{12\varepsilon} - h^2 \frac{u^2 Q_{xx}}{12\varepsilon} = 0 \tag{5.5}$$

The high order spatial error correction in both cases is therefore achieved via inrtoduction of the diffusive terms loaded by the coefficient appropriate for the desired order of accuracy. The cross order derivative term is introduced in the two-dimensional case (5.4), consistently emphasizing its multidimensional origin. Establishing the nature of the high order correction additions gives one an opportunity to compare this present approach to several other methods similarly utilizing space-time correction (mostly diffusive) terms in an attempt to enhance solution accuracy and monotonicity.

5.2 Lax-Wendroff formulation for the linear unsteady case.

Consider the one-dimensional unsteady linear advection-diffusion equation:

$$L(q) = \frac{\partial q}{\partial t} + u \frac{\partial q}{\partial x} - \varepsilon \frac{\partial^2 q}{\partial x^2} = 0 \tag{5.6}$$

Lax-Wendroff Taylor formulation is specifically designed to develop high order time discretization. Two forward Taylor series, for a full timestep $\triangle t$ and for a partial timestep $(1 - \alpha)\triangle t$ and two corresponding backward series are used towards this goal as shown in Chapter 4.

A linear combination of the four series is then taken to eliminate the third order terms yielding

$$q^{n+1} - q^n - \triangle t \left[\theta \frac{\partial q^{n+1}}{\partial t} + (1+\theta)\frac{\partial q^n}{\partial t}\right] =$$

$$- \frac{\triangle t^2}{6}\left[(3\theta - 1)\frac{\partial^2 q^{n+1}}{\partial t^2} + (3\theta - 2)\frac{\partial^2 q^n}{\partial t^2}\right] \tag{5.7}$$

$$- \frac{\triangle t^4}{72}\left[-(3\theta - 1)^2\frac{\partial^4 q^{n+1}}{\partial t^4} + (3\theta - 2)^2\frac{\partial^4 q^n}{\partial t^4}\right] + H.O.T.$$

where $\theta = (\alpha + 1)/3$.

The left had side is the θ-implicit approximation, and the right hand side consists of the correction error terms. A standard procedure is now to replace time derivatives with their space counterparts via the Lax-Wendroff substitution utilizing the original equation (5.6) as

$$\frac{\partial q}{\partial t} = \left(-u\frac{\partial}{\partial x} + \varepsilon\frac{\partial^2}{\partial x^2}\right) q \tag{5.8}$$

$$\frac{\partial^2 q}{\partial t^2} = \left(-u\frac{\partial}{\partial x} + \varepsilon\frac{\partial^2}{\partial x^2}\right)\left(-u\frac{\partial}{\partial x} + \varepsilon\frac{\partial^2}{\partial x^2}\right) q = \left(u^2 - 2u\varepsilon\frac{\partial}{\partial x} + \varepsilon^2\frac{\partial^2}{\partial x^2}\right)\frac{\partial^2 q}{\partial x^2} \tag{5.9}$$

Clearly, a non-linear case would add some extra algebraic complexity in evaluating these terms.

Finally, substituting (5.8-5.9) into (5.7) yields the following semi-discrete PDE

$$\begin{aligned} q^{n+1} - q^n &- \triangle t\theta \left(-u\frac{\partial q^{n+1}}{\partial x} + \varepsilon \frac{\partial^2 q^{n+1}}{\partial x^2} \right) \\ &- \triangle t(1-\theta) \left(-u\frac{\partial q^{n}}{\partial x} + \varepsilon \frac{\partial^2 q^{n}}{\partial x^2} \right) \\ &+ \frac{\triangle t^2(3\theta - 1)}{6} \left(u^2 \frac{\partial^2 q^{n+1}}{\partial x^2} - 2u\varepsilon \frac{\partial^3 q^{n+1}}{\partial x^3} + \varepsilon^2 \frac{\partial^4 q^{n+1}}{\partial x^4} \right) \\ &+ \frac{\triangle t^2(3\theta - 2)}{6} \left(u^2 \frac{\partial^2 q^{n}}{\partial x^2} - 2u\varepsilon \frac{\partial^3 q^{n}}{\partial x^3} + \varepsilon^2 \frac{\partial^4 q^{n}}{\partial x^4} \right) = 0 \end{aligned} \tag{5.10}$$

The time discretization technique described herein provides a potentially infinitely accurate approximation in time achievable by correcting for progressively higher order truncation error terms. Including only $\triangle t$ order terms in (5.10) would produce the second order time accurate method, while retaining terms of the order $\triangle t^2$ would increase the corresponding order of accuracy to four. This procedure can be continued to the desired approximation degree. Of course, as usual, accuracy would come at a price. As can be seen from (5.10), fourth order time accurate method would require one to discretize third and fourth order space derivatives, thus increasing computational costs by expanding the solution matrix bandwidth.

The order of the spatial discretization would also become an issue in this case, since a low (lower than four) order space approximation will offset the advantage of using high order accurate time method by introducing low order errors into the numerical solution. Therefore tradeoffs persist, the most common being the use of

the substitutions (5.8-5.9) derived for a strictly hyperbolic (zero physical diffusion) problem in a more general case (5.6) while arguing that the focus is on the problems with zero or small physical diffusion. Sometimes it is simply stated that retaining third and fourth order derivative approximations produces an undesirable increase in solution matrix bandwidth and all derivations proceed from there with (5.10) reduced to

$$q^{n+1} - q^n - \triangle t\theta\left(-u\frac{\partial q^{n+1}}{\partial x} + \varepsilon\frac{\partial^2 q^{n+1}}{\partial x^2}\right) - \triangle t(1-\theta)\left(-u\frac{\partial q^n}{\partial x} + \varepsilon\frac{\partial^2 q^n}{\partial x^2}\right) + \frac{\triangle t^2(3\theta-1)}{6}u^2\frac{\partial^2 q^{n+1}}{\partial x^2} + \frac{\triangle t^2(3\theta-2)}{6}u^2\frac{\partial^2 q^n}{\partial x^2} = 0 \tag{5.11}$$

or taking $\triangle t \to \gamma \geq 0$

$$\frac{\partial q}{\partial t} + u\frac{\partial q}{\partial x} - \varepsilon\frac{\partial^2 q}{\partial x^2} - \frac{\triangle t u^2}{2}\frac{\partial^2 q}{\partial x^2} = 0 \tag{5.12}$$

The correction term resulting from this analysis is a diffusive second order derivative of magnitude $\triangle t u^2/2$ which is notably independent of the viscosity parameter ε and is immediately recognized as the TWS formulation β correction term.

5.3. Generalized Taylor Weak Statement approach.

For the purposes of the theoretical analysis, the general multi-dimensional advection-diffusion equation is assumed to be sufficiently approximated by its convectional component (Chaffin, 1997). In index notation

$$\frac{\partial q}{\partial t} + u_j\frac{\partial q}{\partial x_j} = 0 \tag{5.13}$$

The higher order time derivatives are replaced by the equivalent spatial derivatives as outlined in the previous section in the case of the linear equation resulting in

$$\frac{\partial^2 q}{\partial t^2} = -u_j \frac{\partial}{\partial x_j}\frac{\partial q}{\partial t} = u_k \frac{\partial}{\partial x_k}\left(u_j \frac{\partial q}{\partial x_j}\right) \tag{5.14}$$

$$\frac{\partial^3 q}{\partial t^3} = u_k \frac{\partial}{\partial x_k}\left(u_j \frac{\partial}{\partial x_j}\frac{\partial q}{\partial t}\right) = -u_l \frac{\partial}{\partial x_l}\left(u_k \frac{\partial}{\partial x_k}\left(u_j \frac{\partial q}{\partial x_j}\right)\right) \tag{5.15}$$

Weighted combinations of (5.14) and (5.15) are taken with weight coefficients $-\alpha + \beta \approx 1$ and $\gamma - \mu \approx 1$ yielding

$$\frac{\partial^2 q}{\partial t^2} = 2\alpha\left(u_j \frac{\partial}{\partial x_j}\frac{\partial q}{\partial t}\right) + 2\beta\left(u_k \frac{\partial}{\partial x_k}\left(u_j \frac{\partial q}{\partial x_j}\right)\right) \tag{5.16}$$

$$\frac{\partial^3 q}{\partial t^3} = 6\gamma\left(u_k \frac{\partial}{\partial x_k}\left(u_j \frac{\partial}{\partial x_j}\frac{\partial q}{\partial t}\right)\right) + 6\mu\left(u_l \frac{\partial}{\partial x_l}\left(u_k \frac{\partial}{\partial x_k}\left(u_j \frac{\partial q}{\partial x_j}\right)\right)\right) \tag{5.17}$$

Substituting these forms in the series time Taylor series expansion and proceeding to take $\triangle t \to \gamma \geq 0$ yields the modified system

$$\frac{\partial q}{\partial t} + u_j \frac{\partial q^{n+\theta}}{\partial x_j}$$

$$-\triangle t(\alpha\left(u_j \frac{\partial}{\partial x_j}\frac{\partial q}{\partial t}\right) + \beta\left(u_k \frac{\partial}{\partial x_k}\left(u_j \frac{\partial q}{\partial x_j}\right)\right)) \tag{5.18}$$

$$-\triangle t^2(\gamma\left(u_k \frac{\partial}{\partial x_k}\left(u_j \frac{\partial}{\partial x_j}\frac{\partial q}{\partial t}\right)\right) + \mu\left(u_l \frac{\partial}{\partial x_l}\left(u_k \frac{\partial}{\partial x_k}\left(u_j \frac{\partial q}{\partial x_j}\right)\right)\right)) = 0$$

specification of the coefficient set $\alpha, \beta, \gamma, \mu$ is usually a subject of numerical trial-and-error approach with larger amounts of diffusion achieved by increasing coefficient β

where required by trial solution runs. Possible optimization approaches were also suggested by Chaffin (1997).

As seen from (5.1) and (5.4), the high order correction error term obtained in the present development is identical in appearance to the modified TWS β term. The expected high order spatial accuracy of the TWS method is therefore theoretically verified. Another important consequence of the present analysis is that application of the correction term is now governed by the theoretically sound principles rather than numerical experimentation. The theory therefore provides a highly efficient dispersion error control mechanism whose application is based on the specifics of the solution domain discretization and physics of the problem. These derivations are of fundamental importance for the real-world application problems.

5.4 Upwind formulation.

Low order centered discretization of the convection term in (5.6), via for example a GWS FE formulation is known to result in spurious oscillations which is illustrated in previous sections. Using the upwind finite difference representation instead,

$$\frac{\partial q}{\partial x} = \frac{Q_j - Q_{j-1}}{h} \tag{5.19}$$

prevents this from occuring. The result is the first order space accurate scheme which in a one-dimensional case produces the following computational stencil expression

$$-(1 + \frac{uh}{\varepsilon})Q_{j-1} + 2(1 + \frac{uh}{2\varepsilon})Q_j - Q_{j+1} = 0 \tag{5.20}$$

Expanding (5.20) in Taylor series, collecting the terms and neglecting high order error contributions yields

$$u\frac{\partial q}{\partial x} - \varepsilon\left(1 + \frac{uh}{2\varepsilon}\right)\frac{\partial^2 q}{\partial x^2} = 0 \tag{5.21}$$

and the use of the first order upwind formula (5.19), thus introduces artificial diffusion of the amount $uh/2$.

Note, that unlike the high order correction of the fourth order method, both Lax-Wendroff and upwind error corrections are independent of the physics of the problem (via viscosity parameter ε). In fact, for $u = 1$ both are linearly proportional to the time/space discretization size hinting similarity of the underlying ideas albeit transient vs spatial interpretations. The next subsection thus concentrates on comparing upwind and high order corrections in the steady-state case, with a unified time-space correction approach investigated later on in the chapter.

5.5. Upwind vs. High order = monotonicity vs. accuracy.

Two seemingly similar, but distinctly different problems, namely shock capturing and sharp boundary layer resolution, piecefully coexist in the realm of analytical research in the CFD field. It is well known that while first order upwind type methods are preferable to deal with the first problem, with high order methods failing miserably in the shock capturing task, high order resolution is required in the later case. Various methods have been developed recently to deal exclusively with shock wave problems

(Leonard 1991, Hu and Shu, 1998, Iannelli, 1999) with solution monotonicity being the driving force behind the method derivation. The accuracy is clearly not an issue in this case and the first order deals with the problem, providing excellent solutions.

Sharp boundary layers of the convection dominated problems present a significantly different challenge. While at the first glance, sharp boundary layers have a shock-like appearance, they are not infinitisemally small surfaces along which solution properties change in a jump, but rather finite, if not very sizable, subdomains with abrupt but continuous change in solution characteristics. Solution resolution inside of the layer as opposed to simply identifying its location, thus becomes extremely important, and cannot be achieved by shock capturing methods with their design low order of accuracy.

Figure 5.1 [1] presents solutions obtained for the steady-state one-dimensional advection diffusion equation (5.6) with viscosity parameter set to $\varepsilon = 0.001$ on a uniform 21-node mesh. Figure 5.1a presents fourth order solution, while Figure 5.1b. illustrates numerical solution obtained using the upwind formulation (5.20). In accordance with the previous results, high order solution is overdiffused, signaling insufficient mesh refinement for adequate layer resolution. In contrast upwind solution evidences expected monotonicity and allows for identifying boundary layer location. As expected, upwind formulation does a better job in its design goal of effectively

[1] all figures may be found in Appendix I

locating potential solution discontinuities. As illustrated earlier high order method would require additional mesh refinement.

Figure 5.2 shows comparative method performance in resolving solution inside of the layer. Figure 5.2a gives solution computed over the entire solution domain for $\varepsilon = 0.05$ on a uniform 11-node mesh, while for illustrative purposes only Figures 5.2b and 5.2c are limited to the portion of the domain containing the boundary layer. Results in Figure 5.2b were computed for $\varepsilon = 0.01$ on a 41-node uniform mesh, while Figure 5.2c is for $\varepsilon = 0.001$ on a 401-node uniform mesh. Exact solution is shown as a dash line for comparison.

Numerical results confirm that high order correction method allows for superior resolution of interior layer features. Its performance is enhanced by the error correction dependence on the value of the viscosity parameter ε, which provides an optimal amount of artificial diffusion for various levels of physical diffusivity. First order accurate upwind formulation fails to resolve the layer and additional mesh refinement does not result in significant improvement. These results emphasize the important distinction between shock capturing and layer resolution.

5.6. Uniformly high order time-space corrections.

The high order spatial discretization approach developed above provides a unique way of unifying time-space correction approaches. The spatial discretization correction theory complements the Lax-Wendroff error corrections with its spatial counter-

parts, thus allowing for a uniform high order approximation in both time and space, while retaining solution matrix bandwidth of lower order methods. Since the initial three-node spatial discretization is the theoretical goal of algorithm development in one dimension, it is important to avoid the use of third and higher order space derivatives at time step $n+1$ in (5.10). This can be achieved by setting $\theta=1/3$. The remaining second order time derivative, which in turn introduces third and fourth order space derivatives into (5.10) via (5.8-5.9), is then evaluated at the time step n which does not increase the computation cost in any meaningful way, since these become parts of the residual (right hand side) formation. The solution matrix bandwidth does not increase in this case. It is necessary to note at this point, that while in general the non-diffusive trapezoidal rule $\theta=1/2$ is the weapon of choice in evaluating (5.10), and $\theta=1/3$ algorithm by itself usually produces unacceptable computational results, the developed high order correction theory is demonstrated below to completely remedy this problem, allowing for a uniformly high order space-time discretization.

The fourth order accurate time algorithm written for $\theta=1/3$ requires the following evaluation of (5.9)

$$\begin{aligned} q^{n+1} - q^n - \frac{\triangle t}{3}\left(-u\frac{\partial q^{n+1}}{\partial x} + \varepsilon\frac{\partial^2 q^{n+1}}{\partial x^2}\right) - \frac{2\triangle t}{3}\left(-u\frac{\partial q^{n}}{\partial x} + \varepsilon\frac{\partial^2 q^{n}}{\partial x^2}\right) \\ - \frac{\triangle t^2}{6}\left(u^2\frac{\partial^2 q^n}{\partial x^2} - 2u\varepsilon\frac{\partial^3 q^n}{\partial x^3} + \varepsilon^2\frac{\partial^4 q^n}{\partial x^4}\right) = 0 \end{aligned} \tag{5.22}$$

The three-node spatial discretization of (5.22) is

$$
\begin{aligned}
&Q_j^{n+1} - Q_j^n + \frac{\triangle t u}{3}(a_1 Q_{j-1}^{n+1} + a_2 Q_j^{n+1} + a_3 Q_{j+1}^{n+1}) \\
&-\frac{\varepsilon \triangle t}{3}(a_4 Q_{j-1}^{n+1} + a_5 Q_j^{n+1} + a_6 Q_{j+1}^{n+1}) = \\
&-\frac{2\triangle t u}{3}(a_1 Q_{j-1}^{n} + a_2 Q_j^{n} + a_3 Q_{j+1}^{n}) \\
&+\frac{2\triangle t \varepsilon}{3}(a_4 Q_{j-1}^{n} + a_5 Q_j^{n} + a_6 Q_{j+1}^{n}) \\
&+\frac{\triangle t^2 u^2}{6}(a_4 Q_{j-1}^{n} + a_5 Q_j^{n} + a_6 Q_{j+1}^{n}) \\
&-\frac{\triangle t^2 u \varepsilon}{3}(b_1 Q_{j-2}^{n} + b_2 Q_{j-1}^{n} + b_3 Q_j^{n} + b_4 Q_{j+1}^{n} + b_5 Q_{j+2}^{n}) \\
&+\frac{\triangle t^2 \varepsilon^2}{6}(c_1 Q_{j-2}^{n} + c_2 Q_{j-1}^{n} + c_3 Q_j^{n} + c_4 Q_{j+1}^{n} + c_5 Q_{j+2}^{n})
\end{aligned}
\tag{5.23}
$$

where Q_j^n replaces q^n as a fully discrete nodal solution and $b_i, c_i, i = 1, ..., 5$ are the coefficients of the central five-node discretizations of third and fourth order derivatives respectively. Note that both are evaluated at the time step n and thus do not result in the solution matrix of larger bandwidth. Coefficients are given by

$$
b_1 = -\frac{1}{2h^3}, \qquad b_2 = \frac{1}{h^3}, \qquad b_3 = 0, \qquad b_4 = -\frac{1}{h^3}, \qquad b_5 = \frac{1}{2h^3} \tag{5.24}
$$

$$
c_1 = \frac{1}{h^4}, \qquad c_2 = -\frac{4}{h^4}, \qquad c_3 = \frac{6}{h^4}, \qquad c_4 = -\frac{4}{h^4}, \qquad c_5 = \frac{1}{h^4} \tag{5.25}
$$

The discrete expression in (5.23) provides a fourth order time, second order space approximation. The fourth order space correction terms are derived via the theoretical approach of the previous sections to provide a uniform high order space-time discretization. With Q^n replacing Q_j^n for clarity, Taylor series expansion of (5.23) provides

$$\begin{aligned} Q^{n+1} + \frac{\triangle tu}{3}Q_x^{n+1} + \frac{\triangle tuh^2}{18}Q_{xxx}^{n+1} - \frac{\varepsilon\triangle t}{3}Q_{xx}^{n+1} - \frac{\varepsilon\triangle th^2}{36}Q_{xxxx}^{n+1} = \\ Q^n - \frac{2\triangle tu}{3}Q_x^n - \frac{\triangle tuh^2}{9}Q_{xxx}^n + \left(\frac{2\triangle t\varepsilon}{3} + \frac{\triangle t^2u^2}{6}\right)Q_{xx}^n \\ + \left(\frac{\triangle t\varepsilon}{18} + \frac{\triangle t^2u^2}{72}\right)h^2Q_{xxxx}^n - \frac{\triangle t^2u\varepsilon}{3}Q_{xxx}^n - \frac{\triangle t^2u\varepsilon h^2}{12}Q_{xxxx}^n \\ + \frac{\triangle t^2\varepsilon^2}{6}Q_{xxxx}^n + \frac{\triangle t^2\varepsilon^2h^2}{36}Q_{xxxxxx}^n \end{aligned} \tag{5.26}$$

To eliminate spatial derivatives of the order greater than two at time step $n+1$, whose evaluation would result in larger solution matrix bandwidth, one can now introduce higher order correction terms as demonstrated earlier in the previous sections. Rewritting (5.26) and neglecting the terms of the order greater or equal to two as shown in (3.14) yields the following expressions

$$\begin{aligned} Q_{xx}^{n+1} = &\frac{3}{\varepsilon\triangle t}Q^{n+1} + \frac{u}{\varepsilon}Q_x^{n+1} - \frac{3}{\varepsilon\triangle t}Q^n + \frac{2u}{\varepsilon}Q_x^n \\ &- \left(2 + \frac{\triangle tu^2}{2\varepsilon}\right)Q_{xx}^n + \triangle tuQ_{xxx}^n - \frac{\triangle t\varepsilon}{2}Q_{xxxx}^n \end{aligned} \tag{5.27}$$

Differentiating (5.27) repeatedly with respect to x yields

$$\begin{aligned} Q^{n+1}_{xxx} =& \frac{3}{\varepsilon\triangle t}Q^{n+1}_{x} + \frac{u}{\varepsilon}Q^{n+1}_{xx} - \frac{3}{\varepsilon\triangle t}Q^{n}_{x} + \frac{2u}{\varepsilon}Q^{n}_{xx} \\ & - \left(2 + \frac{\triangle t u^2}{2\varepsilon}\right) Q^{n}_{xxx} + \triangle t u Q^{n}_{xxxx} - \frac{\triangle t \varepsilon}{2} Q^{n}_{xxxxx} \end{aligned} \tag{5.28}$$

$$\begin{aligned} Q^{n+1}_{xxxx} =& \frac{3}{\varepsilon\triangle t}Q^{n+1}_{xx} + \frac{u}{\varepsilon}Q^{n+1}_{xxx} - \frac{3}{\varepsilon\triangle t}Q^{n}_{xx} + \frac{2u}{\varepsilon}Q^{n}_{xxx} \\ & - \left(2 + \frac{\triangle t u^2}{2\varepsilon}\right) Q^{n}_{xxxx} + \triangle t u Q^{n}_{xxxxx} - \frac{\triangle t \varepsilon}{2} Q^{n}_{xxxxxx} \end{aligned} \tag{5.29}$$

Substituting (5.28) and (5.29) back into (5.26) allows for expressing the truncation error in the form

$$\begin{aligned} & Q^{n+1} + \frac{\triangle t u}{3}Q^{n+1}_{x} - \frac{\varepsilon\triangle t}{3}Q^{n+1}_{xx} - Q^{n} + \frac{2\triangle t u}{3}Q^{n}_{x} \\ & - \left(\frac{2\triangle t\varepsilon}{3} + \frac{\triangle t^2 u^2}{6}\right) Q^{n}_{xx} + \frac{\triangle t^2 u\varepsilon}{3}Q^{n}_{xxx} - \frac{\triangle t^2\varepsilon^2}{6}Q^{n}_{xxxx} \\ & + h^2\triangle t[\frac{u}{12\varepsilon\triangle t}Q^{n+1}_{x} + \left(\frac{u^2}{36\varepsilon} - \frac{1}{12\triangle t}\right) Q^{n+1}_{xx} - \frac{u}{12\varepsilon\triangle t}Q^{n}_{x} \\ & + \left(\frac{u^2}{18\varepsilon} + \frac{1}{12\triangle t}\right) Q^{n}_{xx} - \frac{\triangle t u^3}{72\varepsilon}Q^{n}_{xxx} + \frac{\triangle t u^2}{36}Q^{n}_{xxxx} \\ & + \frac{\triangle t u\varepsilon}{24}Q^{n}_{xxxxx} - \frac{\triangle t\varepsilon^2}{72}Q^{n}_{xxxxxx}] = 0 \end{aligned} \tag{5.30}$$

The unsteady analog of the modified PDE concept developed in the previous sections for the steady-state case can be now obtained by reversing signs on the

h^2 terms in (5.30). Note that only first and second order spatial derivatives need to be evaluated at the time step $n+1$ thus containing solution matrix bandwidth expansion. Also fifth and sixth order spatial derivatives are now required at the time step n. The uniformly fourth order space-time algorithm for the original equation (5.6) now becomes

$$Q_j^{n+1} + \left(\frac{\triangle tu}{3} - \frac{h^2 u}{12\varepsilon}\right)(a_1 Q_{j-1}^{n+1} + a_2 Q_j^{n+1} + a_3 Q_{j+1}^{n+1})$$

$$+ \left(\frac{h^2}{12} - \frac{h^2 u^2 \triangle t}{36\varepsilon} - \frac{\varepsilon \triangle t}{3}\right)(a_4 Q_{j-1}^{n+1} + a_5 Q_j^{n+1} + a_6 Q_{j+1}^{n+1}) =$$

$$Q_j^n - \left(\frac{2\triangle tu}{3} + \frac{h^2 u}{12\varepsilon}\right)(a_1 Q_{j-1}^n + a_2 Q_j^n + a_3 Q_{j+1}^n)$$

$$+ \left(\frac{2\triangle t\varepsilon}{3} + \frac{\triangle t^2 u^2}{6} + \frac{h^2 u^2 \triangle t}{18\varepsilon} + \frac{h^2}{12}\right)(a_4 Q_{j-1}^n + a_5 Q_j^n + a_6 Q_{j+1}^n) \tag{5.31}$$

$$- \left(\frac{\triangle t^2 u\varepsilon}{3} + \frac{h^2 \triangle t^2 u^3}{72\varepsilon}\right)(b_1 Q_{j-2}^n + b_2 Q_{j-1}^n + b_3 Q_j^n + b_4 Q_{j+1}^n + b_5 Q_{j+2}^n)$$

$$+ \left(\frac{\triangle t^2 \varepsilon^2}{6} + \frac{h^2 \triangle t^2 u^2}{36}\right)(c_1 Q_{j-2}^n + c_2 Q_{j-1}^n + c_3 Q_j^n + c_4 Q_{j+1}^n + c_5 Q_{j+2}^n)$$

$$+ \frac{h^2 \triangle t^2 u\varepsilon}{24}(d_1 Q_{j-3}^n + d_2 Q_{j-2}^n + d_3 Q_{j-1}^n + d_4 Q_j^n + d_5 Q_{j+1}^n + d_6 Q_{j+2}^n + d_7 Q_{j+3}^n)$$

$$- \frac{h^2 \triangle t^2 \varepsilon^2}{72}(e_1 Q_{j-3}^n + e_2 Q_{j-2}^n + e_3 Q_{j-1}^n + e_4 Q_j^n + e_5 Q_{j+1}^n + e_6 Q_{j+2}^n + e_7 Q_{j+3}^n)$$

Nodal coefficients d_i, e_i responsible for seven-node discretization of the fifth and sixth order spatial derivatives in (5.31) are given by

$$\begin{aligned} d_1 &= -\frac{1}{2h^5}, \quad d_2 = \frac{2}{h^5}, \quad d_3 = -\frac{5}{2h^5}, \quad d_4 = 0 \\ d_5 &= \frac{5}{2h^5}, \quad d_6 = -\frac{2}{h^5}, \quad d_7 = \frac{1}{2h^5} \end{aligned} \tag{5.32}$$

$$\begin{aligned} e_1 &= \frac{1}{h^6}, \quad e_2 = -\frac{6}{h^6}, \quad e_3 = \frac{15}{h^6}, \quad e_4 = -\frac{20}{h^6} \\ e_5 &= \frac{15}{h^6}, \quad e_6 = -\frac{6}{h^6}, \quad e_7 = \frac{1}{h^6} \end{aligned} \tag{5.33}$$

Chapter 6

High order formulation for non-linear equation systems.

6.1 Flows in a converging-diverging nozzle. Euler equations.

6.1.1 Problem statement.

Consider isenropic flow in a converging-diverging nozzle with geometry definition as (Iannelli, 1999)

$$A(x) = \begin{cases} 1.75 - 0.75\cos[2(x-0.5)\pi], & 0.0 \le x \le 0.5 \\ \\ 1.25 - 0.25\cos[2(x-0.5)\pi], & 0.5 \le x \le 1.0 \end{cases} \tag{6.1}$$

The flow in the converging part is subsonic and if the oulet pressure is low enough there will be supersonic flow in the diverging portion. When the back pressure is equal to the design pressure ratio specific to a particular nozzle geometry the diverging flow is entirely supersonic, otherwise a normal shock occurs in the diverging section, with its location uniquely defined by the back pressure. Analytical steady solution is well-known and is readily available (see for example White, 1979).

The quasi-one dimensional inviscid (Euler) equations describing the flow are

$$L(q) = \frac{\partial q}{\partial t} + \frac{\partial f}{\partial x} - s = 0 \tag{6.2}$$

where

$$q = \begin{pmatrix} \rho \\ m \\ E \end{pmatrix}, \qquad f = \begin{pmatrix} m \\ \frac{m^2}{\rho} + p \\ \frac{(E+p)m}{\rho} \end{pmatrix}, \qquad s = \begin{pmatrix} -m\frac{d\ln A(x)}{dx} \\ -\frac{m^2}{\rho}\frac{d\ln A(x)}{dx} \\ -\frac{(E+p)m}{\rho}\frac{d\ln A(x)}{dx} \end{pmatrix} \tag{6.3}$$

$$p = (\gamma - 1)\left[E - \frac{m^2}{2\rho}\right] \tag{6.4}$$

Here ρ is density, E volume specific total energy, p pressure, $A(x)$ nozzle cross sectional area distribution, γ ratio of specific heats. For a perfect gas this system is closed by the polytropic equation of state

$$E = \frac{p}{\gamma - 1} + \frac{1}{2}\rho u^2 \tag{6.5}$$

where $u = m/\rho$ is the flow velocity. The verification steady state test corresponds to the impulsive decrease of the subsonic-outlet boundary condition to $p_{out} = 0.84$ which places the normal shock at the area ratio $A_s/A_{in} = 1.09896$, which corresponds to $x = 0.64675$. The exact shock Mach numbers are $M_{sup} = 1.36989$ and $M_{sub} = 0.75274$ (Iannelli, 1999).

This problem is usually employed to test algorithm capability to provide stable transition of shocked flows to the corresponding steady-state regime (Baker et al., 1999, Iannelli, 1999). The nozzle cross-section area distribution while continuous with continuous slopes, evidences a discontinuous slope curvature which provides additional insight into algorithm resolution. Since the goal of this work is to investigate

the effect of high order spatial approximation on the algorithm performance, furher developments concentrate on the steady-state form of (6.2) with the Dirichlet boundary conditions set by the corresponding analytical solution.

6.1.2 High order formulation.

Using (6.3) one can expand (6.2) in the form

$$\begin{cases} \frac{d\rho u}{dx} + \rho u \frac{d\ln A(x)}{dx} = 0 \\ 0.8\frac{d\rho u^2}{dx} + 0.4\frac{dE}{dx} + \rho u^2 \frac{d\ln A(x)}{dx} = 0 \\ 1.4\frac{dEu}{dx} - 0.2\frac{d\rho u^3}{dx} + (1.4Eu - 0.2\rho u^3)\frac{d\ln A(x)}{dx} = 0 \end{cases} \tag{6.6}$$

or

$$\begin{cases} \rho\frac{du}{dx} + u\frac{d\rho}{dx} + \rho u \frac{d\ln A(x)}{dx} = 0 \\ 1.6\rho u\frac{du}{dx} + 0.8u^2\frac{d\rho}{dx} + 0.4\frac{dE}{dx} + \rho u^2 \frac{d\ln A(x)}{dx} = 0 \\ 1.4E\frac{du}{dx} + 1.4u\frac{dE}{dx} - 0.6\rho u^2\frac{du}{dx} - 0.2u^3\frac{d\rho}{dx} + (1.4Eu - 0.2\rho u^3)\frac{d\ln A(x)}{dx} = 0 \end{cases} \tag{6.7}$$

The second order discretization of (6.7) is obtained from (22) as

$$R_j(a_1U_{j-1} + a_2U_j + a_3U_{j+1}) + U_j(a_1R_{j-1} + a_2R_j + a_3R_{j+1}) + R_jU_jS_j = 0 \tag{6.8}$$

$$\begin{aligned} 1.6R_jU_j(a_1U_{j-1} + a_2U_j + a_3U_{j+1}) + 0.8U_j^2(a_1R_{j-1} + a_2R_j + a_3R_{j+1}) \\ + 0.4(a_1E_{j-1} + a_2E_j + a_3E_{j+1}) + R_jU_j^2S_j = 0 \end{aligned} \tag{6.9}$$

$$\begin{aligned} 1.4E_j(a_1U_{j-1} + a_2U_j + a_3U_{j+1}) + 1.4U_j(a_1E_{j-1} + a_2E_j + a_3E_{j+1}) \\ -0.6R_jU_j^2(a_1U_{j-1} + a_2U_j + a_3U_{j+1}) - 0.2U_j^3(a_1R_{j-1} + a_2R_j + a_3R_{j+1}) \\ +(1.4E_jU_j - 0.2R_jU_j^3)S_j = 0 \end{aligned} \tag{6.10}$$

Here, $\{R_j\}, \{U_j\}, \{E_j\}$ are the unknown nodal values of density (ρ), velocity (u) and energy (E), coefficints a_i are given by (23), and

$$S_j = \frac{d \ln A(x_j)}{dx} \tag{6.11}$$

In order to develop a fourth order approximation to (6.7), it is critically important to note that each equation of the system must be considered separately. In that, while three equations form the system, the modified PDE obtained by a Taylor series expansion is a unique characteristic of the expanded difference equation itself. Any term substitution among equations inside the system would therefore compromise the consistency of the original conservation law system. This can potentially complicate applicability of the current approach since each equation in a system includes several independent variables thus making it difficult to reduce the order of the perturbed PDE via differentiation.

With this in mind, proceeding with a Taylor series expansion of (6.8-6.10) at node j, the following modified system is obtained

$$RU_x + UR_x + RUS + \frac{h^2}{6}[RU_{xxx} + UR_{xxx}] + H.O.T. = 0 \tag{6.12}$$

$$\begin{gathered} 1.6RUU_x + 0.8U^2R_x + 0.4E_x + RU^2S \\ + \frac{h^2}{6}[1.6RUU_{xxx} + 0.8U^2R_{xxx} + 0.4E_{xxx}] + H.O.T. = 0 \end{gathered} \tag{6.13}$$

$$1.4EU_x + 1.4UE_x - 0.6RU^2U_x - 0.2U^3R_x + (1.4EU - 0.2RU^3)S$$
$$+\frac{h^2}{6}[1.4EU_{xxx} + 1.4UE_{xxx} - 0.6RU^2U_{xxx} - 0.2U^3R_{xxx}] + H.O.T. = 0 \tag{6.14}$$

where R, U, E, S replace the corresponding nodal values of R_j, U_j, E_j, S_j for simplicity, and subscripts denote partial derivative of the corresponding order.

Differntiating each equation twice with respect to x yields

$$RU_{xxx} + UR_{xxx} = -3R_{xx}U_x - 3R_xU_{xx} - R_{xx}US$$
$$-2R_xU_xS - 2R_xUS_x - RU_{xx}S - 2RU_xS_x - RUS_{xx} + H.O.T. \tag{6.15}$$

$$1.6RUU_{xxx} + 0.8U^2R_{xxx} + 0.4E_{xxx} = -4.8R_{xx}UU_x - 4.8R_xU_x^2$$
$$-4.8RU_xU_{xx} - R_{xx}U^2S - 4R_xUSU_x - 2R_xU^2S_x - 2RU_x^2S - 4RUS_xU_x \tag{6.16}$$
$$-2RUSU_{xx} - RU^2S_{xx} - 4.8R_xUU_{xx} + H.O.T.$$

$$1.4EU_{xxx} + 1.4UE_{xxx} - 0.6RU^2U_{xxx} - 0.2U^3R_{xxx} = -4.2E_xU_{xx}$$
$$+1.8R_{xx}U^2U_x + 3.6R_xUU_x^2 + 1.8R_xU^2U_{xx} + 1.2RU_x^3 + 3.6RUU_xU_{xx}$$
$$-2.8SE_xU_x - 1.4SUE_{xx} - 1.4SEU_{xx} + 1.2SR_xU^2U_x + 0.2SU^3R_{xx} \tag{6.17}$$
$$+1.2SRUU_x^2 + 0.6SRU^2U_{xx} - 2.8S_xUE_x - 2.8S_{xx}EU_x + 0.4S_xU^3R_x$$
$$+1.2S_xRU^2U_x - 1.4S_{xx}EU + 0.2S_{xx}RU^3 - 4.2E_{xx}U_x + H.O.T.$$

Substituting these back into (6.12-6.14), the perturbed ODE system leading to the fourth order approximation of (6.7) is

$$\rho\frac{du}{dx}+u\frac{d\rho}{dx}+\rho u\frac{d\ln A(x_j)}{dx}+\frac{h^2}{6}[3\frac{d^2\rho}{dx^2}\frac{du}{dx}+3\frac{d^2u}{dx^2}\frac{d\rho}{dx}$$
$$+us\frac{d^2\rho}{dx^2}+2s\frac{d\rho}{dx}\frac{du}{dx}+2u\frac{d\rho}{dx}\frac{ds}{dx}+2\rho\frac{du}{dx}\frac{ds}{dx}+\rho s\frac{d^2u}{dx^2}+\rho u\frac{d^2s}{dx^2}]=0 \tag{6.18}$$

$$1.6\rho u\frac{du}{dx}+0.8u^2\frac{d\rho}{dx}+0.4\frac{de}{dx}+\rho u^2\frac{d\ln A(x_j)}{dx}$$
$$+\frac{h^2}{6}[4.8u\frac{d^2\rho}{dx^2}\frac{du}{dx}+4.8\frac{d\rho}{dx}\left(\frac{du}{dx}\right)^2+4.8u\frac{d\rho}{dx}\frac{d^2u}{dx^2}+4.8\rho\frac{du}{dx}\frac{d^2u}{dx^2}$$
$$+u^2s\frac{d^2\rho}{dx^2}+4us\frac{du}{dx}\frac{d\rho}{dx}+2u^2\frac{ds}{dx}\frac{d\rho}{dx}+2\rho s\left(\frac{du}{dx}\right)+4\rho u\frac{ds}{dx}\frac{du}{dx} \tag{6.19}$$
$$+2\rho us\frac{d^2u}{dx^2}+\rho u^2\frac{d^2s}{dx^2}]=0$$

$$1.4e\frac{du}{dx}+1.4u\frac{de}{dx}-0.6\rho u^2\frac{du}{dx}-0.2u^3\frac{d\rho}{dx}$$
$$+(1.4eu-0.2\rho u^3)\frac{d\ln A(x_j)}{dx}+\frac{h^2}{6}[4.2\frac{du}{dx}\frac{d^2e}{dx^2}+4.2\frac{de}{dx}\frac{d^2u}{dx^2}$$
$$-1.8u^2\frac{du}{dx}\frac{d^2\rho}{dx^2}-3.6u\left(\frac{du}{dx}\right)^2\frac{d\rho}{dx}-1.8u^2\frac{d\rho}{dx}\frac{d^2u}{dx^2}-1.2\rho\left(\frac{du}{dx}\right)^3 \tag{6.20}$$
$$+2.8s\frac{de}{dx}\frac{du}{dx}+1.4su\frac{d^2e}{dx^2}+1.4se\frac{d^2u}{dx^2}-1.2su^2\frac{du}{dx}\frac{d\rho}{dx}-0.2su^3\frac{d^2\rho}{dx^2}$$
$$-1.2s\rho u\left(\frac{du}{dx}\right)^2-0.6s\rho u^2\frac{d^2u}{dx^2}+2.8u\frac{ds}{dx}\frac{de}{dx}+2.8e\frac{ds}{dx}\frac{du}{dx}-0.4u^3\frac{ds}{dx}\frac{d\rho}{dx}$$
$$-1.2\rho u^2\frac{ds}{dx}\frac{du}{dx}+1.4eu\frac{d^2s}{dx^2}-0.2\rho u^3\frac{d^2s}{dx^2}-3.6\rho u\frac{du}{dx}\frac{d^2u}{dx^2}]=0$$

6.1.3 Diffusion term introduction.

The high order formulation of the previous section is applied directly to the original system (6.2). Since a well-known characteristic feature of the physics of the problem is the development of normal shock wave upstream of the nozzle throat, one may expect the numerical solution to become oscillatory in the vicinity of the wave. High order discretizations are known to exaggerate the problem due to the Gibbs phenomenon (Harten et al., 1987, Morton and Sweby, 1987) suggesting low order interpolation across the wave front. This leads one to look for ways of adapting the designed theoretical procedure to solve the problem at hand.

Since most of the numerical methods attempt to resolve shocks by resorting to various diffusion mechanisms, one immediately obvious way to proceed is to directly outfit both fourth and second order methods with the corresponding diffusion terms and compare their relative performance. Towards this goal diffusive terms of the form

$$-\varepsilon\frac{\partial^2\rho}{\partial x^2}, \qquad -\varepsilon\frac{\partial^2 u}{\partial x^2}, \qquad -\varepsilon\frac{\partial^2 e}{\partial x^2} \tag{6.21}$$

were added to their respective equations in both methods. Approximation of these terms could be carried out in a manner consistent with (4.8) with no additional modifications made to the developed fourth order system (6.18-6.20). As a result its approximation order is reduced to that of the second order system. Of course, this rather rude development is not expected to produce very accurate results. In fact, the resulting numerical solution is overly diffused as shown in Chapter 7.

While one might argue that a uniformly fourth order method could remedy the situation, all attempts to design one directly following the theoretical procedure developed above did not succeed, due to the lack of symmetry in the partial derivative groups, which was the direct result of adding the diffusive terms. For the uniformly fourth order approximation to be achieved, it is therefore necessary to search for some other ideas for implementing this strategy.

6.1.4 High order formulation for Euler equations.

As noted, the theory applicability rests on the possibility of expressing higher order derivatives via their lower order counterparts achieved via repeated differentiation of the corresponding modified equation which is in turn obtained by a Taylor series expansion. For this technique to work for conservation law systems the approximating difference equations must possess certain symmetry among different partial derivative group entries of the system equations. It seems that in general some additional work is required to formulate the system in a desirable *symmetrical* form. In the particular case of Euler equations one can achieve this goal by a relatively straight forward analysis outlined in this section.

Since any implementation of the developed theory implies the ability to express high order derivatives via those of lower order, introduction of a second order diffusion term is a necessary condition. As shown in the previous section, direct introduction does not yield satisfactory results, hence the approach requires optimization. It is

clear from the theory developed for the advection-diffusion problem that the equation of the type

$$\frac{dq(x)}{dx} - \varepsilon \frac{d^2q(x)}{dx^2} + s(x) = 0 \tag{6.22}$$

can be efficiently approximated by the designed discretization procedure, regardless of the exact form of the functions $q(x), s(x)$. The later is true since the unknown function $q(x)$ is to be included symmetrically into the modified equation as defined by approximation (4.8). The source function $s(x)$ is to be differentiated twice in developing the fourth order modified equation, thus producing various combinations of at most second order derivatives of the unknown variables, whose three-node discretization is then available via (4.8).

With this in mind consider the following substitution

$$\begin{cases} f_1(x) = \rho(x)u(x) \\ f_2(x) = 0.8\rho(x)u^2(x) + 0.4e(x) \\ f_3(x) = 1.4e(x)u(x) - 0.2\rho(x)u^3(x) \end{cases} \tag{6.23}$$

The backward transformation is provided by

$$\begin{cases} \rho(x) = \frac{f_1(x)}{u(x)} \\ e(x) = 2.5f_2(x) - 2f_1(x)u(x) \\ 3f_1(x)u^2(x) - 3.5f_2(x)u(x) + f_3(x) = 0 \end{cases} \tag{6.24}$$

Hence, for given $f_1(x), f_2(x), f_3(x)$ and $u(x)$, the nodal values of $\rho(x), e(x)$ can be

found via (6.24). The parent Euler equation system (6.2) is now replaced by

$$\begin{cases} \frac{df_1(x)}{dx} - \varepsilon \frac{d^2 f_1(x)}{dx^2} + f_1(x) \frac{d \ln A(x_j)}{dx} = 0 \\ \frac{df_3(x)}{dx} - \varepsilon \frac{d^2 f_3(x)}{dx^2} + f_3(x) \frac{d \ln A(x_j)}{dx} = 0 \\ \frac{df_2(x)}{dx} - \varepsilon \frac{d^2 f_2(x)}{dx^2} + f_1(x) u(x) \frac{d \ln A(x_j)}{dx} = 0 \\ 3 f_1(x) u^2(x) - 3.5 f_2(x) u(x) + f_3(x) = 0 \end{cases} \tag{6.25}$$

with the corresponding Dirichlet boundary conditions found from (6.23). Substitution (6.24) appears to be rather general and can be applied when dealing with multidimensional steady inviscid equations. It results in a system (6.25) which is larger than that approximated via the perturbed PDE analysis of the previous sections. The disadvantage of solving larger number of equations is therefore offset by the ability to efficiently implement a high order formulation.

In the present case this substitution results in further simplification. The first two equations are linear and not coupled with the rest of the system. They can be solved independently, providing the nodal values of $f_1(x)$ and $f_3(x)$. With these in hand $f_2(x)$ and $u(x)$ are then found by solving

$$\begin{cases} \frac{df_2(x)}{dx} - \varepsilon \frac{d^2 f_2(x)}{dx^2} + f_1(x) u(x) \frac{d \ln A(x_j)}{dx} = 0 \\ 3 f_1(x) u^2(x) - 3.5 f_2(x) u(x) + f_3(x) = 0 \end{cases} \tag{6.26}$$

and the nodal values of $\rho(x), e(x)$ are determined from (6.24) by simple substitution.

The second order approximation of (6.25) is obtained via (23). Development of the fourth order formulation starts by noting that the first two equations are of the form (6.22), which is considered as a general generic equation. Its second order formulation

via (23), followed by Taylor series expansion leads to the following modified equation

$$F_x - \varepsilon F_{xx} + FS + \frac{h^2}{6}\left[F_{xxx} - \frac{\varepsilon}{2}F_{xxxx}\right] + H.O.T. = 0 \tag{6.27}$$

Here, $F = F_j$ are the nodal values of the unknown function $f(x)$, and $S = S_j$ are the nodal values of the source function given by (6.11). Rewriting (6.27) and differentiating the resultant expression by x and xx yields

$$F_{xx} = \frac{1}{\varepsilon}[F_x + FS] + H.O.T. \tag{6.28}$$

$$F_{xxx} = \frac{1}{\varepsilon}[F_{xx} + F_x S + FS_x] + H.O.T. \tag{6.29}$$

$$F_{xxxx} = \frac{1}{\varepsilon}[F_{xxx} + F_{xx}S + 2F_x S_x + FS_{xx}] + H.O.T. \tag{6.30}$$

Substituting (6.28-6.30) back into (6.27), then reversing the signs of the correction error terms, provides the generic fourth order perturbed ODE in the form

$$\frac{df}{dx} - \varepsilon\frac{d^2f}{dx^2} + f\frac{d\ln A(x_j)}{dx} - \frac{h^2}{12\varepsilon}\left[\frac{d^2f}{dx^2} + s\frac{df}{dx} + f\frac{ds}{dx}\right] + \frac{h^2}{12}\left[s\frac{d^2f}{dx^2} + 2\frac{ds}{dx}\frac{df}{dx} + f\frac{d^2f}{dx^2}\right] = 0 \tag{6.31}$$

The next step is development of the fourth order approximation of (6.26). Since the second equation in (6.26) does not contain partial derivatives, hence will not produce truncation error terms upon its discretization, only the first equation of the

system requires modification. Noting again that the exact form of the source term is of no relevance in the present analysis, and making the convenient substitution

$$y(x) = f_1(x)u(x)\frac{d\ln A(x_j)}{dx}, \qquad Y = Y_j = F_{1j}U_jS_j \tag{6.32}$$

one obtains the following modified equation

$$F_x - \varepsilon F_{xx} + Y + \frac{h^2}{6}[F_{xxx} - \frac{\varepsilon}{2}F_{xxxx}] + H.O.T. = 0 \tag{6.33}$$

Rewriting (6.33) and differentiating it repeatedly with respect to x yields the following expressions

$$F_{xx} = \frac{1}{\varepsilon}[F_x + Y] + H.O.T. \tag{6.34}$$

$$F_{xxx} = \frac{1}{\varepsilon}[F_{xx} + Y_x] + H.O.T. \tag{6.35}$$

$$F_{xxxx} = \frac{1}{\varepsilon}[F_{xxx} + Y_{xx}] + H.O.T. \tag{6.36}$$

which upon substitution into (6.33) results in the following fourth order perturbed ODE

$$\frac{df_2}{dx} - \varepsilon\frac{d^2f_2}{dx^2} + y(x) - \frac{h^2}{12\varepsilon}\left(\frac{d^2f_2}{dx^2} + \frac{dy}{dx}\right) + \frac{h^2}{12}\frac{d^2y}{dx^2} = 0 \tag{6.37}$$

The complete fourth order perturbed system is now

$$\begin{cases} \frac{df_1}{dx} - \varepsilon\frac{d^2f_1}{dx^2} + f_1\frac{d\ln A(x_j)}{dx} - \frac{h^2}{12\varepsilon}\left[\frac{d^2f_1}{dx^2} + s\frac{df_1}{dx} + f_1\frac{ds}{dx}\right] + \\ \frac{h^2}{12}\left[s\frac{d^2f_1}{dx^2} + 2\frac{ds}{dx}\frac{df_1}{dx} + f_1\frac{d^2f_1}{dx^2}\right] = 0 \\ \frac{df_3}{dx} - \varepsilon\frac{d^2f_3}{dx^2} + f_3\frac{d\ln A(x_j)}{dx} - \frac{h^2}{12\varepsilon}\left[\frac{d^2f_3}{dx^2} + s\frac{df_3}{dx} + f_3\frac{ds}{dx}\right] + \\ \frac{h^2}{12}\left[s\frac{d^2f_3}{dx^2} + 2\frac{ds}{dx}\frac{df_3}{dx} + f_3\frac{d^2f_3}{dx^2}\right] = 0 \\ \frac{df_2}{dx} - \varepsilon\frac{d^2f_2}{dx^2} + f_1u\frac{d\ln A(x_j)}{dx} - \frac{h^2}{12\varepsilon}\left[\frac{d^2f_2}{dx^2} + us\frac{df_1}{dx} + f_1s\frac{du}{dx} + f_1u\frac{ds}{dx}\right] + \\ \frac{h^2}{12}\left[us\frac{d^2f_1}{dx^2} + 2s\frac{du}{dx}\frac{df_1}{dx} + 2u\frac{ds}{dx}\frac{df_1}{dx} + 2f_1\frac{ds}{dx}\frac{du}{dx} + f_1s\frac{d^2u}{dx^2} + f_1u\frac{d^2s}{dx^2}\right] = 0 \\ 3f_1(x)u^2(x) - 3.5f_2(x)u(x) + f_3(x) = 0 \end{cases} \tag{6.38}$$

6.1.5. Spatial filtering.

The numerical solution computed using the developed fourth order method may still require some additional work in and around the sonic throat. Spatial filtering technique outlined by Visbal and Gaitonde (1998), is the method of choice in this section. Being a postprocessing operation this method allows for selective phase filtering of dispersive error modes, while retaining a uniformly high order of the filtered numerical solution. Denoting a component of the solution vector by Q, filtered values Q^f can be obtained by solving the following tridiagonal algebraic system

$$\alpha_f Q^f_{i-1} + Q^f_i + \alpha_f Q^f_{i+1} = \sum_{n=0}^{N} \frac{a_n}{2}(Q_{i+n} + Q_{i-n}) \tag{6.39}$$

This formula provides Nth order filter with a $2N+1$ node stencil. It can be shown that the spectral function of the filtering operator (6.39) is

$$SF(\omega) = \frac{\sum_{n=0}^{N} a_n cos(n\omega)}{1 + 2\alpha_f cos(\omega)} \tag{6.40}$$

The symmetry of the operator (6.39) provides for SF to be real and non-dispersive. The $N+1$ unknowns a_i are derived by Taylor series analysis, while α_f is retained as a free variable which must remain within the range $-0.5 \leq \alpha_f \leq 0.5$, where $\alpha_f = -0.5$ delivers the largest amount of diffusion. Derivation of the 8th-order filter is given below for clarity.

Derivation of the 8th-order filter requires setting $N = 4$ and (6.39) is rewritten as

$$\begin{aligned} \alpha_f Q^f_{i-1} + Q^f_i + \alpha_f Q^f_{i+1} = \frac{a_4}{2}(Q_{i+4} + Q_{i-4}) + \frac{a_3}{2}(Q_{i+3} + Q_{i-3}) \\ + \frac{a_2}{2}(Q_{i+2} + Q_{i-2}) + \frac{a_1}{2}(Q_{i+1} + Q_{i-1}) + a_0 Q_i \end{aligned} \tag{6.41}$$

Performing Taylor series expansion of nodal solution entries in (6.41) around node j yields

$$Q_{i+1} + Q_{i-1} = 2Q_i + h^2 Q_i^{(2)} + \frac{h^4}{12} Q_i^{(4)} + \frac{h^6}{360} Q_i^{(6)} + H.O.T. \tag{6.42}$$

$$Q_{i+2} + Q_{i-2} = 2Q_i + 4h^2 Q_i^{(2)} + \frac{4h^4}{3} Q_i^{(4)} + \frac{8h^6}{45} Q_i^{(6)} + H.O.T. \tag{6.43}$$

$$Q_{i+3} + Q_{i-3} = 2Q_i + 9h^2 Q_i^{(2)} + \frac{27h^4}{4} Q_i^{(4)} + \frac{81h^6}{40} Q_i^{(6)} + H.O.T. \tag{6.44}$$

$$Q_{i+4} + Q_{i-4} = 2Q_i + 16h^2 Q_i^{(2)} + \frac{64h^4}{3} Q_i^{(4)} + \frac{512h^6}{45} Q_i^{(6)} + H.O.T. \tag{6.45}$$

Substituting (6.42-6.45) into (6.41) results in

$$(2\alpha_f + 1)Q_i^f + h^2\alpha_f Q_i^{f(2)} + \frac{\alpha_f h^4}{12}Q_i^{f(4)} + \frac{\alpha_f h^6}{360}Q_i^{f(6)} =$$

$$Q_i(a_0 + a_1 + a_2 + a_3 + a_4) + h^2 Q_i^{(2)}(\frac{a_1}{2} + 2a_2 + \frac{9a_3}{2} + 8a_4) \tag{6.46}$$

$$+h^4 Q_i^{(4)}(\frac{a_1}{24} + \frac{2a_2}{3} + \frac{27a_3}{8} + \frac{32a_4}{3}) + h^6 Q_i^{(6)}(\frac{a_1}{720} + \frac{4a_2}{45} + \frac{81a_3}{80} + \frac{256a_4}{45})$$

Since the goal is to match the coefficients of the corresponding series up to the 8th-order, (6.46) provides four equations for five variables. The missing equation is given by the condition $SF(\pi) = 0$ which eliminates the odd-even mode. Solving the system yields

$$\begin{aligned} a_0 &= \frac{93 + 70\alpha_f}{128}, \qquad a_1 = \frac{7 + 18\alpha_f}{16}, \qquad a_2 = \frac{-7 + 14\alpha_f}{32} \\ a_3 &= \frac{1}{16} - \frac{\alpha_f}{8}, \qquad a_4 = -\frac{1}{128} + \frac{\alpha_f}{64}, \qquad a_5 = 0 \end{aligned} \tag{6.47}$$

6.1.6 Time dependent formulation

Now consider the time dependent formulation. The governing Euler system of equations remains (6.2). Introducing the second order diffusive derivatives and following the substitution pattern accepted for the steady-state case modifies it to

$$\begin{cases} \frac{\partial q}{\partial t} + \frac{\partial f}{\partial x} - \varepsilon\frac{\partial^2 q}{\partial x^2} + s(x) = 0 \\ \\ 3f_1(x)u^2(x) - 3.5f_2(x)u(x) + f_3(x) = 0 \end{cases} \tag{6.48}$$

where q, f and s are given in (6.3). Unlike the steady-state case, this is a coupled system of four equations and its only advantage over conventional high order formulations is in the equation symmetry, which in turn allows for containing solution

matrix bandwidth expansion. Note that the extra compatibility condition is a simple algebraic equation which must hold at all nodes of the solution domain. Its implementation does not require computational effort and extensive theoretical analysis usually accompanying numerical solution of differential equations.

The initial conditions are provided by the exact sonic, shock-free isentropic flow solution. The Dirichlet boundary conditions at the inlet are set equal to the initial condition. The outlet pressure is fixed to result in the normal shock wave propagating upstream as discussed for the steady-state case. This condition is relaxed when supersonic flow is achieved at the outlet during a numerical calculation.

Assuming sufficient continuity and performing semi-discretization in time using the standard θ-implicit method approximation yields

$$Q^{n+1} = Q^n + \triangle t \left(\theta \frac{dQ^{n+1}}{dt} + (1-\theta) \frac{dQ^n}{dt} \right) + O(\triangle t^2) \tag{6.49}$$

Here, Q is the nodal value of state variable q and n is the current time step.

Substituting (6.48) into (6.49), selecting non-dissipative trapesoidal rule (θ=1/2) for time integration and neglecting high order time derivative terms results in

$$\begin{aligned} Q^{n+1} = Q^n &+ \frac{\triangle t}{2} \left(-\frac{\partial F^{n+1}}{\partial x} + \varepsilon \frac{\partial^2 F^{n+1}}{\partial x^2} + S^{n+1} \right) \\ &+ \frac{\triangle t}{2} \left(-\frac{\partial F^n}{\partial x} + \varepsilon \frac{\partial^2 F^n}{\partial x^2} + S^n \right) \end{aligned} \tag{6.50}$$

where F, S are nodal values of functions $f_i(x)$ defined by the substitution (6.23) and source function $s(x)$ respectively.

Rewritting (6.50) in the form

$$\begin{aligned} &Q^{n+1} + \frac{\triangle t}{2}\left(\frac{\partial F^{n+1}}{\partial x} - \varepsilon\frac{\partial^2 F^{n+1}}{\partial x^2} - S^{n+1}\right) = \\ &Q^{n} + \frac{\triangle t}{2}\left(-\frac{\partial F^{n}}{\partial x} + \varepsilon\frac{\partial^2 F^{n}}{\partial x^2} + S^{n}\right) \end{aligned} \tag{6.51}$$

and introducing second order spatial discretization via (22) yields

$$\begin{aligned} &Q_j^{n+1} + \frac{\triangle t}{2}(a_1 F_{j-1}^{n+1} + a_2 F_j^{n+1} + a_3 F_{j+1}^{n+1}) \\ &\quad - \frac{\triangle t\varepsilon}{2}(a_4 F_{j-1}^{n+1} + a_5 F_j^{n+1} + a_6 F_{j+1}^{n+1}) - \frac{\triangle t}{2} S_j^{n+1} = \\ &Q_j^{n} - \frac{\triangle t}{2}(a_1 F_{j-1}^{n} + a_2 F_j^{n} + a_3 F_{j+1}^{n}) \\ &\quad + \frac{\triangle t\varepsilon}{2}(a_4 F_{j-1}^{n} + a_5 F_j^{n} + a_6 F_{j+1}^{n}) + \frac{\triangle t}{2} S_j^{n} \end{aligned} \tag{6.52}$$

This completes development of the second order numerical formulation. The fourth order spatial approximation is now thought via Taylor series analysis. Making the usual assumption of spatial mesh being sufficiently refined, expanding the second order stencil form (6.52) around node j, one obtains the modified PDE in the form

$$\begin{aligned} &Q^{n+1} + \frac{\triangle t}{2}F_x^{n+1} + \frac{\triangle t h^2}{12}F_{xxx}^{n+1} - \frac{\triangle t\varepsilon}{2}F_{xx}^{n+1} - \frac{\triangle t\varepsilon h^2}{24}F_{xxxx}^{n+1} - \frac{\triangle t}{2}S^{n+1} = \\ &= Q^{n} - \frac{\triangle t}{2}F_x^{n} - \frac{\triangle t h^2}{12}F_{xxx}^{n} + \frac{\triangle t\varepsilon}{2}F_{xx}^{n} + \frac{\triangle t\varepsilon h^2}{24}F_{xxxx}^{n} + \frac{\triangle t}{2}S^{n} + H.O.T. \end{aligned} \tag{6.53}$$

where Q, F, S replace nodal values Q_j, F_j, S_j for clarity and subscript denotes the corresponding spatial derivative. Collecting the terms of the order h^2 and neglecting

higher order terms leads to

$$\begin{aligned} & Q^{n+1} - Q^n + \frac{\triangle t}{2} F_x^{n+1} + \frac{\triangle t}{2} F_x^n - \frac{\triangle t\varepsilon}{2} F_{xx}^{n+1} - \frac{\triangle t\varepsilon}{2} F_{xx}^n - \frac{\triangle t}{2} S^{n+1} \\ & - \frac{\triangle t}{2} S^n + \frac{h^2 \triangle t}{12} [F_{xxx}^{n+1} - \frac{\varepsilon}{2} F_{xxxx}^{n+1} + F_{xxx}^n - \frac{\varepsilon}{2} F_{xxxx}^n] = 0 \end{aligned} \tag{6.54}$$

The following relationships then follow from (6.54) by differentiation. Recall that the fact that higher order terms in the modified equation (6.53) can now be neglected was proven in (3.14).

$$\frac{\triangle t\varepsilon}{2} F_{xx}^{n+1} = Q^{n+1} - Q^n + \frac{\triangle t}{2} F_x^{n+1} + \frac{\triangle t}{2} F_x^n - \frac{\triangle t\varepsilon}{2} F_{xx}^n - \frac{\triangle t}{2} S^{n+1} - \frac{\triangle t}{2} S^n \tag{6.55}$$

$$F_{xx}^{n+1} = \frac{2}{\triangle t\varepsilon} Q^{n+1} - \frac{2}{\triangle t\varepsilon} Q^n + \frac{1}{\varepsilon} F_x^{n+1} + \frac{1}{\varepsilon} F_x^n - F_{xx}^n - \frac{1}{\varepsilon} S^{n+1} - \frac{1}{\varepsilon} S^n \tag{6.56}$$

$$F_{xxx}^{n+1} = \frac{2}{\triangle t\varepsilon} Q_x^{n+1} - \frac{2}{\triangle t\varepsilon} Q_x^n + \frac{1}{\varepsilon} F_{xx}^{n+1} + \frac{1}{\varepsilon} F_{xx}^n - F_{xxx}^n - \frac{1}{\varepsilon} S_x^{n+1} - \frac{1}{\varepsilon} S_x^n \tag{6.57}$$

$$F_{xxxx}^{n+1} = \frac{2}{\triangle t\varepsilon} Q_{xx}^{n+1} - \frac{2}{\triangle t\varepsilon} Q_{xx}^n + \frac{1}{\varepsilon} F_{xxx}^{n+1} + \frac{1}{\varepsilon} F_{xxx}^n - F_{xxxx}^n - \frac{1}{\varepsilon} S_{xx}^{n+1} - \frac{1}{\varepsilon} S_{xx}^n \tag{6.58}$$

These can now be substituted back into (6.54), to express third and fourth order spatial derivatives via their first and second order counterparts, thus allowing a three-

node spatial discretization.

$$
\begin{aligned}
&Q^{n+1} + \frac{\triangle t}{2} F_x^{n+1} - \frac{\triangle t\varepsilon}{2} F_{xx}^{n+1} - \frac{\triangle t}{2} S^{n+1} \\
&+\frac{h^2 \triangle t}{12}[\frac{1}{\triangle t\varepsilon} Q_x^{n+1} - \frac{1}{\triangle t} Q_{xx}^{n+1} + \frac{1}{2\varepsilon} F_{xx}^{n+1} - \frac{1}{2\varepsilon} S_x^{n+1} + \frac{1}{2} S_{xx}^{n+1}] = \\
&Q^n - \frac{\triangle t}{2} F_x^n + \frac{\triangle t\varepsilon}{2} F_{xx}^n + \frac{\triangle t}{2} S^n \\
&-\frac{h^2 \triangle t}{12}[-\frac{1}{\triangle t\varepsilon} Q_x^n + \frac{1}{\triangle t} Q_{xx}^n + \frac{1}{2\varepsilon} F_{xx}^n - \frac{1}{2\varepsilon} S_x^n + \frac{1}{2} S_{xx}^n]
\end{aligned}
\tag{6.59}
$$

The modified time-discretized PDE providing the fourth order spatial discretization is obtained from (6.59) by reversing the signs on the h^2 correction terms as

$$
\begin{aligned}
&Q^{n+1} + \frac{\triangle t}{2} F_x^{n+1} - \frac{\triangle t\varepsilon}{2} F_{xx}^{n+1} - \frac{\triangle t}{2} S^{n+1} \\
&-\frac{h^2 \triangle t}{12}[\frac{1}{\triangle t\varepsilon} Q_x^{n+1} - \frac{1}{\triangle t} Q_{xx}^{n+1} + \frac{1}{2\varepsilon} F_{xx}^{n+1} - \frac{1}{2\varepsilon} S_x^{n+1} + \frac{1}{2} S_{xx}^{n+1}] = \\
&Q^n - \frac{\triangle t}{2} F_x^n + \frac{\triangle t\varepsilon}{2} F_{xx}^n + \frac{\triangle t}{2} S^n \\
&+\frac{h^2 \triangle t}{12}[-\frac{1}{\triangle t\varepsilon} Q_x^n + \frac{1}{\triangle t} Q_{xx}^n + \frac{1}{2\varepsilon} F_{xx}^n - \frac{1}{2\varepsilon} S_x^n + \frac{1}{2} S_{xx}^n]
\end{aligned}
\tag{6.60}
$$

Fully discrete computational implementation is now obtained by using regular second order spatial approximation formulation (4.8), with the correction terms provided by the modified PDE analysis increasing the spatial approximation order to four. Time intergration is still carried out via the trapesoidal rule (6.49), thus result-

ing in the second order time accurate algorithm.

$$
\begin{aligned}
&Q_j^{n+1} + \frac{\triangle t}{2}(a_1 F_{j-1}^{n+1} + a_2 F_j^{n+1} + a_3 F_{j+1}^{n+1}) \\
&- \left(\frac{\triangle t\varepsilon}{2} + \frac{h^2 \triangle t}{24\varepsilon}\right)(a_4 F_{j-1}^{n+1} + a_5 F_j^{n+1} + a_6 F_{j+1}^{n+1}) - \frac{\triangle t}{2} S_j^{n+1} \\
&- \frac{h^2}{12\varepsilon}(a_1 Q_{j-1}^{n+1} + a_2 Q_j^{n+1} + a_3 Q_{j+1}^{n+1}) + \frac{h^2}{12}(a_4 Q_{j-1}^{n+1} + a_5 Q_j^{n+1} + a_6 Q_{j+1}^{n+1}) \\
&+ \frac{h^2 \triangle t}{24\varepsilon} S1_j^{n+1} - \frac{h^2 \triangle t}{24} S2_j^{n+1} = \\
&Q_j^n - \frac{\triangle t}{2}(a_1 F_{j-1}^n + a_2 F_j^n + a_3 F_{j+1}^n) \\
&+ \left(\frac{\triangle t\varepsilon}{2} + \frac{h^2 \triangle t}{24\varepsilon}\right)(a_4 F_{j-1}^n + a_5 F_j^n + a_6 F_{j+1}^n) + \frac{\triangle t}{2} S_j^n \\
&+ \frac{h^2}{12\varepsilon}(a_1 Q_{j-1}^n + a_2 Q_j^n + a_3 Q_{j+1}^n) - \frac{h^2}{12}(a_4 Q_{j-1}^n + a_5 Q_j^n + a_6 Q_{j+1}^n) \\
&- \frac{h^2 \triangle t}{24\varepsilon} S1_j^n + \frac{h^2 \triangle t}{24} S2_j^n
\end{aligned}
\tag{6.61}
$$

Here $S1_j, S2_j$ denote first and second order derivatives of the source term (6.11).

6.2 Incompressible Navier-Stokes equations.

6.2.1 Ω-Ψ algorithm.

Navier Stokes equation set governing two-dimensional flow of viscous incompressible fluid is written as (see for example Baker, 1983)

$$\frac{\partial u_j}{\partial x_j} = 0 \tag{6.62}$$

$$\frac{\partial u_i}{\partial t} + \frac{\partial}{\partial x_j}\left(u_i u_j + \frac{p}{\rho_0}\delta_{ij} - \sigma_{ij}\right) + \frac{b_i}{Fr} = 0 \tag{6.63}$$

where ρ_0 is the constant density, u_j is the two-dimensional velocity vector, b_i is the body force, p is pressure, σ_{ij} is the Stokes stress tensor defined as

$$\sigma_{ij} = \frac{\nu}{Re}\left(\frac{\partial u_i}{\partial x_j} + \frac{\partial u_j}{\partial x_i}\right) \tag{6.64}$$

and nondimensional groups are defined as

$$Re = \frac{U_\infty L}{\nu_\infty} \tag{6.65}$$

$$Fr = \frac{U_\infty^2}{Lg} \tag{6.66}$$

The constant density restriction allows for introduction of streamfunction and vorticity variable set ψ, ω via

$$\mathbf{u} \equiv \bigtriangledown \times \psi\mathbf{k} \tag{6.67}$$

$$\omega \equiv \bigtriangledown \times \mathbf{u} \cdot \mathbf{k} \tag{6.68}$$

which recasts the original system (6.62-6.63) into

$$\frac{\partial \omega}{\partial t} + (\bigtriangledown \times \psi\mathbf{k} \cdot \bigtriangledown)\omega - \frac{1}{Re} \bigtriangledown^2 \omega = 0 \tag{6.69}$$

$$\bigtriangledown^2 \psi + \omega = 0 \tag{6.70}$$

with pressure being determined as a postprocessing operation via

$$\frac{1}{\rho_0} \bigtriangledown^2 p - \omega^2 + \frac{\partial^2 \psi}{\partial x^2} + \frac{\partial^2 \psi}{\partial y^2} + 2\frac{\partial^2 \psi}{\partial x \partial y} = 0 \tag{6.71}$$

Neglecting body force contribution, writing (6.69) in a component form and remembering definitions (6.67-6.68) yields the Navier Stokes system in the form

$$\frac{\partial \omega}{\partial t} + u\frac{\partial \omega}{\partial x} + v\frac{\partial \omega}{\partial y} - \frac{1}{Re}\frac{\partial^2 \omega}{\partial x^2} - \frac{1}{Re}\frac{\partial^2 \omega}{\partial y^2} = 0 \tag{6.72}$$

$$\frac{\partial^2 \psi}{\partial x^2} + \frac{\partial^2 \psi}{\partial y^2} + \omega = 0 \tag{6.73}$$

$$u = \frac{\partial \psi}{\partial y} \tag{6.74}$$

$$v = \frac{\partial \psi}{\partial x} \tag{6.75}$$

6.2.2 High order formulation

Equation (6.72) is recognized as unsteady advection-diffusion equation whose high order fomulation was developed in the previous sections. Completion of the high order formulation for this problem class therefore rests on the corresponding development for the stream-function Poisson equation. Assuming existence of the appropriate boundary conditions, generality of the developed theory readily provides a required extension. Here, one proceeds along a well established by now design sequence.

Spatial discretization of (6.73) on a nine-node computational stencil results in

$$W_{ij} + c_1\Psi_{i-1,j-1} + c_2\Psi_{i,j-1} + c_3\Psi_{i+1,j-1} + c_4\Psi_{i-1,j} + c_5\Psi_{i,j} +$$

$$+c_6\Psi_{i+1,j} + c_7\Psi_{i-1,j+1} + c_8\Psi_{i,j+1} + c_9\Psi_{i+1,j+1} = 0 \tag{6.76}$$

The approximation requirement as dictated by (6.73) and Taylor series expansion of (6.76) is

$$\sum_{n=1}^{9} c_n = 0$$

$$-c_1 + c_3 - c_4 + c_6 - c_7 + c_9 = 0$$

$$-c_1 - c_2 - c_3 + c_7 + c_8 + c_9 = 0$$

$$c_1 + c_3 + c_4 + c_6 + c_7 + c_9 = \frac{2}{h^2}$$

$$c_1 + c_2 + c_3 + c_7 + c_8 + c_9 = \frac{2}{h^2} \tag{6.77}$$

$$c_1 - c_3 - c_7 + c_9 = 0$$

$$c_9 - c_1 = 0$$

$$c_9 + c_1 = \frac{1}{3h^2}$$

$$c_3 - c_7 = 0$$

which results in

$$c_1 = \frac{1}{6h^2}, \qquad c_2 = \frac{2}{3h^2}, \qquad c_3 = \frac{1}{6h^2}, \qquad c_4 = \frac{2}{3h^2}, \qquad c_5 = -\frac{10}{3h^2} \tag{6.78}$$

$$c_6 = \frac{2}{3h^2}, \qquad c_7 = \frac{1}{6h^2}, \qquad c_8 = \frac{2}{3h^2}, \qquad c_9 = \frac{1}{6h^2} \tag{6.79}$$

and reduces the corresponding truncation error expression to

$$\omega + \psi_{xx} + \psi_{yy} + \frac{h^2}{12}\psi_{xxxx} + \frac{h^2}{12}\psi_{yyyy} + \frac{h^2}{6}\psi_{xxyy} + H.O.T. = 0 \tag{6.80}$$

Differentiating (6.80) by xx and yy, neglecting high order terms and taking the linear combination of the resulting expressions, yields

$$\psi_{xxxx} + 2\psi_{xxyy} + \psi_{yyyy} = -\omega_{xx} - \omega_{yy} \tag{6.81}$$

Substituting (6.81) into (6.80) and reversing the error term signs provides the desirable fourth order accurate perturbed PDE in the form

$$\omega + \frac{\partial^2 \psi}{\partial x^2} + \frac{\partial^2 \psi}{\partial y^2} + \frac{h^2}{12}\left(\frac{\partial^2 \omega}{\partial x^2} + \frac{\partial^2 \omega}{\partial y^2}\right) = 0 \tag{6.82}$$

The modified continuous system comprised of four coupled equations written for four variables ω, ψ, u, v now is

$$\frac{\partial \omega}{\partial t} + \mathbf{u} \cdot \nabla \omega - \frac{1}{Re}\nabla \cdot \nabla \omega - \frac{h^2 Re}{12}\mathbf{u} \cdot \nabla(\mathbf{u} \cdot \nabla \omega) = 0 \tag{6.83}$$

$$\omega + \nabla \cdot \nabla\psi + \frac{h^2}{12}\nabla \cdot \nabla\omega = 0 \tag{6.84}$$

$$u = \frac{\partial \psi}{\partial y} \tag{6.85}$$

$$v = \frac{\partial \psi}{\partial x} \tag{6.86}$$

with pressure being determined via (6.71) as a postprocessing operation.

6.2.3. High order formulation for general Navier-Stokes equation forms.

The two-dimensional Navier-Stokes momentum equation is

$$\frac{\partial u_i}{\partial t} + \frac{\partial}{\partial x_j}\left(u_i u_j + \frac{1}{\rho_0} p\delta_{ij} - \frac{1}{Re}\frac{\partial u_i}{\partial x_j}\right) = 0 \tag{6.87}$$

In order to derive a high order perturbed PDE for a general form in (6.87) the pressure contribution is momentarily neglected and equation is expanded as

$$\frac{\partial u_i}{\partial t} + u_i\frac{\partial u_j}{\partial x_j} + u_j\frac{\partial u_i}{\partial x_j} - \frac{1}{Re}\frac{\partial^2 u_i}{\partial x_j^2} = 0 \tag{6.88}$$

In the case of incompressible equations (6.62), equation (6.88) is reduced to

$$\frac{\partial u_i}{\partial t} + u_j\frac{\partial u_i}{\partial x_j} - \frac{1}{Re}\frac{\partial^2 u_i}{\partial x_j^2} = 0 \tag{6.89}$$

and its high order counterpart recalling the pressure contribution is given as (6.83)

$$\frac{\partial u_i}{\partial t} + \frac{\partial}{\partial x_j}\left(u_j u_i + \frac{1}{\rho_0} p\delta_{ij} - \frac{1}{Re}\frac{\partial u_i}{\partial x_j} - \frac{h^2 Re}{12} u_j u_k \frac{\partial u_i}{\partial x_k}\right) = 0 \tag{6.90}$$

For the current theoretical analysis to be applicable in a more general case (6.87), equation is symmetrized as

$$\frac{\partial u_i}{\partial t} + u_i \frac{\partial u_j}{\partial x_j} + u_j \frac{\partial u_i}{\partial x_j} - \frac{1}{Re} \frac{\partial^2 u_i}{\partial x_j^2} - \tau \frac{\partial^2 u_j}{\partial x_j^2} = 0 \tag{6.91}$$

where $\tau \to 0$ is a parameter similar to the viscosity parameter of the advection-diffusion formulation.

From symmetry, recalling the theoretical developments detailed in Chapter 4 one easily arrives at the high order perturbed PDE for the general form (6.87) as

$$\begin{aligned} &\frac{\partial u_i}{\partial t} + \frac{\partial}{\partial x_j} \left(u_i u_j + \frac{1}{\rho_0} p \delta_{ij} - \frac{1}{Re} \frac{\partial u_i}{\partial x_j} - \tau \frac{\partial u_j}{\partial x_j} \right) \\ &\quad - \frac{\partial}{\partial x_j} \left(\frac{h^2 Re}{12} u_j u_k \frac{\partial u_i}{\partial x_k} + \frac{h^2}{12\tau} u_i u_k \frac{\partial u_j}{\partial x_k} \right) = 0 \end{aligned} \tag{6.92}$$

thus recovering the general TWS formulation form as outlined by Noronha and Baker (1989) (see also Noronha (1989)). This high order formulation will remain essentially unchanged in three dimensions, provided the mesh size measure h is generalized via an appropriate combination of $\triangle x$, $\triangle y$ and $\triangle z$. Of course, the application of the correction terms is again governed by the physics of the problem as dictated by the theoretical design. It is important to emphasize that this latest development (6.92) is only true in the case when general compressible equation forms are under consideration.

6.2.4. FE-like matrix formulation. Assembly procedure

If finite element based software is to be employed in numerical computations, one may needs to establish a clear connection between the computational stencil expression characteristic of the developed high order approach and matrix formulations resulting from finite element variational statements. Once discrete stencil expressions are converted to matrix notation, the entire formulation can be implemented using any finite element computing environment. Since a nine-node stencil of the form (6.76) is used in present theoretical formulations, this section concentrates on finite element formulations employing bilinear test and trial function sets.

The end point of a variational formulation as applied on a single element of the solution domain is the derivation of the corresponding matrix statement written on this element, whose subsequent assembly results in a computable stencil expression similar to the one in (6.76) which in turn provides the numerical solution over the entire computational domain.

When bilinear basis is used in a formulation, the matrix statment for a linear steady-state problem is always expressed as (Baker, 1983, Chaffin, 1997)

$$\begin{bmatrix} a_{11} & a_{12} & a_{13} & a_{14} \\ a_{21} & a_{22} & a_{23} & a_{24} \\ a_{31} & a_{32} & a_{33} & a_{34} \\ a_{41} & a_{42} & a_{43} & a_{44} \end{bmatrix} \begin{Bmatrix} Q_1 \\ Q_2 \\ Q_3 \\ Q_4 \end{Bmatrix} = \{0\} \tag{6.93}$$

where Q_j is the nodal numerical solution and the coefficients a_{ij} depend on the trial

and test function sets and on the partial differential equation itself. A nine-node discrete stencil expression obtained via assembling (6.93) on four adjacent elements then is derived as (Chaffin, 1997)

$$\begin{aligned} & a_{31}Q_{i-1,j-1} + (a_{32} + a_{41})Q_{i,j-1} + a_{42}Q_{i+1,j-1} + (a_{34} + a_{21})Q_{i-1,j} \\ & \qquad + (a_{11} + a_{22} + a_{33} + a_{44})Q_{ij} \\ & +(a_{43} + a_{12})Q_{i+1,j} + a_{24}Q_{i-1,j+1} + (a_{23} + a_{14})Q_{i,j+1} + a_{13}Q_{i+1,j+1} = 0 \end{aligned} \tag{6.94}$$

Comparing (6.94) to (6.76) one easily obtains the following relationship between the discrete stencil coefficients

$$\begin{aligned} & c_1 = a_{31}, \qquad c_2 = a_{32} + a_{41}, \qquad c_3 = a_{42}, \qquad c_4 = a_{34} + a_{21} \\ & \qquad\qquad\qquad\qquad c_5 = a_{11} + a_{22} + a_{33} + a_{44} \\ & c_6 = a_{43} + a_{12}, \qquad c_7 = a_{24}, \qquad c_8 = a_{23} + a_{14}, \qquad c_9 = a_{13} \end{aligned} \tag{6.95}$$

This system provides a set of conditions that must be satisfied to establish a one to one correspondence between the bilinear matrix forms of the finite element method and the developed high order spatial formulation.

Denoting as $\{\Omega\}$ and $\{\Psi\}$ the solution vectors corresponding to continuous variables ω and ψ in (6.72-6.75), and using expressions (6.78-6.79), (6.95) yields the

following fourth order accurate discrete stencil expression for (6.76)

$$\begin{aligned}
&\Omega_{ij} + \frac{1}{6h^2}\Psi_{i-1,j-1} + \frac{2}{3h^2}\Psi_{i,j-1} + \frac{1}{6h^2}\Psi_{i+1,j-1} + \frac{2}{3h^2}\Psi_{i-1,j} - \frac{10}{3h^2}\Psi_{ij} \\
&\quad + \frac{2}{3h^2}\Psi_{i+1,j} + \frac{1}{6h^2}\Psi_{i-1,j+1} + \frac{2}{3h^2}\Psi_{i,j+1} + \frac{1}{6h^2}\Psi_{i+1,j+1} \\
&\quad + \frac{1}{12}\left[\Omega_{i-1,j} - 2\Omega_{ij} + \Omega_{i+1,j}\right] + \frac{1}{12}\left[\Omega_{i,j-1} - 2\Omega_{ij} + \Omega_{i,j+1}\right] = 0
\end{aligned} \tag{6.96}$$

which can then be transformed into the matrix statement

$$\begin{bmatrix} -\frac{10}{3h^2} & \frac{2}{3h^2} & 0 & \frac{2}{3h^2} \\ \frac{2}{3h^2} & 0 & 0 & \frac{1}{6h^2} \\ \frac{1}{6h^2} & \frac{2}{3h^2} & 0 & 0 \\ 0 & \frac{1}{6h^2} & 0 & 0 \end{bmatrix} \begin{Bmatrix} \Psi_1 \\ \Psi_2 \\ \Psi_3 \\ \Psi_4 \end{Bmatrix} + \begin{bmatrix} \frac{2}{3} & \frac{1}{12} & 0 & \frac{1}{12} \\ \frac{1}{12} & 0 & 0 & 0 \\ 0 & \frac{1}{12} & 0 & 0 \\ 0 & 0 & 0 & 0 \end{bmatrix} \begin{Bmatrix} \Omega_1 \\ \Omega_2 \\ \Omega_3 \\ \Omega_4 \end{Bmatrix} = \{0\} \tag{6.97}$$

ready to be used by a finite element computing environment. With the TWS numerical implementation details of (6.72) given by Chaffin (1997), this concludes the development of the high order formulation for the incompressible Navier-Stokes equation class.

Chapter 7

Results and discussion.

7.1 Undetermined coefficients approach.

7.1.1 Convergence study results.

Since an analytical solution is not generally available, the following analysis (Baker, 1991) is used to confirm predicted convergence rate of the developed methods. For the lead term of the truncation series expansion given in the form

$$error^h \simeq C_k h_e^{2k} \tag{7.1}$$

and using

$$T^h + e^h = T_{exact} = T^{h/2} + e^{h/2} \tag{7.2}$$

one can easily verify, that

$$e^h = (2^{2k}) e^{h/2} \tag{7.3}$$

and therefore

$$T^{h/2} - T^h = (2^{2k} - 1) e^{h/2}, \qquad e^{h/2} = \frac{\triangle T^{h/2}}{2^{2k} - 1} \tag{7.4}$$

Here $\triangle T^{h/2} = T^{h/2} - T^h$ denotes the computed difference in the two approximate solutions. Selecting a *log* representation, the slope of the convergence curve should be

$$slope = \frac{log(e^{h/M}) - log(e^{h/2M})}{log(h) - log(h/2)} = \frac{log(e^{h/M}/e^{h/2M})}{log(2)} \tag{7.5}$$

Results of a convergence study computed for (3.1) on uniformly refined discretizations for $\varepsilon = 0.1$ at the mid-node of the solution domain are shown in Table 1 [2]. All presented solutions computed for $u = 1$ were smooth (oscillation-free). The data adhere to the theoretical convergence prediction, confirming the order of the lead truncation error term for each method.

7.1.2. One-dimensional steady-state problems.

Solution evolution for $\varepsilon = 0.001$ is shown in Figure 7.1 with number of nodes *Nnode*. Presented are numerical solutions computed using fourth order (3.18) and Galerkin linear basis (3.7) methods. Even for this modest value of ε, Galerkin linear basis solution remains oscillatory in the boundary region for all considered discretizations. The well known monotonicity constraint (Fletcher, 1991, Roy and Baker, 1997) applied to $\varepsilon = 0.001$ states that at least 500 nodes are needed for Galerkin linear basis discretization to produce a non-oscillatory (monotone) solution.

In contrast, fourth order method solutions remain monotone independent of *Nnode,* albeit overdiffused on the coarse (*Nnode*=21) mesh, in full agreement with high order method results reported by Fletcher (1991). While the coarse mesh solution is clearly overdiffused, a reasonable 121-node discretization of the solution domain allows for computing an acceptable solution. Further refinement results in a highly accurate monotone solution for *Nnode*=221.

[2] all Tables may be found in Appendix II

Figure 7.2 illustrates solution evolution for the stationary wave problem, as obtained for $\varepsilon = 0.001$ and various discretizations. The equation remains (3.1), while boundary conditions are modified to

$$q(0) = -1 \qquad\qquad q(1) = 1 \tag{7.6}$$

and

$$u = \begin{cases} -1 & for \quad 0 \leq x < \frac{1}{2} \\ 1 & for \quad \frac{1}{2} < x \leq 1 \end{cases} \tag{7.7}$$

The numerical data confirm the trends in Figure 7.1, in that the fourth order method solution is monotone for all discretizations, with solution accuracy improvment on refined meshes. The Galerkin linear basis solutions remain oscillatory for all cases.

7.1.3. One-dimensional unsteady problems.

Numerical experiments were conducted for $u = 1$, $0.2 \leq t \leq 1.4$, on a 41-node uniform mesh with $h = 0.05$. The time step was varied to produce different Courant numbers. The analytical solution (3.27) was used to set initial and Dirichlet boundary conditions.

Figure 7.3 shows solution evolution for $\varepsilon = 0.01$ and $\varepsilon = 0.001$. Compared are the fourth order (3.39) and the Galerkin linear basis method solutions. Achieving a uniform fourth order accuracy in space and time would require a fourth order time

integration algorithm. Instead, the non-dissipative trapesoidal rule is used to focus on solution dependency on the order of spatial approximation. Both methods are therefore second order accurate in time.

Both methods performed equally well for $\varepsilon = 0.01$ producing accurate solutions for a considered range of Courant number. Decreasing the value of ε steepens the propagating wavefront creating difficulties in resolving the resulting gradient. The fourth order method evidences leading dispersive oscillations, that diminish with increase of the Courant number and completely disappear for $C = 1$. This is particularly attractive, since for a fixed spatial discretization size larger Courant number means larger time step, thus allowing for a faster solution process. This trend is completely reversed for the Galerkin linear basis solution. In that, all considered solutions are unacceptably polluted by the trailing dispersive errors, with magnitude of the oscillations increasing with Courant number.

The fourth order method performance for $C = 1$ is examined in Figures 7.4a and 7.4b for different values of the viscosity parameter ε. Both simulations produced monotone error-free results. For small values of ε, the original advection-diffusion equation (3.26) asymptoticaly approaches the non-diffusive hyperbolic equation

$$\frac{\partial q(x,t)}{\partial t} + u\frac{\partial q(x,t)}{\partial x} = 0 \tag{7.8}$$

The ability of the fourth order method to resolve sharp shock-like wavefront gradients

for C=1 corresponds to solving (7.8) with ε approaching zero in (3.39). Figures 7.4c-7.4f document the results obtained using (3.39) with ε set to 0.0000001 for the initial wave front a sine wave, Figure 7.4c, and a two-node square wave, Figure 7.4e. Initial condition is shown as a dashed line on all plots. Wavefront locations are shown after 18 and 20 time steps respectively. Fourth order method simulations produced excellent results, while the Galerkin linear basis comparison solutions, presented for comparison, are totaly destroyed by oscillations. One must note that, while several methods can produce nodally exact results for equation (7.8) with Courant number of one, the developed fourth order method solutions presented in Figure 7.4 are never nodally exact.

7.1.4. Two-dimensional steady-state problems.

Data as generated for the convergence study obtained for the fourht order method (3.59) and the sixth order method (3.64), on uniformly refined discretizations for $\varepsilon = 1$ at the mid-node of the solution domain, are shown in Table 2. All presented solutions were computed for u=v=1. Data adherence to the convergence curves confirm the order of the lead truncation error term for each method.

Numerical solutions computed on a uniform 11x11 square mesh for various values of ε are presented in Figure 7.5. Compared are the fourth order method (3.59) and the Galerkin bilinear basis solutions. Both methods produce acceptable solutions for $\varepsilon =$ 1, with the fourth order method solution being nearly nodally-exact. The Galerkin

bilinear basis solution is totally destroyed for the convection dominated problem with $\varepsilon = 0.001, 0.00001$. Conversely, the fourth order method yields nodally accurate monotone solutions, demonstrating the theory's ability to resolve sharp gradients in a boundary layer, as formed due to the small value of ε.

Figure 7.6 depicts the method's performance when applied to the slightly more challenging problem, corresponding to boundary conditions (3.42) while (3.43) is replaced by the adiabatic conditions,

$$\frac{\partial q(x,1)}{\partial \mathbf{n}} = \frac{\partial q(1,y)}{\partial \mathbf{n}} = 0 \tag{7.9}$$

This allows examining solution behavior in the absence of exact nodal boundary data, hence admitting more severe boundary layer oscillations.

Solutions were generated at $\varepsilon = 0.005$ for progressively refined computational grids. The general trends remained unchanged from those shown in Figure 7.1 for the one-dimensional case. The Galerkin bilinear basis solution is oscillatory in the boundary layer region for all considered discretizations, with oscillation magnitude decreasing with increased mesh density. The fourth order method yields monotone results on all discretizations, including the inaccurate, overdiffused solution on the coarse 11x11 grid. It significantly improves with modest mesh refinement, resulting in an acceptable, while still diffused, solution on a 31x31 node mesh. It showes sharp boundary layer resolution on a 51x51 node mesh. Note again, that the bandwidth of the solution matrix remains the same in all cases.

7.2. Perturbed equation approach.

7.2.1. One-dimensional problems on uniform mesh.

Convergence data computed for the derived methods are presented in the Table 3 and Table 4. Table 3 lists data obtained for the scalar case (4.19), Table 4 for the non-linear case (4.24). All data were computed for $\varepsilon = 0.1$.

Computed slope values confirm Taylor series-predicted convergence rates of the developed methods. When compared to the exact solution $Q(x = 0.75) = 0.0820433$ in the scalar case ($\varepsilon = 0.1$) the fourth order method evidences superior performance. Specifically, monotone and accurate results are obtained on a relatively coarse mesh. A tenfold mesh refinement would be required for the second order method to produce comparable results. This seemingly insignificant "third digit" observation will become extremely important in costly real-life computations.

Solution evolution for Case problem 1 for $\varepsilon = 0.001$ is shown in Figure 7.7 with number of nodes *Nnode* . Presented are numerical solutions computed using fourth order and second order methods. While the high order formulation developed via the perturbed equation approach differs from that obtained via the undetermined coefficients analysis of Chapter 3, the high order solution trends remain unchanged and can be directly compared to the results shown in Figure 7.1.

Results computed for the Burger's equation case are shown in Figure 7.8 for $\varepsilon = 0.001$. The fourth order accurate solutions are presented for various discretiza-

tions. Presented solutions follow general trends observed for the linear case, higlighting continuity of the developed theoretical approach. All solutions are monotone with highly accurate results obtained on sufficiently refined discretizations. Second order method solution (not shown here) was highly divergent. In fact, continuing the iteration process (up to 50 iterations, not shown) does not improve the solution, but rather exaggerates its divergent behavior.

Overall, computational results illustrate two main points. Namely, high order methods can achieve desirable error levels on coarser meshes, and for a given mesh high order methods produce more accurate results. The developed theoretical approach allows for exercising these advantages at no added computational cost, which is usually associated with solution matrix bandwidth expansion of high order accurate methods.

7.2.2. One-dimensional problems on non-uniform mesh.

Figure 7.9 presents results obtained on a strongly non-uniform mesh with geometric progression $p = 0.8$ for the scalar $u = 1$ one-dimensional steady-state case. Compared are third order (4.48) and Galerkin linear basis methods. As expected packing mesh at the wall allows for resolving solution gradients on a small number of nodes for virtually any value of viscosity parameter ε. Similarly to the uniform mesh results, higher order approximation allows for monotone resolution of the boundary layer on a coarser mesh.

Since exact location of the boundary layer is required for efficient utilization of non-uniform discretizations, Figures 7.10 and 7.11 present results obtained on *locally* uniform meshes. In that, solution domain is subdivided into several uniformly discretized subdomains. Those potentially containing sharp discontinuities and/or boundary layers are then packed with nodes, while the rest are treated with coarse mesh. This approach does not require the exact knowledge of trouble-spot locations, just some general prediction based on the physics of the problem at hand. Figure 7.10 compares the results computed for the linear case with the fourth order and Galerkin linear basis methods. Locally non-uniform meshing at the nodes connecting adjacent subdomains is handled via third (4.48) and first (4.36) order methods respectively. Figure 7.11 shows the results obtained with the fourth order method (4.17) for the Burgers equation case (4.24). Here n, m and l represent the number of nodes in each of the solution subdomains. Here again the fourth order method produces excellent monotone results on coarse meshes for all tested values of the viscocity parameter ε.

7.2.3. Two-dimensional steady-state problems.

Uniform mesh refinement results confirming predicted convergence rates of the developed fourth order method are shown in Table 5.

All data were computed at the center node of the solution domain $x = 0.5, y = 0.5$. For the purpose of establishing convergence rate of the method the linear problem

(4.66) with the exact boundary conditions

$$q(1,1) = 1 \qquad q(0,y) = q(x,0) = 0 \tag{7.10}$$

$$q(x,1) = \frac{e^{\frac{ux}{\varepsilon}} - 1}{e^{\frac{1}{\varepsilon}} - 1} \qquad q(1,y) = \frac{e^{\frac{vy}{\varepsilon}} - 1}{e^{\frac{1}{\varepsilon}} - 1} \tag{7.11}$$

was considered in the mesh refinement study.

Numerical results are shown in Figures 7.12, 7.13. Figure 7.12 compares solutions to the linear problem computed on uniform meshes of different density for $\varepsilon = 0.005$, while Figure 7.13 shows results for the non-linear problem (4.18) obtained for various values of the viscosity parameter ε on a uniform 31x31 node mesh. In both cases the boundary conditions (7.11) were replaced with the adiabatic conditions

$$\frac{\partial q(x,1)}{\partial \mathbf{n}} = \frac{\partial q(1,y)}{\partial \mathbf{n}} = 0 \tag{7.12}$$

Solutions of the linear problem (4.16) using the fourth order method developed via "perturbed PDE" approach closely follow the trends obtained earlier with the fourth order method resulted from the undetermined coefficients analysis. One must again note that both theoretical approaches result in distinctly different stencil coefficients, while retaining the same theoretically predicted fourth order convergence rate and efficient nine-node implementation of lower order two-dimensional constructions. Presented numerical results thus confirm the earlier findings. In that, the fourth order method yields monotone results on all discretizations. An inaccurate, overdiffused solution on a coarse 11x11 grid is significantly improved after a modest mesh

refinement (Figure 7.12b). Further mesh refinement produces an excellent solution on a 51x51 node mesh. Companion Galerkin bilinear basis results were presented in earlier sections and were shown to remain oscillatory for all considered meshes.

The computational results shown in Figure 7.13 demonstrate the algorithm applicability to non-linear steady-state problems. Here, a good initial approximation in the Newton algorithm allows for sustaining excellent monotone solutions and sharp gradient resolution for a broad range of the viscosity parameter ε.

7.2.4. Two-dimensional unsteady problems.

To investigate the accuracy of the developed fourth order spatial approximation in two dimensions, the problem of a Gaussian hill translating with a uniform velocity $\mathbf{u} = \frac{1}{\sqrt{2}}\mathbf{i} + \frac{1}{\sqrt{2}}\mathbf{j}$ and spreading isotropically with diffusivity ε is considered. The analytical solution has the form (Donea, 1984)

$$q(r,t) = \frac{1}{\sigma(t)} exp\left(-\frac{1}{2\sigma(t)^2}(r - r_0 - \mathbf{u}t)^2\right) \tag{7.13}$$

where $\sigma(t) = \sigma_0(1 + 2\varepsilon t/\sigma_0^2)^{1/2}$. The width of the hill at the initial time $t = 0$ is set to $\sigma_0 = 0.07$ and solution is time-iterated on a uniform 26 by 26 node mesh until time $t = 0.5$ is reached. Viscosity parameter was set to $\varepsilon = 0.005$. The perturbed PDE (4.93) reduces to

$$Q^{n+1} + \frac{\triangle tu}{2}Q_x^{n+1} + \frac{\triangle tv}{2}Q_y^{n+1} - \frac{\triangle t\varepsilon}{2}Q_{xx}^{n+1} - \frac{\triangle t\varepsilon}{2}Q_{yy}^{n+1}$$

$$-\frac{h^2\triangle t}{2}\left(\frac{u}{6\triangle t\varepsilon}Q_x^{n+1}+\frac{v}{6\triangle t\varepsilon}Q_y^{n+1}+Q_{xx}^{n+1}(\frac{u^2}{12\varepsilon}-\frac{1}{6\triangle t})\right)$$

$$+\frac{h^2\triangle t}{2}\left(Q_{yy}^{n+1}(\frac{v^2}{12\varepsilon}-\frac{1}{6\triangle t})+\frac{uv}{6\varepsilon}Q_{xy}^{n+1}\right)= \tag{7.14}$$

$$Q^n-\frac{\triangle tu}{2}Q_x^n-\frac{\triangle tv}{2}Q_y^n+\frac{\triangle t\varepsilon}{2}Q_{xx}^n+\frac{\triangle t\varepsilon}{2}Q_{yy}^n$$

$$+\frac{h^2\triangle t}{2}\left(-\frac{u}{6\triangle t\varepsilon}Q_x^n-\frac{v}{6\triangle t\varepsilon}Q_y^n+Q_{xx}^n(\frac{u^2}{12\varepsilon}+\frac{1}{6\triangle t})\right)$$

$$+\frac{h^2\triangle t}{2}\left(Q_{yy}^n(\frac{v^2}{12\varepsilon}+\frac{1}{6\triangle t})+\frac{uv}{6\varepsilon}Q_{xy}^n\right)$$

Figure 7.14 shows the initial and final analytical distributions. Figure 7.15 depicts computational results obtained for different values of the Courant number. Compared are the fourth order (4.93) and second order accurate spatial methods.

The use of the higher order spatial approximation allowed for reducing the oscillatory dispersion error for all considered values of Courant number by eliminating higher order error terms, which results in more accurate solutions. The developed theory was shown to be time/space complete with unsteady perturbed PDE forms reducing to those of the steady-state case via temporal terms reduction. Both second and fourth order spacial implementations required the same computational effort with more accurate results being obtained at no added cost.

7.2.5. Two-dimensional hyperbolic problems.

The problem of the Gaussian hill distribution probagation with a uniform constant velocity along the solution domain diagonal was considered. The perturbed PDE (4.101) reduces to

$$Q^{n+1} + \frac{\triangle tu}{2} Q_x^{n+1} + \frac{\triangle tv}{2} Q_y^{n+1} + \frac{h^2 \triangle t}{2} \left(\frac{1}{3\triangle t} Q_{xx}^{n+1} + \frac{1}{3\triangle t} Q_{yy}^{n+1} \right) =$$

$$Q^n - \frac{\triangle tu}{2} Q_x^n - \frac{\triangle tv}{2} Q_y^n + \frac{h^2 \triangle t}{2} \left(\frac{1}{3\triangle t} Q_{xx}^n + \frac{1}{3\triangle t} Q_{yy}^n \right) \qquad (7.15)$$

Figure 7.16 shows hill distribution on a uniform 31 by 31 node mesh at time $t = 0$ and that after 10 time iterations with Courant number set to 0.1 using the developed fourth order space accurate method. The presented computational result demonstrates a rather unfortunate theoretical consistency. In that, order of the method increase does not result in accurate solutions for hyperbolic problems requiring other optimization approaches.

7.3 Non-linear equation systems.

7.3.1 Flows in a converging-diverging nozzle.

To confirm predicted convergence rates of the developed fourth order method (6.18-6.20), the model problem (6.2) was modified to avoid potential difficulties resulting from the stationary shock wave in the diverging part of the nozzle. Hence, only the converging portion of the nozzle with the corresponding Dirichlet boundary conditions

was considered in the convergence study. Convergence data for the flow velocity computed at the node $x = 0.25$ is presented in Table 6.

Obtained convergence slopes confirm the design order of the method. Unfortunately, when applied to the model problem, the numerical solution is divergent for both methods. This is easily explained by the presence of the normal shock, whose resolution cannot be improved by increasing the order of the method. This leads one to look for ways of adapting the designed theoretical procedure to solve the problem at hand.

Towards this goal diffusive terms of the form

$$-\varepsilon\frac{\partial^2\rho}{\partial x^2}, \qquad -\varepsilon\frac{\partial^2 u}{\partial x^2}, \qquad -\varepsilon\frac{\partial^2 e}{\partial x^2} \tag{7.16}$$

were added to their respective equations in both methods. Approximation of these terms was carried out in a manner consistent with (1.1) and no additional modifications were made to the developed fourth order system (6.18-6.20). As a result its approximation order was reduced to that of the second order system. Viscosity parameter ε was varied, in an attempt to make the diffused solution assymptotically approach solution of the original system (6.2). Numerical results obtained for both methods are presented in Figure 7.17. All solutions were computed on a 101 node uniform mesh. Exact analytical solution is shown with a solid line, and numerical solution is represented by nodal (circle) symbols. The fourth order method results were computed for $\varepsilon = 0.02$ and the second order method results were computed for

$\varepsilon = 0.0008$.

The fourth order method solution is clearly unacceptable, and while the second order method by comparison seems to produce a somewhat better looking solution, it is still greatly overdiffused and quite modest oscillations can be seen behind the shock. While one might argue that a uniformly fourth order method could remedy the situation, all attempts to design one directly following the theoretical procedure developed herein did not succeed, due to the lack of symmetry in the partial derivative groups, which was the direct result of adding the diffusive terms. For the uniformly fourth order approximation to be achieved, it is therefore necessary to search for some other ideas for implementing this strategy.

Introduction of the substitution (6.23) outlined in Chapter 6 results in improved solution properties to be illustrated below. To confirm predicted convergence rates of the developed fourth order method (6.38), the model problem was again modified to include only the converging portion of the nozzle. Convergence data for the flow velocity computed at the node $x = 0.25$ for $\varepsilon = 0.1$ is presented in Table 7.

Computational results obtained for both methods for various values of viscosity parameter ε are shown in Figures 7.18 and 7.19. The solid lines indicates the exact analytical solution, while circles denote the computed nodal numerical solution.

The developed formulation allows for designing a uniformly fourth order approximation while introducing a stabilizing diffusion mechanism into the original equation

system. As a result, both second and fourth order methods provide excellent resolution of the stationary shock wave in the diverging part of the nozzle. Both methods have a significant problem at the nozzle-throat sonic point, and the fourth order method proves to be somewhat less inaccurate. In agreement with the computational results obtained for the advection-diffusion equation, the fourth order method solution is monotone, unlike that of the second order method which develops oscillations for small values of the viscocity parameter, Figure 7.19. As expected, the smaller the value of the viscosity parameter ε, the closer the numerical solution follows that calculated analytically. This observation makes monotonicity of the fourth order solution even more attractive. Both methods become divergent for $\varepsilon < 0.0004$.

Numerical solution is further improved via spatial filtering (6.39) algorithm, with the results shown in Figure 7.20. Maximum amount of diffusion $\alpha = -0.49$ was used in this case. Note, being more accurate to begin with, the fourth order solution requires a smaller amount of additional diffusion.

Time-dependent formulation (6.48) allows one to investigate a genuinly transient physical problem. Computational results are shown in Figure 7.21, with the solid line representing the exact analytical steady-state solution, and symbols representing that obtained numerically. Compared are the second and fourth order spatial approximation formulations (6.52), (6.61). In both cases, time integration is performed via the second order trapezoidal rule algorithm. Viscosity parameter is set to $\varepsilon = 0.0008$

with solutions diverging for smaller values. CFL number was set to 0.3 and spatial filtering was performed after every time step to promote solution monotonicity.

Employing higher order spatial discretization allows for computing more accurate solution, which is in an excellent agreement with theory. Higher order accuracy results in a better resolution of solution characteristics, while requiring smaller amounts of additional diffusion as provided by spatial filtering. As a reminder, $\alpha \sim 0.5$ in (6.40) provides minimum amounts of diffusion, with $\alpha \sim -0.5$ corresponding to the maximum amount. The sonic-throat point is clearly resolved and the normal shock discontinuity is acceptably positioned on two nodes by the fourth order formulation. In turn, the second order formulation remains oscillatory around the shock front resolved on three nodes signaling the need for more diffusion, which would further flatten the shock.

While higher order approximation becomes unstable for CFL$\geq$0.5, second order method accompanied by modest amounts of spatial filtering remains stable for larger timesteps, allowing one to quickly progress towards the steady-state solution. This result is illustrated in Figure 7.22. Solution is computed using the second order spatial discretization, CFL number is set to 20, viscocity parameter is 0.000001 and steady-state solution is achieved in as little as 17 time steps. Here again, solid line represents the exact analytical solution. While larger amounts of diffusion $\alpha = -0.05$ are needed to maintain solution monotonicity in this case, the small number of time

steps helps to somewhat offset this problem, resulting in a perfectly acceptable two-node shock resolution. Shock position is clearly a bit off, but if a good inexpensive first approximation of the steady-state regime is desired, this is one way to achieve the goal. As always, there is no free lunch.

7.3.2. Driven cavity benchmark solutions.

The driven-cavity problem is a well-known validation benchmark problem (Baker, 1983, Williams, 1993, Roy, 1994, Chaffin, 1997). The solution domain is the unit square, with the lid defined to slide across the domain at a uniform velocity.

The high order formulation (6.83-6.86) developed for the incompressible Navier-Stokes vorticity-streamfunction formulation was shown to incorporate the fundamentals of the classic TWS analysis. The correction error terms necessary for the appropriate order of accuracy are combined via vector analysis to provide the β term of the TWS formulation. The theoretical analysis results in a highly efficient dispersion error control mechanism whose application is based on the specifics of the solution domain discretization and physics of the problem. It is this theoretically sound control mechanism that distinguishes this development, allowing for selective application of optimal amounts of diffusion for maximum accuracy as dictated by the high order accuracy formulation. It is important to note that unlike TWS formulation, present development also includes the reformulated Poisson streamfunction equation (6.84) as an integral part of a uniformly high order accurate solution.

Numerical results for a range of Reynolds numbers are shown in Figures 7.23, 7.24. Compared are GWS, TWS and newly developed high order method formulations. For a modest value of Re=1000 all solutions are of reasonable engineering quality, with GWS vorticity solution showing some oscillatory behavior. Oscillations are significantly reduced via TWS β-term application and are non-existent on the fourth order method solution.

The picture changes significantly as Reynolds number is increased to 3000. As shown in Figure 7.24, GWS and TWS solutions are unacceptably polluted by oscillations, with high order formulation providing excellent monotone solution on a rather coarse locally-uniform mesh. This locally-uniform discretization is quantized via the aPSE notation as X1: [33(0. 8R1.0 .02 16R1.0 .98 8R1.0 1)] and X2: [-33(0. 20R1.0 .98 12R1.0 1)], which reads for X1: "from 0 to 0.02 place 8 nodes with the progression ratio of 1.0 (uniformly), from 0.02 to 0.98 uniformly place 16 nodes and finally from 0.98 to 1.0 uniformly place 8 nodes". Similarly, notation for X2 reads: "from 0 to 0.98 uniformly place 20 nodes, from 0.98 to 1.0 uniformly place 12 nodes".

The numerical results illustrate a definite advantage of theoretically predicted selective application of numerical diffusion provided by the error correction terms over the entire solution domain. Note that packing more nodes at the boundaries of the solution domain would result in monotone solutions for both GWS and TWS formulations. Of course, the price one pays is the information lost on the interior of

the solution domain with the discretization nodes migrating to the boundaries.

Importance of considering a uniform high order formulation consisting of the perturbed PDEs for both vorticity and streamfunction equations in illustrated in Figures 7.25, 7.26 and 7.27. Figures 7.25, 7.26 show the results obtained when the high order formulation is only used for the vorticity equation while the streamfunction remains (6.73). Solution is comparable to that of the TWS method in Figure 7.24. In contrast, Figure 7.27 shows the solution computed when only the streamfunction equation is modified with vorticity being calculated via the original equation (6.72). One may conclude that for this particular problem class high order modification of the streamfunction equation is more significant as compared to that of the vorticity equation, but both are required for a consistent high order formulation.

Results from the uniform mesh convergence study conducted for stream-function variable in energy norm using both GWS and high order formulation with Re=10 and Re=100 are shown in Table 8. All solutions were time-iterated to steady-state. Obtained convergence data indicate near-second order convergence for both methods reflecting time-integration second order of accuracy. While the nominal order of accuracy in the high order formulation is reduced, the desirable performance trends of the high order method is nevertheless preserved. This is seen from the convergence data obtained for Re=100 on coarser (9×9 and 17×17) discretizations. Consistent with the results reported for the model advection-diffusion problem, high order formula-

tion achieves monotone solutions on coarser meshes resulting in higher convergence rates and more accurate numerical results. The convergence data computed for the high order formulation illustrates the relative importance of the terms neglected in designing the continuous vector form of the perturbed PDE in (4.60). These terms are of greater significance when dealing with low Reynolds number flows, resulting in lower convergence rates. When Reynolds number increases, the convergence rate improves due to the diminished contribution from the neglected terms.

The accuracy of the GWS, TWS and high order formulations was tested by comparing their respective numerical solutions to fine-mesh benchmark results established on a 256×256 mesh by Ghia et. al. (1982). Table 9 summarizes driven cavity benchmark data comparisons. For the purpose of obtaining near-monotone solutions for all considered methods, uniform 33×33 node discretization was used for Re=100, 400, 1000, while the locally-uniform discretization quantized as X1: [33(0. 9R1.0 .02 14R1.0 .98 9R1.0 1)], X2: [-33(0. 18R1.0 .98 14R1.0 1)] was used for Re=3200. The study compares the maximum values of the stream-function variable achieved over the entire solution domain (ψ_{max}) together with the values of the vorticity variable computed at the same nodal location, as produced by the considered methods. For consistency, the TWS β parameter was set to 0.2 in all computations. High order and GWS formulations yield similar results with high order method being consistently more accurate. The TWS method results are overdiffused via the β parameter

selection for Re=100, 400 and produce accurate results for Re=1000.

Overall, the numerical results obtained for the driven cavity benchmark problem confirm the advantages of using the developed uniform high order formulation. It allows for achieving monotone accurate numerical solutions on coarser discretizations as compared to GWS and TWS methods. This preserves the high order solution trends illustrated for the model advection-diffusion problem and provides for a better resolution of the interior of the solution domain. The application of the correction error terms developed herein is governed by physics of the problem and does not require many a knob and several a switch to run the problem.

Chapter 8
Summary and conclusions.

A new approach to designing high order accurate CFD methods has been developed and tested for a range of problem statements including compressible Euler and incompressible Navier-Stokes equation systems. The systematic construction of progressively higher order spatial approximations is achieved via a modified equation analysis, which allows one to determine the computational stencil coefficients appropriate to a desired accuracy order. The resulting high order error correction terms are shown to be consistent with the β term characteristic of the TWS finite element formulation. This confirms the expected high order of spatial accuracy in TWS constructions and provides a highly efficient dispersion error control mechanism whose application is based on the specifics of the solution domain discretization and physics of the problem.

Theoretical development utilizes fundamentals of the finite element weak statement formulation, and truncation error analysis, to characterize error in the numerical solution process. It then offers a computationally inexpensive way of constructing equation specific higher order approximations. A distinguishing desirable property of the developed method is solution matrix bandwidth, which always remains equal to that of the second order discretizations. This permits combining the computational efficiency of the lower order methods with superior accuracy inherent in high

order approximations. Generality of the underlying principles is shown to provide a natural transition of the concepts derived for one-dimensional steady-state case to multi-dimensional and unsteady problems. The perturbed PDE analysis is further demonstrated to be widely applicable to Navier-Stokes non-linear equation law system, with the theoretical development yielding the continuous vector forms needed for the appropriate error corrections.

Numerical simulations compare performance of the developed method to that of the GWS and TWS formulations. Uniform mesh refinement convergence results confirm the order of truncation error for each method. High order formulation is shown to require significantly fewer nodes to accurately resolve solution gradients for convection dominated problems. Benchmark problem applications for the compressible Euler and incompressible Navier-Stokes equations complete the manuscript. In both cases the developed high order formulation is shown to result in more accurate solutions on coarser discretizations, thus preserving the design trends illustrated for the model advection-diffusion equation. The theoretical development is therefore complete.

Bibliography

1. C.Baiocchi and F.Brezzi, 'Virtual bubbles and Galerkin-least-squares type methods', *Comp. Methods in Appl. Mech. Engrg.,* **105,** 125-141 (1993).

2. A.J.Baker and J.W.Kim, 'A Taylor weak-statement algorithm for hyperbolic conservation laws', *Int. J. Numer. Methods Fluids,* **7,** 489-520 (1987).

3. A.J.Baker, *Finite element computational fluid dynamics,* Hemisphere, New York, 1983.

4. A.J.Baker and D.W.Pepper, *Finite elements* 1-2-3, McGraw-Hill, 1991.

5. A.J.Baker, *Weak statement CFD: I Incompressible Flow,* CFD tutorial, 1997.

6. A.J.Baker, D.J.Chaffin, J.S.Iannelli and S.Roy, 'Finite elements for CFD - how does the theory compare?', *Int. J. Numer. Methods Fluids*, **31**, 345-358 (1999).

7. A.N.Brooks and T.J.R. Hughes, 'Streamline upwind Petrov-Galerkin methods for advection dominated flows', *Proc. Third Int. Conf. on Finite Element Methods in Fluid Flow,* Banff, 1980.

8. D.J.Chaffin and A.J.Baker, 'On Taylor weak statement finite element methods for computational fluid dynamics', *Int. J. Numer. Methods Fluids,* **21,** 273-294 (1995).

9. D.J.Chaffin, *A Taylor weak statement finite element method for computational fluid dynamics,* Ph.D. dissertation, The University of Tennessee, Knoxville,

1997.

10. I.Christie and A.R.Mitchell, 'Upwinding of high order Galerkin methods in conduction-convection problems', *Int. J. Numer. Methods Eng.,* **12,** 1764-1771 (1978).

11. L.Collatz, *The numerical treatment of differential equations,* Springer-Verlag, Berlin, 1960.

12. J.Donea, 'A Taylor-Galerkin method for convective transport problems', *Int. J. Numer. Methods Eng.,* **20,** 101-119 (1984).

13. C.A.J.Fletcher, *Computational techniques for fluid dynamics 1: Fundamental and general techniques,* Springer-Verlag, New York, 1991.

14. U.Ghia, K.N.Ghia and C.T.Shin, 'High-Re solutions for incompressible flow using the Navier Stokes equations and a multi-grid method', *J. Comp. Physics*, **48**, 387-411 (1982).

15. A.Harten and S.Osher, 'Uniformly high-order accurate nonoscillatory schemes I', *SIAM J. Numer. Anal.*, **24**, 279-309 (1987).

16. A.Harten, B.Engquist, S.Osher and S.R.Chakravarthy, 'Iniformly high order accurate essentially non-oscillatory schemes III', *J. Comput. Physics*, **71**, 231-303 (1987).

17. J.C.Heinrich, P.S. Huyakorn, O.C.Zienkiewicz and A.R.Mitchell, 'An "upwind" finite element scheme for two-dimensional convective transport equation', *Int. J. Numer. Methods Eng.,* **11,** 131-143 (1977).

18. C.Hu and C.-W.Shu, 'A discontinuous Galerkin finite element method for Hamilton-Jacobi equations', *ICASE Report 98-2,* Jan. 1998.

19. C.Hu and C.-W.Shu, 'Weighted essentially non-oscillatory schemes on triangular meshes', *ICASE Report 98-32*, July 1998.

20. J.Iannelli, 'NEWS: A non-linear element-upstream weak statement for the Euler and Navier-Stokes equations', *AIAA paper 96-0763,* Jan. 1996.

21. J.Iannelli, 'A CFD Euler solver from a physical acoustics-convection flux jacobian decomposition', *Int. J. Numer. Methods Fluids*, **31**, 821-860 (1999).

22. J.W.Kim and D.J.Lee, 'Optimized compact finite difference schemes with maximum resolution', *AIAA Journal,* **34,** 887-893 (1996).

23. J.W.Kim and D.J.Lee, 'Numerical simulation of nonlinear waves using optimized high-order compact schemes', *Comput. F. Dyn. J.,* **5,** 281-300 (1996).

24. Z.Kopal, *Numerical analysis,* Wiley, New York, 1961.

25. P.Lax and B.Wendroff, 'Systems of conservation laws', *Commun. Pure Appl. Math.,* **8,** 217-237 (1960).

26. B.P.Leonard, 'The ULTIMATE conservative difference scheme applied to unsteady one-dimensional advection', *Comput. Methods Appl. Mech. Eng.,* **88,** 17-74 (1991).

27. H.Lomax, 'Recent progress in numerical techniques for flow simulation', *AIAA Journal,* **14,** 512-518 (1976).

28. K.W.Morton and P.K.Sweby, 'A comparison of flux limited difference methods and characteristic Galerkin methods for shock modeling', *J. Comput. Physics*, **73**, 203-230 (1987).

29. W.P.Noronha and A.J.Baker, 'A Taylor weak statement finite element CFD algorithm for 2D incompressible Navier Stokes equations', *AIAA 27th Aerospace Sciences Meeting* , January 9-12, Reno, Nevada (1989).

30. W.P.Noronha, *Accuracy, convergence and stability of finite element algorithms for incompressible fluid flow*, Ph.D. dissertation, The University of Tennessee, Knoxville, 1989.

31. J.T.Oden and J.N.Reddy, *Introduction to the Mathematical Theory of Finite Elements,* Wiley, New York, 1976.

32. J.T.Oden, 'Optimal *h-p* finite element methods', *Comput. Methods Appl. Mech. Engrg.,* **112,** 309-331 (1994).

33. S.Roy and A.J.Baker, 'SGM-Part I', *Int. J. of Numer. Heat Transfer,* **31,** 135-176 (1997).

34. S.Roy and A.J.Baker, 'SGM-Part II', *Int. J. of Numer. Heat Transfer, Part B,* **33,** 5-36 (1998).

35. S.Roy, *On improved methods for monotone CFD solution accuracy*, Ph.D. dissertation, The University of Tennessee, Knoxville, 1994.

36. Yu.I.Shokin, *The method of differential approximation,* Springer-Verlag, 1983.

37. C.-W.Shu, 'Essentially non-oscillatory and weighted essentially non-oscillatory schemes for hyperbolic conservation laws', *ICASE Report 97-65,* Nov. 1997.

38. C.K.W.Tam and J.C.Webb, 'Dispersion-relation preserving finite difference schemes for computational acoustics', *J. Comput. Phys.,* **107,** 262-281 (1993).

39. J.W.Thomas, *Numerical partial differential equations,* Springer-Verlag, New York, 1995.

40. M.R.Visbal and D.V.Gaitonde, 'High-order accurate methods for unsteady vortical flows on curvilinear meshes', *AIAA paper 98-0131,* Jan. 1998.

41. R.F.Warming and B.J.Hyett, 'The modified equation approach to the stability and accuracy analysis of finite difference methods', *J. Comp. Phys.,* **14,** 159-179 (1974).

42. F.M.White, *Fluid Mechanics,* McGraw-Hill, New York, 1979.

43. P.Williams, *A three-dimensional, time-accurate, incompressible, Navier Stokes finite element CFD algorithm*, Ph.D. dissertation, The Unbiversity of Tennessee, Knoxville, 1993.

Appendices

Appendix I
Figures

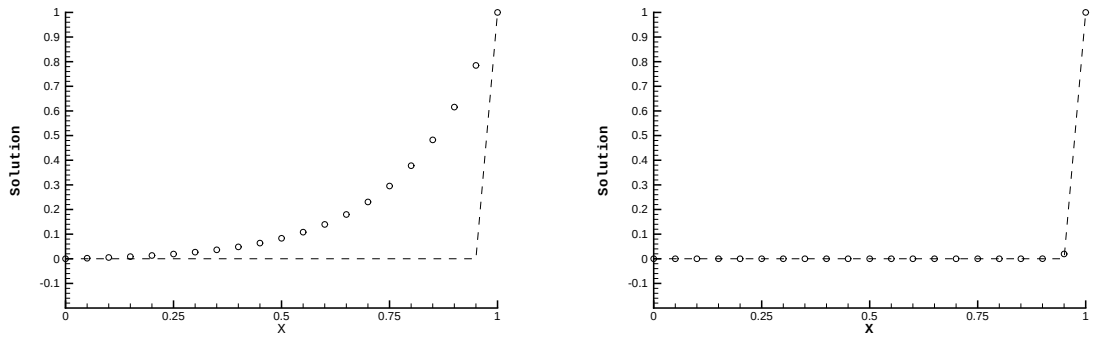

(a) High order formulation

(b) Upwind formulation

Figure 5.1: Steady-state advection-diffusion. Uniform 21-node mesh. Performance comparison for $\varepsilon = 0.001$

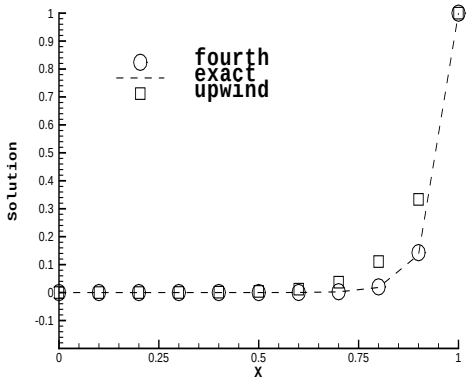

(a) Nnode=11, $\varepsilon = 0.05$

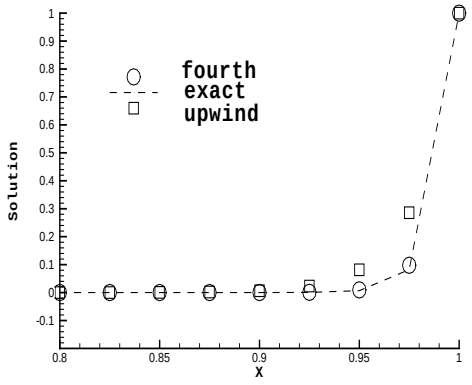

(b) Nnode=41, $\varepsilon = 0.01$

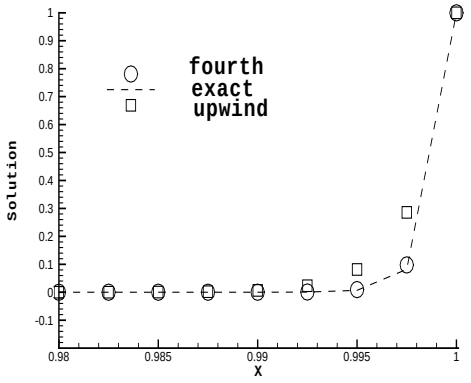

(c) Nnode=401, $\varepsilon = 0.001$

Figure 5.2: Steady-state advection diffusion. Uniform mesh. Performance comparison.

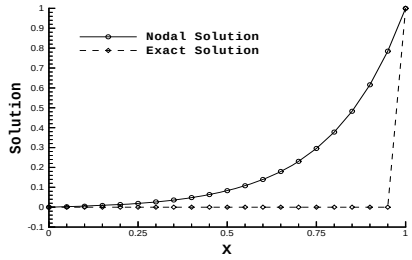

(a) 4^{th} order method, $Nnode$=21

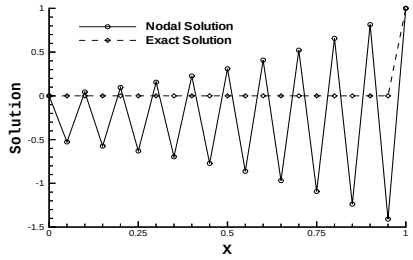

(b) GWS, $Nnode$=21

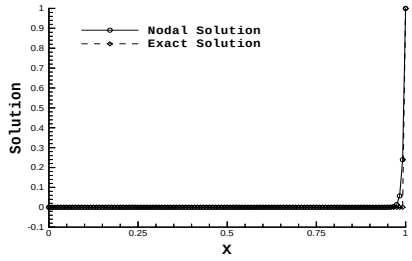

(c) 4^{th} order method, $Nnode$=121

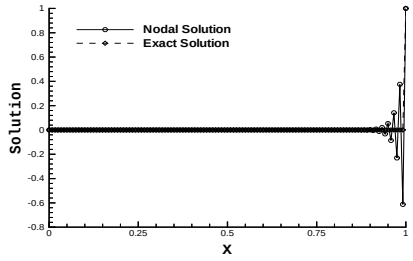

(d) GWS, $Nnode$=121

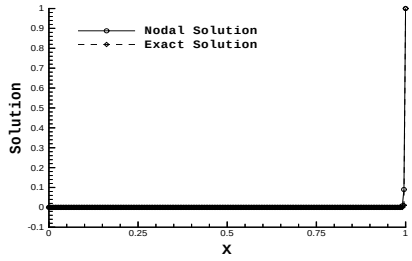

(e) 4^{th} order method, $Nnode$=221

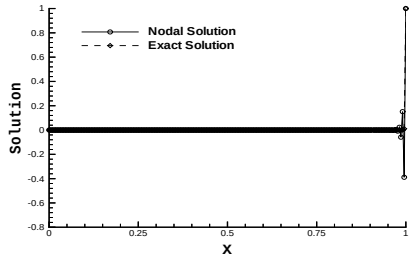

(f) GWS, $Nnode$=221

Figure 7.1: 1D Steady-state problem, solution dependence on $Nnode$, $\varepsilon = 0.001$. High order and GWS performance comparison.

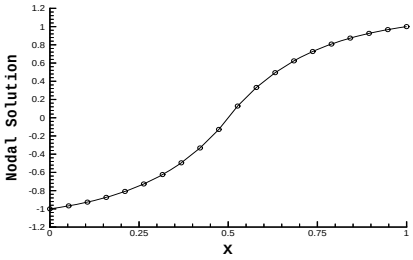

(a) 4^{th} order method, $Nnode$=20

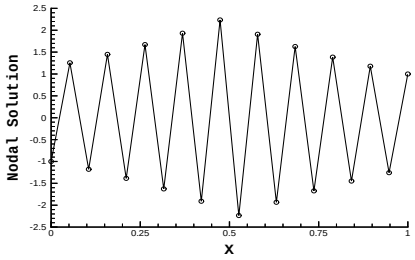

(b) GWS, $Nnode$=20

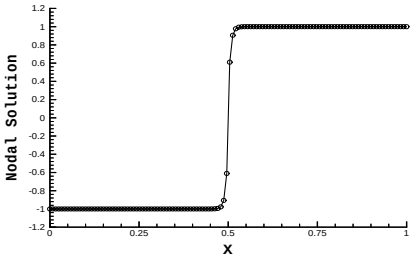

(c) 4^{th} order method, $Nnode$=120

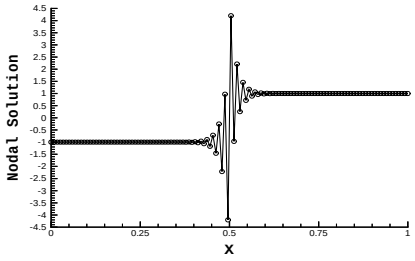

(d) GWS, $Nnode$=120

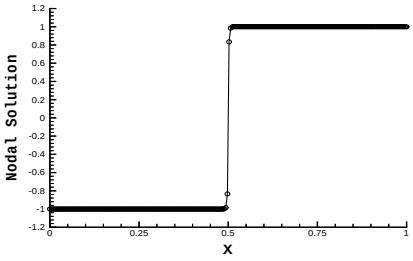

(e) 4^{th} order method, $Nnode$=220

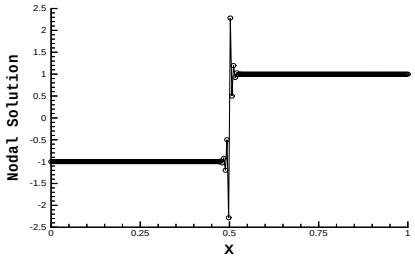

(f) GWS, $Nnode$=250

Figure 7.2: 1D Stationary wave problem, solution dependence on $Nnode$, $\varepsilon = 0.001$. High order and GWS performance comparison.

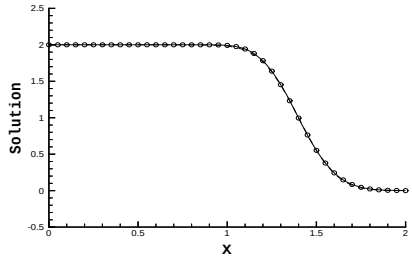

(a) 4^{th} order, C=0.75, ε=0.01

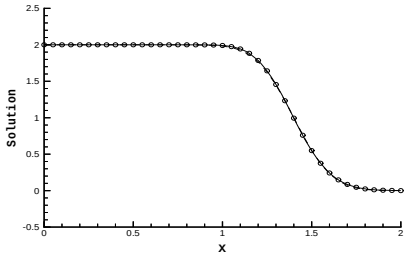

(b) GWS, C=0.75, ε=0.01

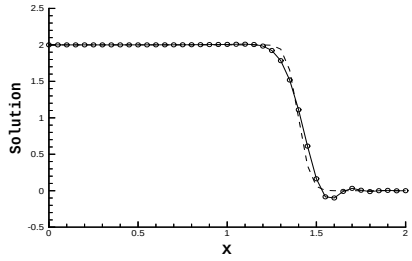

(c) 4^{th} order, C=0.75, ε=0.001

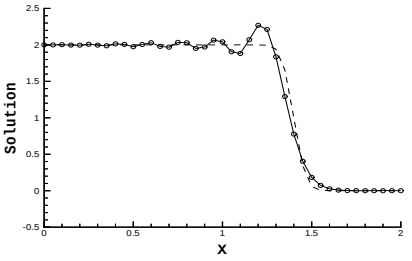

(d) GWS, C=0.75, ε=0.001

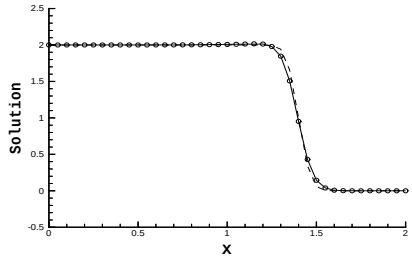

(e) 4^{th} order, C=1, ε=0.001

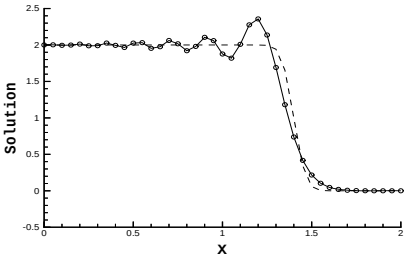

(f) GWS, C=1, ε=0.001

Figure 7.3: 1D Unsteady problem, solution dependence on C and ε. High order and GWS performance comparison.

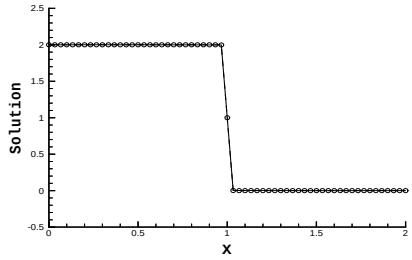

(a) 4^{th} order method, ε=0.000001

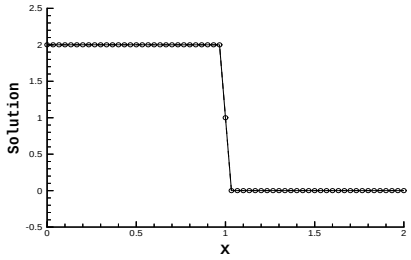

(b) 4^{th} order method, ε=0.0000001

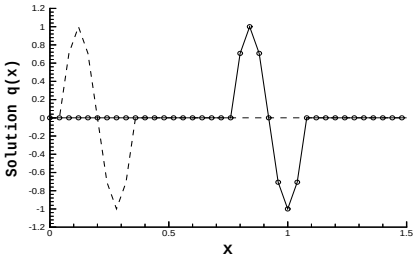

(c) 4^{th} order method solution.

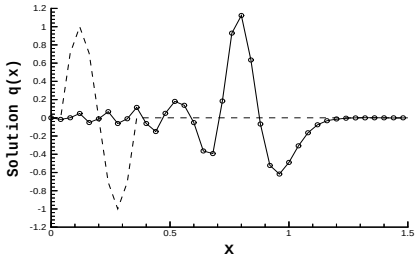

(d) GWS solution.

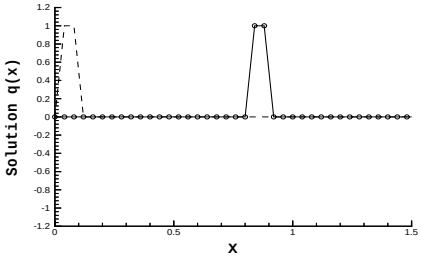

(e) 4^{th} order method solution

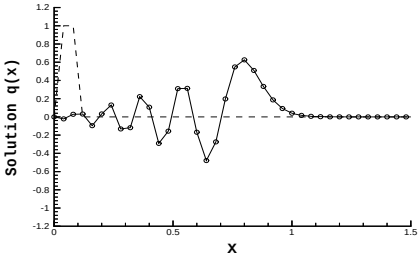

(f) GWS solution.

Figure 7.4: 1D Unsteady problem, solution behavior at small ε, C=1. High order and GWS performance comparison.

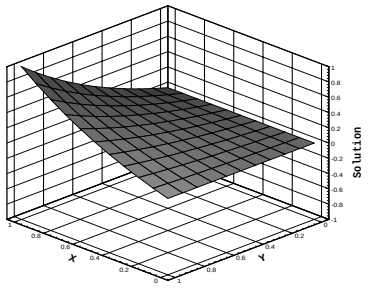

(a) 4^{th} order method, $\varepsilon = 1$

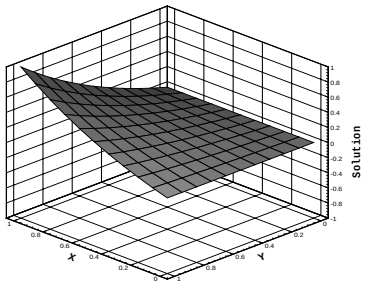

(b) GWS, $\varepsilon = 1$

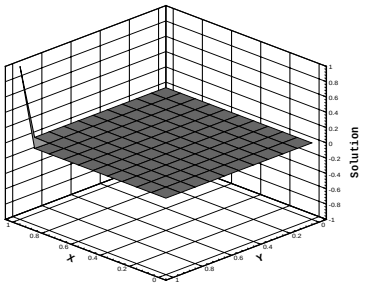

(c) 4^{th} order method, $\varepsilon = 0.001$

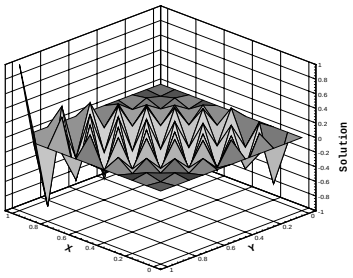

(d) GWS, $\varepsilon = 0.001$

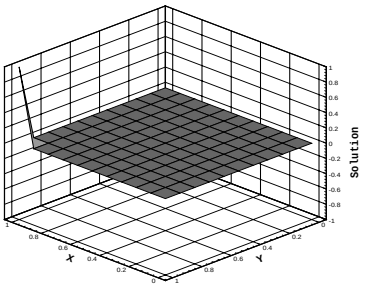

(e) 4^{th} order method, $\varepsilon = 0.00001$

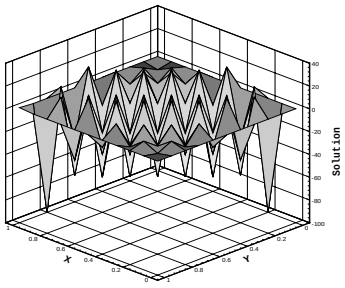

(f) GWS, $\varepsilon = 0.00001$

Figure 7.5: 2D Steady-state problem, solution dependence on ε, 11x11 square mesh. High order and GWS performance comparison.

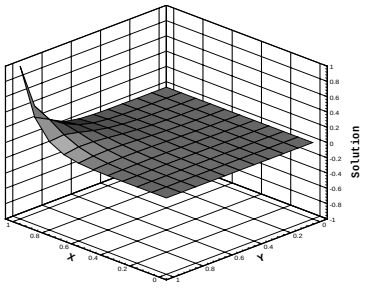

(a) 4^{th} order method, 11x11 mesh

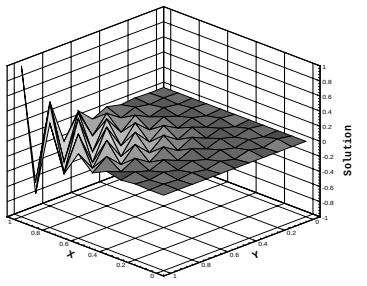

(b) GWS, 11x11 mesh

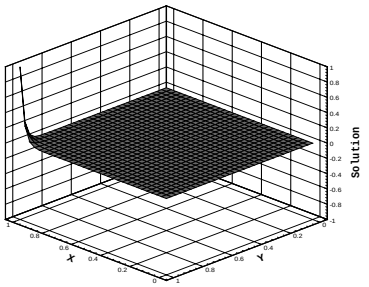

(c) 4^{th} order method, 31x31 mesh

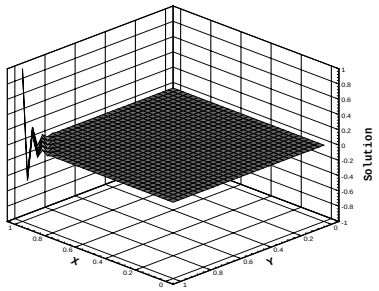

(d) GWS, 31x31 mesh

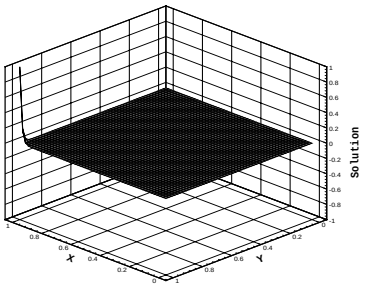

(e) 4^{th} order method, 51x51 mesh

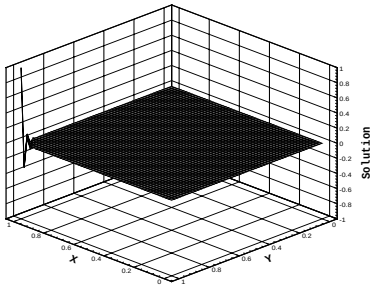

(f) GWS, 51x51 mesh

Figure 7.6: 2D Steady-state problem, solution dependence on $Nnode$, $\varepsilon = 0.005$. High order and GWS performance comparison.

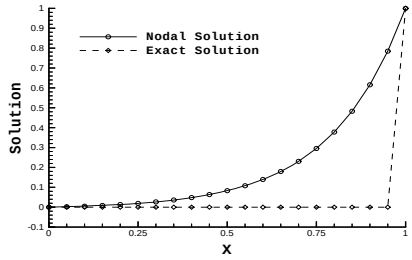

(a) 4^{th} order method, $Nnode$=21

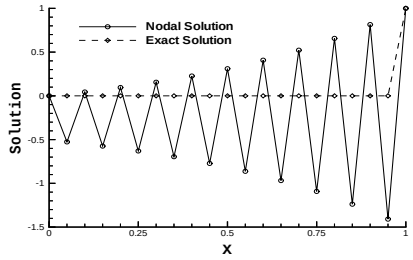

(b) 2^{nd} order method, $Nnode$=21

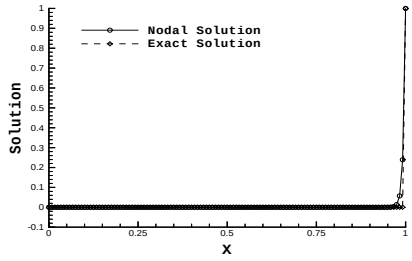

(c) 4^{th} order method, $Nnode$=121

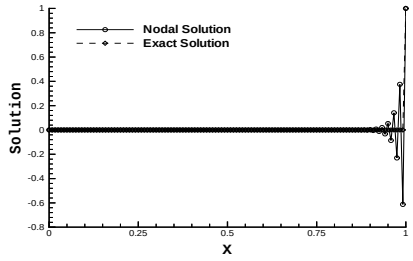

(d) 2^{nd} order method, $Nnode$=121

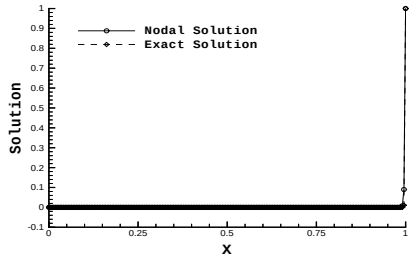

(e) 4^{th} order method, $Nnode$=221

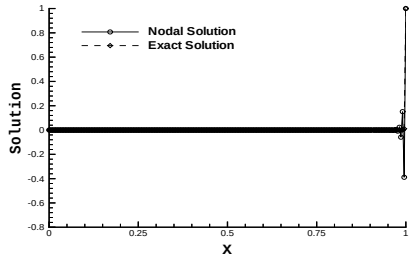

(f) 2^{nd} order method, $Nnode$=221

Figure 7.7: Linear advection-diffusion, solution dependence on $Nnode$, $\varepsilon = 0.001$. High order and GWS performance comparison.

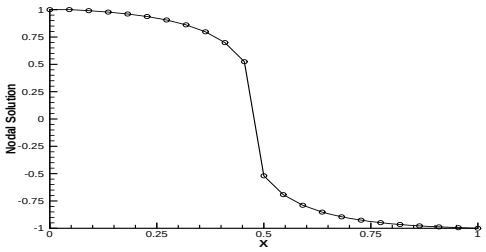

(a) $Nnode$=23

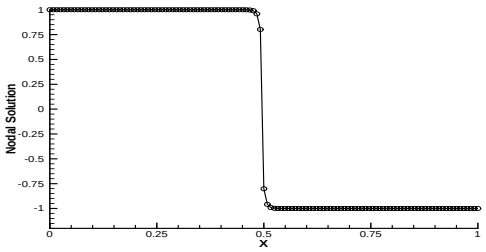

(b) $Nnode$=123

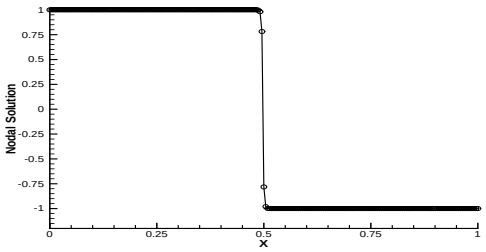

(c) $Nnode$=223

Figure 7.8: Burgers equation. Fourth order method solutions on uniform mesh, $\varepsilon = 0.001$

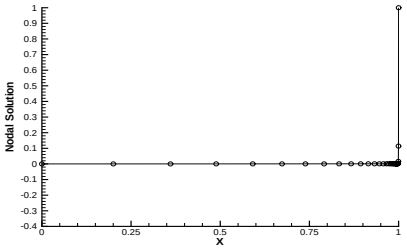

(a) 3^{rd} order method, $Nnode$=31, $\varepsilon = 0.0001$

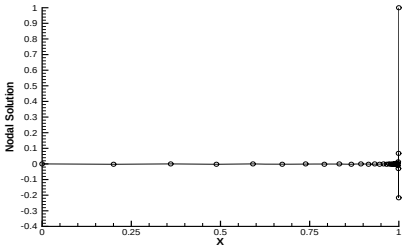

(b) GWS, $Nnode$=31 $\varepsilon = 0.0001$

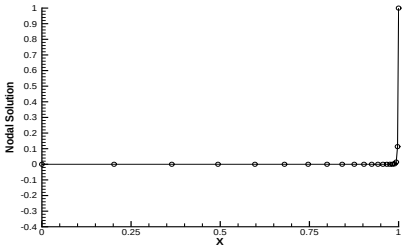

(c) 3^{rd} order method, $Nnode$=21, $\varepsilon = 0.001$

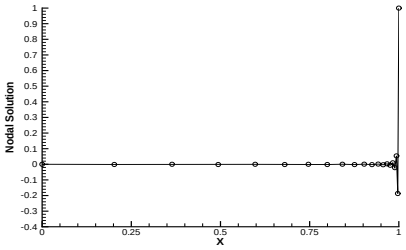

(d) GWS, $Nnode$=21 $\varepsilon = 0.001$

Figure 7.9: Linear advection-diffusion. Non-uniform mesh comparison, p=0.8.

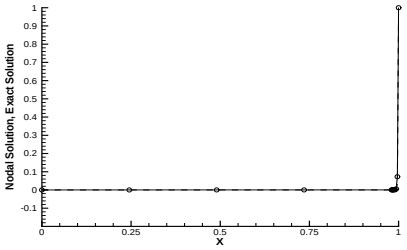

(a) 4^{th} order method, n=5, m=7, $\varepsilon = 0.001$

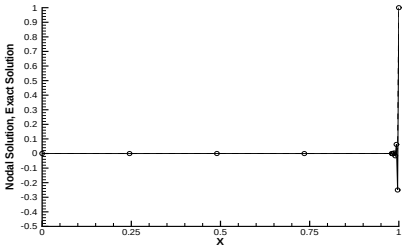

(b) GWS, n=5, m=7 $\varepsilon = 0.001$

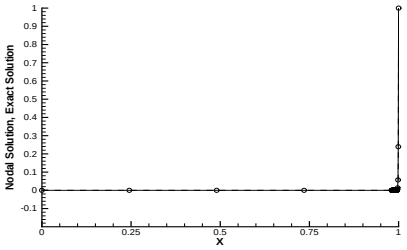

(c) 4^{th} order method, n=5, m=25, $\varepsilon = 0.0001$

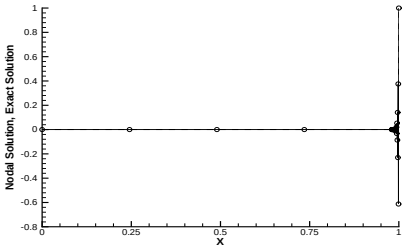

(d) GWS, n=5, m=25 $\varepsilon = 0.0001$

Figure 7.10: Linear advection-diffusion. Locally uniform mesh comparison

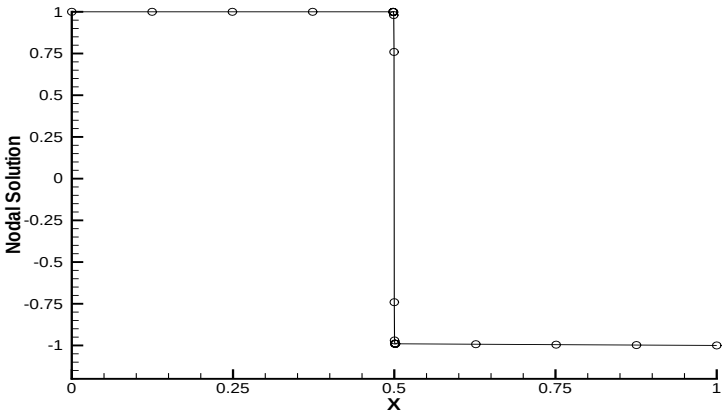

(a) n=5, m=11, l=5, $\varepsilon = 0.0001$

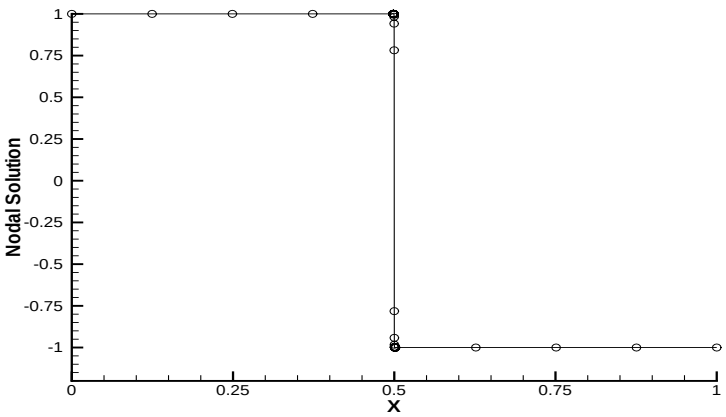

(b) n=5, m=41, l=5, $\varepsilon = 0.00001$

Figure 7.11: Burgers equation. Locally uniform mesh comparison

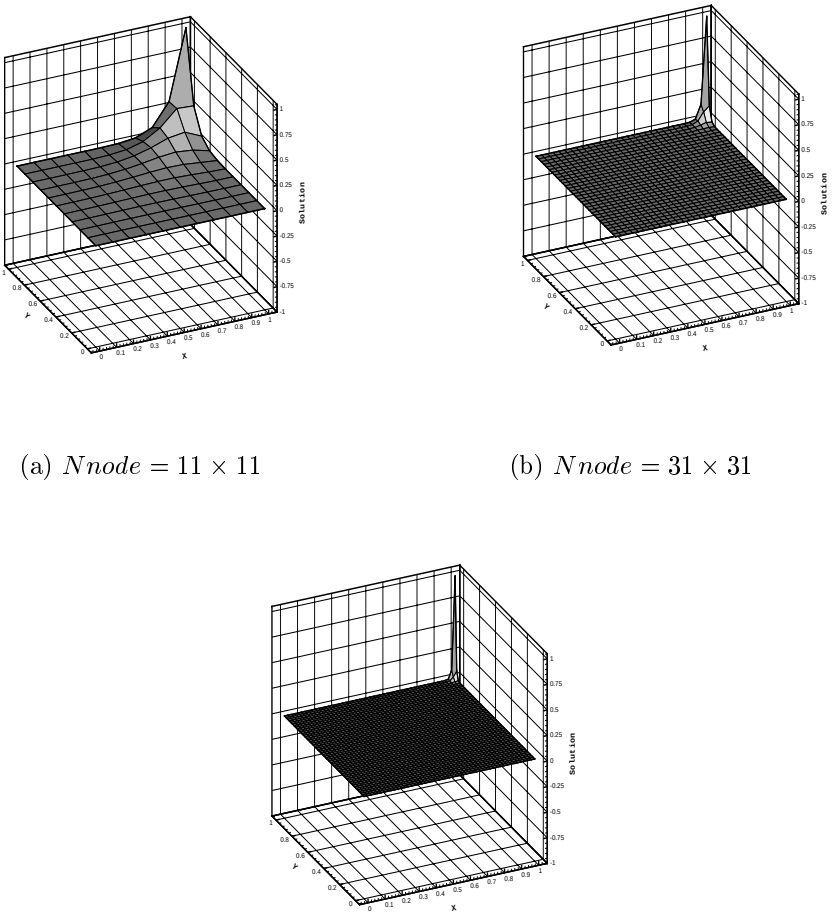

(a) $Nnode = 11 \times 11$

(b) $Nnode = 31 \times 31$

(c) $Nnode = 51 \times 51$

Figure 7.12: Linear advection-diffusion, uniform mesh, solution dependence on $Nnode$, $\varepsilon = 0.005$

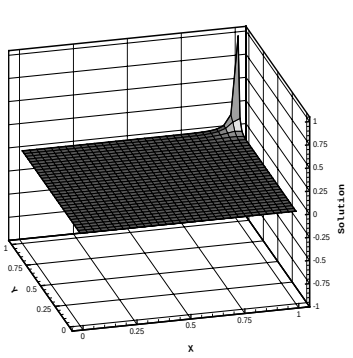

(a) $\varepsilon = 0.01$

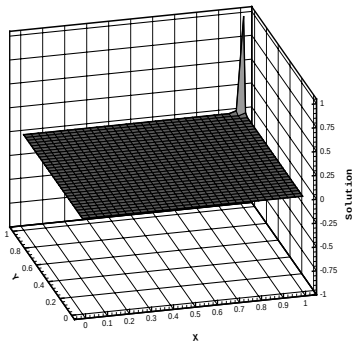

(b) $\varepsilon = 0.0001$

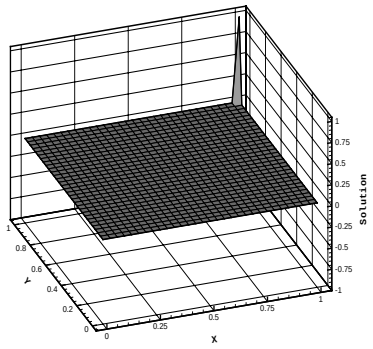

(c) $\varepsilon = 0.000001$

Figure 7.13: Non-linear problem, uniform mesh, solution dependence on ε, $Nnode = 31 \times 31$

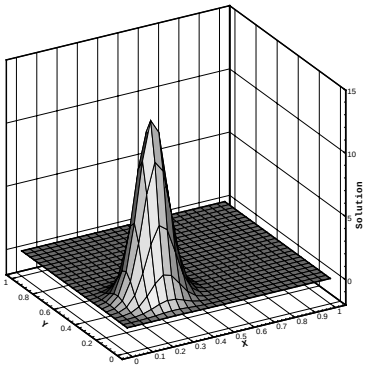

(a) Initial distribution

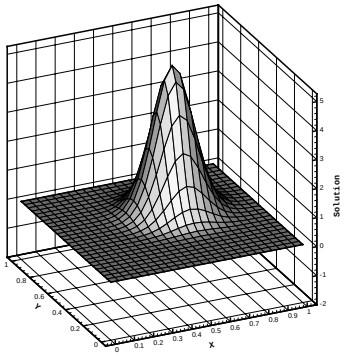

(b) Final distribution at time t=0.5

Figure 7.14: Unsteady advection-diffusion. Analytical distributions

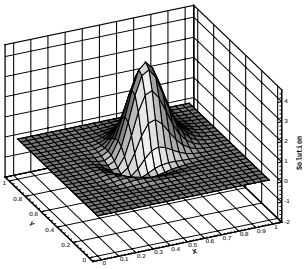

(a) Second order, C=1

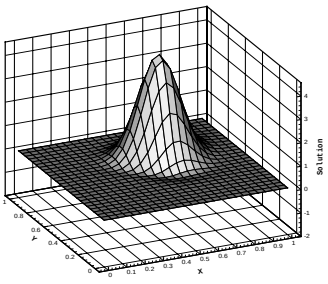

(b) Fourth order, C=1

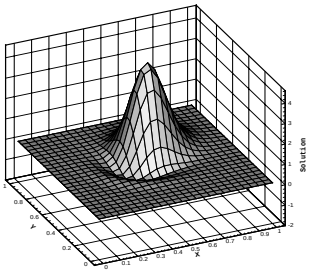

(c) Second order, C=0.75

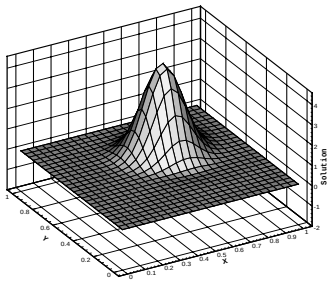

(d) Fourth order, C=0.75

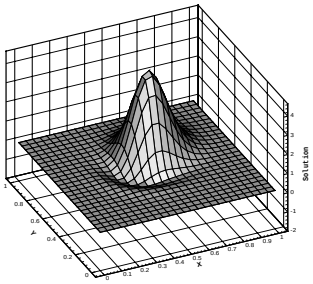

(e) Second order, C=0.5

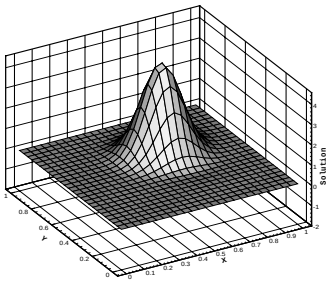

(f) Fourth order, C=0.5

Figure 7.15: Unsteady advection-diffusion. Uniform 26×26-node mesh, $\varepsilon = 0.005$. Solution dependence on Courant number.

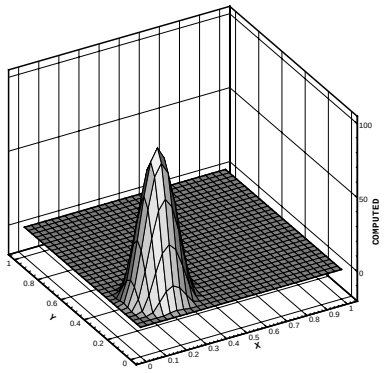

(a) Initial distribution

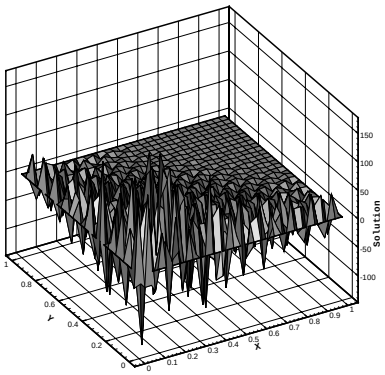

(b) Final distribution

Figure 7.16: Unsteady convection. 31×31-node uniform mesh. High order solution.

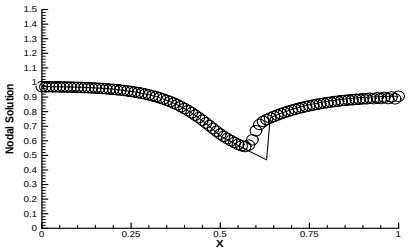

(a) Density, 2^{nd} order method

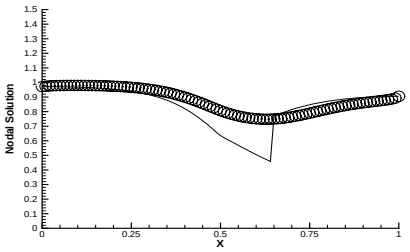

(b) Density, 4^{th} order method

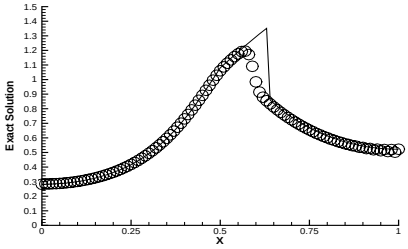

(c) Velocity, 2^{nd} order method

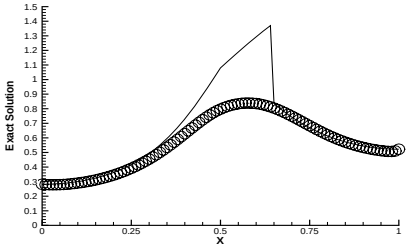

(d) Velocity, 4^{th} order method

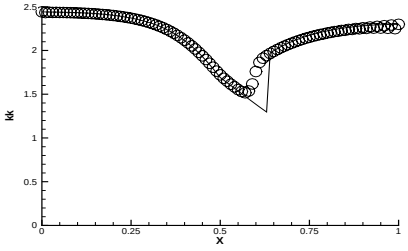

(e) Energy, 2^{nd} order method

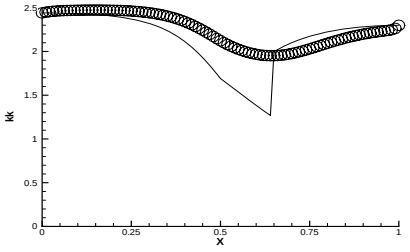

(f) Energy, 4^{th} order method

Figure 7.17: Converging-diverging nozzle flow. Steady-state. Solution comparison, 101-node uniform mesh.

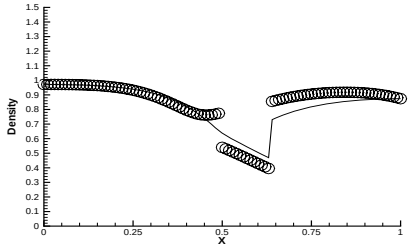

(a) Second order

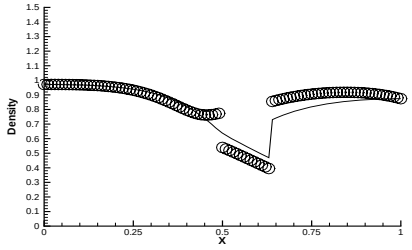

(b) Fourth order

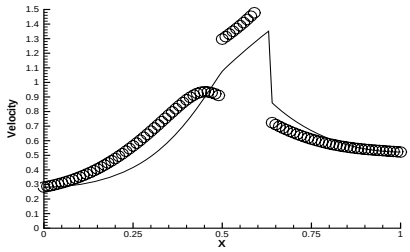

(c) Second order

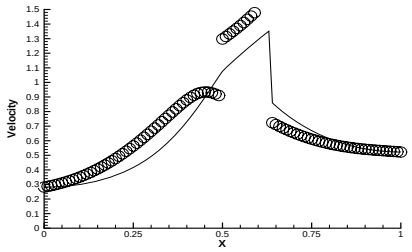

(d) Fourth order

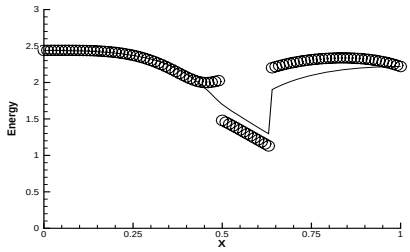

(e) Second order

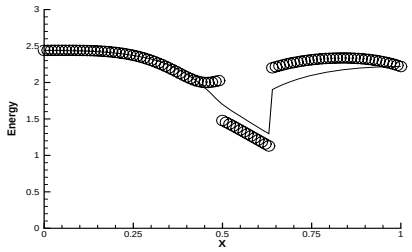

(f) Fourth order

Figure 7.18: Converging-diverging nozzle flow. Steady-state. Fourth/Second order comparison, 101-node uniform mesh, $\varepsilon = 0.1$

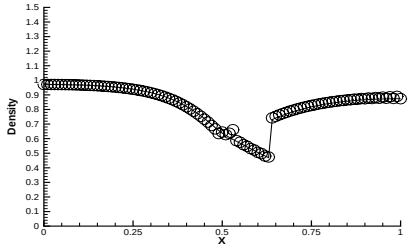

(a) Second order

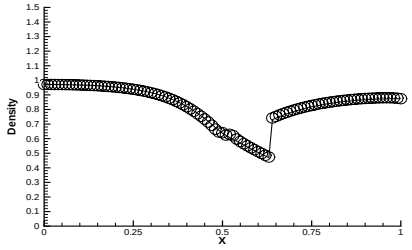

(b) Fourth order

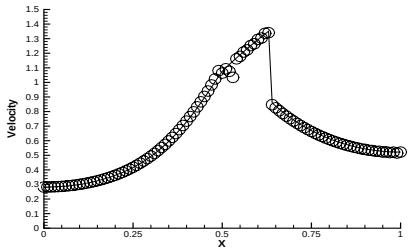

(c) Second order

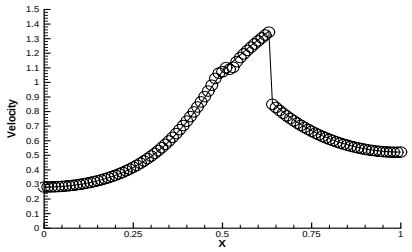

(d) Fourth order

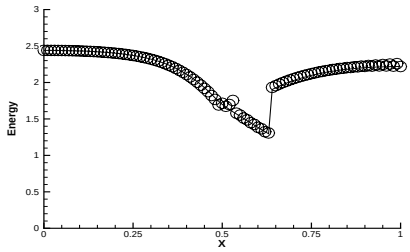

(e) Second order

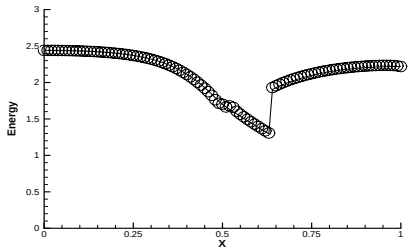

(f) Fourth order

Figure 7.19: Converging-diverging nozzle flow. Steady-state. Fourth/Second order comparison, 101-node uniform mesh, $\varepsilon = 0.0004$

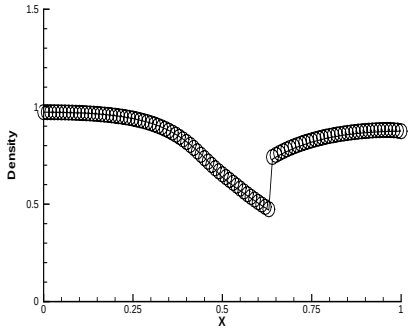

(a) Filtered density

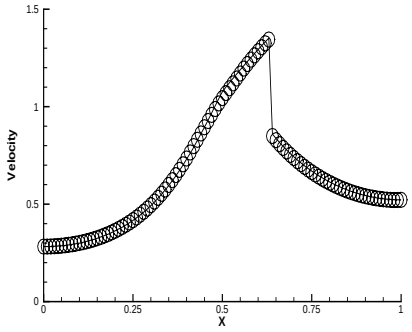

(b) Filtered velocity

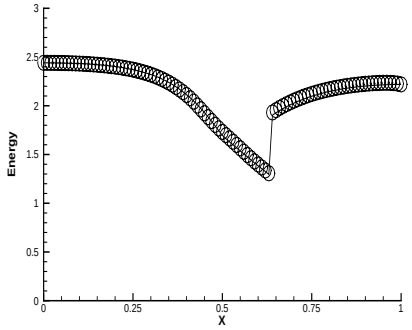

(c) Filtered energy

Figure 7.20: Converging-diverging nozzle flow. Steady-state. Fourth order method with spatial filtering, 101-node uniform mesh, $\varepsilon = 0.0004$, $\alpha = -0.49$

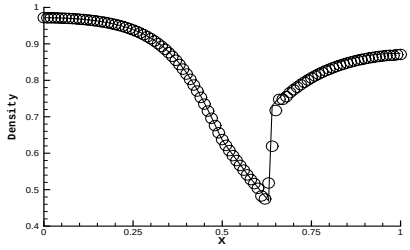

(a) Second order

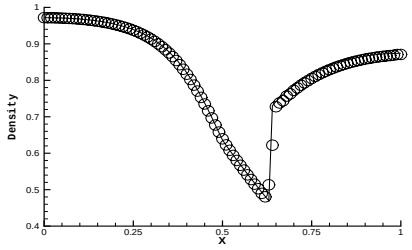

(b) Fourth order

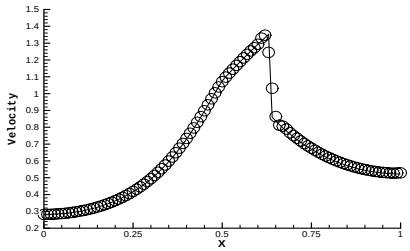

(c) Second order

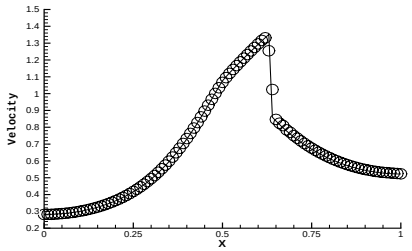

(d) Fourth order

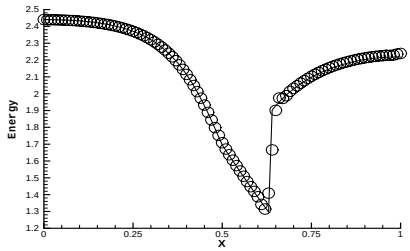

(e) Second order

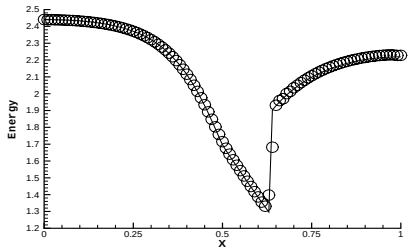

(f) Fourth order

Figure 7.21: Converging-diverging nozzle flow. Transient problem. Fourth/Second order comparison, $\varepsilon = 0.0008$, $\alpha = 0.4$

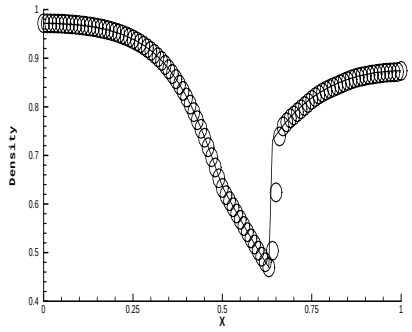

(a) Density

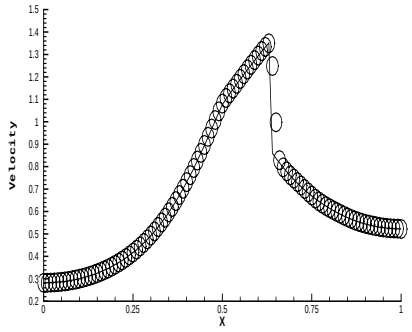

(b) Velocity

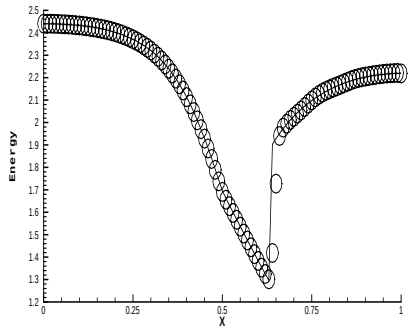

(c) Energy

Figure 7.22: Converging-diverging nozzle flow. Transient problem. Accelerated second order method, $\varepsilon = 0.000001$, $\alpha = -0.05$

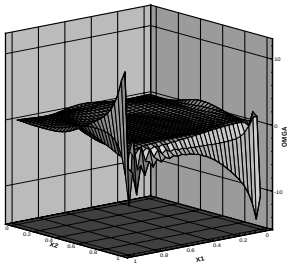

(a) GWS vorticity solution

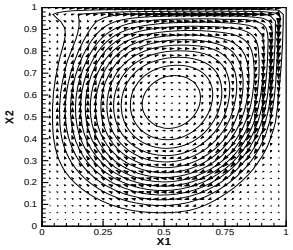

(b) GWS velocity profile

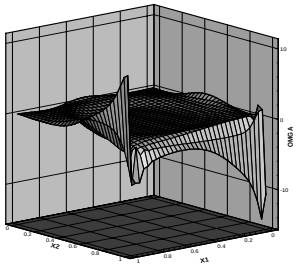

(c) TWS, $\beta = 0.2$, vorticity solution

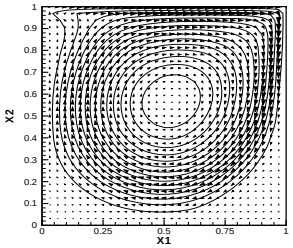

(d) TWS, $\beta = 0.2$, velocity profile

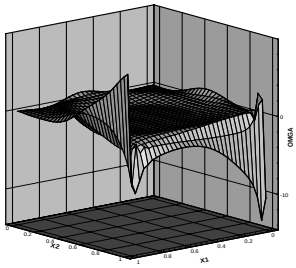

(e) 4^{th} order, vorticity solution

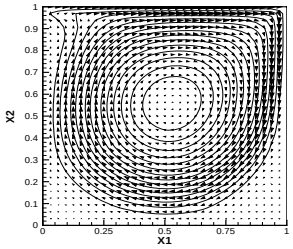

(f) 4^{th} order, velocity profile

Figure 7.23: Driven cavity benchmark solutions. Re=1000, 33×33-node uniform mesh.

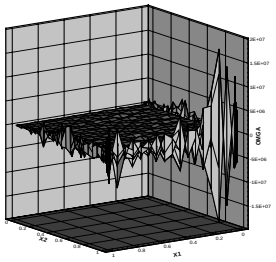

(a) GWS vorticity solution

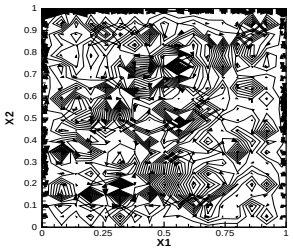

(b) GWS velocity profile

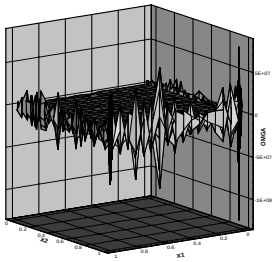

(c) TWS, $\beta = 0.2$, vorticity solution

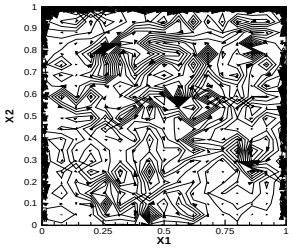

(d) TWS, $\beta = 0.2$, velocity profile

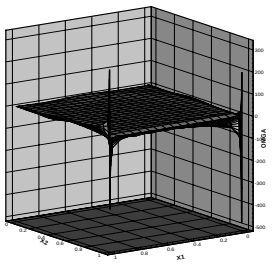

(e) 4^{th} order, vorticity solution

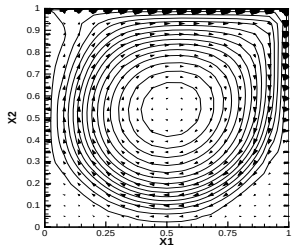

(f) 4^{th} order, velocity profile

Figure 7.24: Driven cavity benchmark solutions. Re=3000, 33×33-node locally-uniform mesh. X1: [33(0. 8R1.0 .02 16R1.0 .98 8R1.0 1)], X2: [-33(0. 20R1.0 .98 12R1.0 1)].

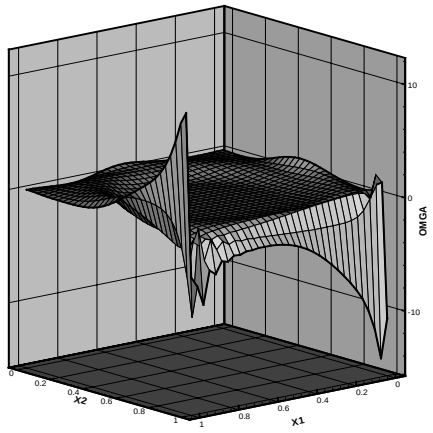

(a) Vorticity solution, Re=1000

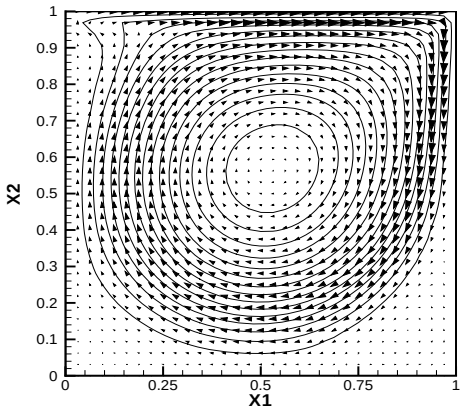

(b) Velocity profile, Re=1000

Figure 7.25: Driven cavity benchmark solutions. Vorticity high order formulation. 33×33-node uniform mesh.

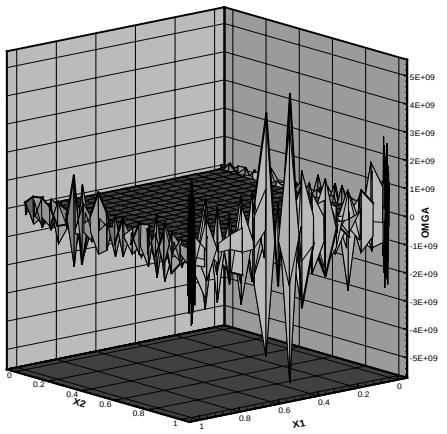

(a) Vorticity solution, Re=3000

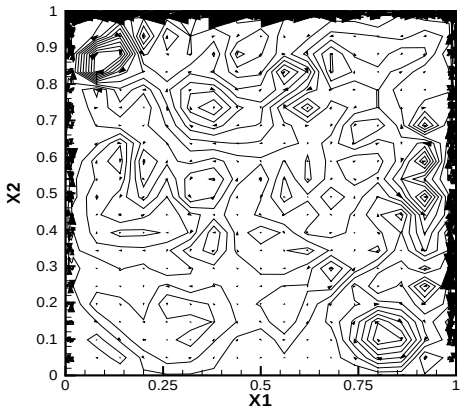

(b) Velocity profile, Re=3000

Figure 7.26: Driven cavity benchmark solutions. Vorticity high order formulation. 33×33-node locally-uniform mesh. X1: [33(0. 8R1.0 .02 16R1.0 .98 8R1.0 1)], X2: [-33(0. 20R1.0 .98 12R1.0 1)].

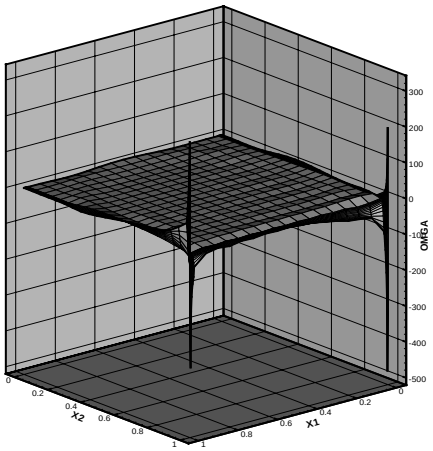

(a) Vorticity solution, Re=3000

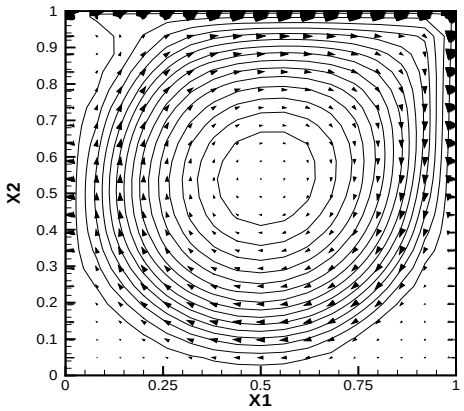

(b) Velocity profile, Re=3000

Figure 7.27: Driven cavity benchmark solutions. Stream-function high order formulation. 33×33-node locally-uniform mesh. X1: [33(0. 8R1.0 .02 16R1.0 .98 8R1.0 1)], X2: [-33(0. 20R1.0 .98 12R1.0 1)].

Appendix II
Tables

Appendix III
Template file for the high order formulation implementation. Driven cavity benchmark.

Appendix IV

Model file for the high order formulation implementation. Driven cavity benchmark.

Appendix V

Driven cavity benchmark. Integer print-field after 40 time steps. High order formulation, Re=3000, 31×31 locally uniform mesh.